1995

NMR studies of lignin models, derivatives and bleaching effluents

Maa, Karen Joy

NMR Studies of Lignin Models, Derivatives and Bleaching Effluents

by

Karen Joy Maa ©

A thesis submitted in partial
fulfillment of the requirements for the degree of
Master of Science

Chemistry Department
Lakehead University
Thunder Bay, Ontario
August 30, 1995

ISBN 0-612-09222-4

Canada

ABSTRACT

NMR problems related to assignment techniques and relaxation restrict the use of NMR in the structural analysis of lignin. These problems have been addressed in three practical studies in this thesis involving a lignin model trimer and peroxide bleaching effluents from spruce and investigation of correlation times of lignin using NMR relaxation. Complete chemical shift assignments for aliphatic and aromatic protons and carbons of a lignin model trimer were made using one- and two-dimensional NMR experiments. Measurements from experiments using the nuclear Overhauser effect were consistent with conformations of this model compound determined from semi-empirical methods and the published experimental crystal structures of model dimers. Structures present in the peroxide bleaching effluents of spruce ground wood were identified using proton, phosphorus and COSY NMR experiments. Correlation times for acetylated kraft lignin fractions varied between 2.7×10^{-8} s and 8.1×10^{-10} s when temperature, molecular weight and concentration were changed. A greater concentration dependence was shown for high mass samples.

ACKNOWLEDGEMENTS

I would like to thank Dr. Jerzy Arct for donating model IIB and for assisting me in preparing the phosphorus derivatizing reagent.

The second floor chemistry staff: Bert Harding, Dave Corbett, Bill Morgan and Ainsley Bharath, graciously supplied or built any special glassware I required as well as supplying chemical reagents.

Keith Pringnitz in the Instrument Lab patiently answered many NMR questions.

A special thank you to my family for their encouragement and support in some very difficult times.

Finally, thank you to Dr. Ted Garver for his patience, understanding and guidance throughout this project.

Funding for this project was provided by NSERC, Mechanical and Chemimechanical Wood-Pulps Network and Lakehead University's Chemistry Department.

TABLE OF CONTENTS

Page

Abstract i

Acknowledgements ii

List of Figures vi

List of Tables ix

Overview 1

Introduction 1

Lignin Structure 1

NMR Analysis 2

One-Dimensional NMR 7

Two-Dimensional NMR 8

PART ONE: MODEL COMPOUNDS 11

Introduction 11

Model Compound 12

Results and Discussion 15

Side Chains 15

Aromatics 22

Methoxyl Protons 31

200 MHz versus 500 MHz 32

NOE and Conformation 35

PART TWO: EFFLUENTS 39

Introduction and Background Information 39

Hydrogen Peroxide 39

α-Ketones and α,β-Unsaturated Aldehydes 40

Reaction of Phenolic Structures 43

Reactions of Beta-O-4 Structures 43

Reactions of Beta-1 Structures 47

Results and Discussion 47
Overview 47
Variation of Structural Elements:
Beta-O-4 Units 50
Phenolic Structures 58
3-Aryl-1-Propanol Units 60
Beta-5-Units 60
Aldehydes 60
Carboxylic Acids 61
Aromatic Protons Adjacent to Carbonyl Groups 64
Carbohydrates 64
Other Structures 64
Conclusion 68
PART THREE: ANALYSIS OF NMR RELAXATION OF DEUTERIUM LABELLED KRAFT LIGNIN FRACTIONS 69
Introduction 69
Deuterium Relaxation 69
Correlation Times 71
Results and Discussion 72
Relaxation Times 72
Concentration and Molecular Weight Dependence 72
Temperature Dependence 72
Conclusion 82
Experimental Section 88
Model Compound 88
Preparation of Kraft Lignin Samples for Deuterium Experiments 88
Preparation of Effluent Samples 88
Preparation of Spruce Kraft Lignin 88
Scheme I Model Compounds 89

Scheme II Deuterium Relaxation....90
Scheme III Preparation of Effluent Samples....91
Scheme IV Preparation of Spruce Kraft Lignin....92
Fractionation of Kraft Lignin....93
Acetylation....93
Scheme V Fraction of Kraft Lignin....94
Scheme VI Acetylation....95
Acetylation Work-Up....96
Hexane Purification....97
Methylation....97
Diazomethane Preparation....97
Sample Preparation....97
Phosphorus-31 NMR....98
Preparation of 1,3,2-dioxaphospholanyl chloride....98
Labelling with 1,3,2-dioxaphospholanyl chloride....99
Deuterium Labelling Methods....99
NMR Experiments....100
Proton NMR....100
Carbon-13....100
COSY....104
NOESY....104
HOESY....104
NOE Difference....104
HMBC....104
HMQC....104
Analysis of Deuterium Relaxation....104
References....110

LIST OF FIGURES

Figure	Title	Page
1	Lignin precursors	3
2	Linkages between phenylpropane units in lignin	5
3	Structural units in spruce lignin and spruce wood	6
4	Acetoguaiacyl-dehydrodi-isoeugenol methyl ether (IIB) with nomenclature	13
5	Aliphatic region on 500 MHz proton spectrum with coupling constants	16
6	200 MHz COSY (Correlated Spectroscopy) with side chain connectivities	17
7	500 MHz decoupled carbon-13 spectrum of IIB	21
8	Aromatic region on 500 MHz proton spectrum	23
9	Aromatic and vinylic regions on the 500 MHz HMQC spectrum	24
10	500 MHz NOE difference spectra	26
11	Models similar in structure to IIB	29
12	Methoxyl regions on various two-dimensional spectra	33
13	Chemical shift dependence on magnetic field strength 200 MHz versus 500 MHz	34
14	Three views of IIB showing conformation	38
15	Peroxide oxidation of α-ketones	41
16	Peroxide oxidation of α,β-unsaturated aldehydes	42
17	Decomposition of α-methylvanillyl alcohol with peroxide	45
18	Major route for peroxide oxidation of β-O-4 model compound guaiacylglycerol-β-aryl ether	46
19	Reaction of peroxide with a β-1 model compound	48
20	Major route for conversion of a stilbene into a quinone by reaction with oxygen	49
21	200 MHz proton spectra of the effluents from the four bleaching stages	51

22 200 MHz COSY spectrum of acetylated effluent from the fourth bleaching stage 53

23 200 MHz phosphorus-31 spectra of the effluents from the four bleaching stages 55

24 Ratios of β-O-4 units to methoxyl groups versus bleaching stage 57

25 Ratios of phenolic hydroxyls to methoxyl groups versus bleaching stage 59

26 Ratios of formyl groups in benzaldehyde units to methoxyl groups versus bleaching stage 62

27 Difference spectrum of acetylated and acetylated/methylated effluent from the first bleaching stage showing the presence of carboxylic acids 63

28 Ratios of aromatic protons with alpha-carbonyl groups to methoxyl groups versus bleaching stage 65

29 Difference spectrum of effluent from the fourth and first bleaching stages showing the presence of carbohydrates 66

30 Ratios of aliphatic hydroxyl to aromatic hydroxyl groups versus bleaching stage 67

31 UV spectrum of spruce Kraft lignin with estimated molecular weights for the fractions 73

32 Spin-lattice relaxation time versus concentration for molecular weights 2300 and 480 74

33 Spin-spin relaxation time versus concentration for molecular weights 2300 and 480 77

34 Ratio of T_1/T_2 versus concentration for molecular weights 2300 and 480 79

35 Rotational correlation time versus concentration for molecular weights 4000, 2300 and 480 80

36 Rotational correlation time versus molar mass 81

37 Spin-lattice relaxation time versus temperature for molecular weights 2800 and 480 83

38 Spin-spin relaxation time versus temperature for molecular weights 2800 and 480....84

39 Correlation time/viscosity*temperature versus temperature for lignin fractions....85

40 200 MHz proton spectra showing the collapse of vanillin multiplets between 7.0-7.5 ppm....101

41 30.7 MHz deuterium spectrum of vanillin....102

42 30.7 MHz deuterium spectrum of ground milled spruce pulp....103

43 Single exponential fit to inversion recovery integral and height data for molecular weight 2300....106

44 Double exponential fit to inversion recovery integral and height data for molecular weight 480....107

45 Theoretical plot of T1/T2 versus correlation time for deuterium at 30.7 MHz....109

LIST OF TABLES

Table	Title	Page
1	Percentages of lignin linkages in softwood	4
2	Expected multiplicities for IIB	14
3	Chemical shifts and coupling constants measured from 500 MHz proton spectrum and 200 MHz coupled carbon-13 spectrum	18
4	Peak assignments from 200 MHz HMQC, HOESY and HMBC experiments	19,20
5	Peak assignments from 200 MHz COSY and 500 MHz NOESY spectra	25
6	Assignments and internuclear distances obtained from 500 MHz NOE difference spectra and MOPAC program	27
7	Chemical shifts for models similar in structure to IIB	30
8	NOESY initial rates from peak intensities	37
9	Rate constants for the reaction of selected model compounds with peroxide	44
10	Peak list for 200 MHz proton spectra of the effluents	52
11	Peak assignments for the COSY spectrum of the effluent from the fourth bleaching stage	54
12	Peak assignments for phosphorus-31 NMR of effluents	56
13	Spin-lattice relaxation times for lignin fractions at various concentrations	75
14	Spin-lattice relaxation times for lignin fractions at various concentrations (double exponential fit)	76
15	Spin-spin relaxation times calculated from line widths for fractionated lignin samples	78

OVERVIEW:

The elucidation of the structure of lignin provides understanding and insight into reactions occuring during pulping and bleaching. Limitations to the application of NMR to the study of lignin were examined in this study. Nuclear magnetic resonance spectroscopy was used to examine lignin samples from a model compound, bleaching effluents and deuterium labelled kraft lignin. The model compound was well suited to the many two-dimensional NMR experiments involving spin exchange and some potentially useful information was derived from the data analysis. These experiments led to a systematic approach to the NMR of lignin molecules as well as the conformation of the model. Larger lignin molecules present in effluents from peroxide brightening of spruce proved to be more difficult to analyse due to their size, complex spectra and relaxation. Nevertheless, the experiments used in effluent analysis allowed important lignin structural units to be identified and semi-quantified. Structural moieties are discussed in light of a review of relevant reactions from the literature. Relaxation studies on samples with molecular weights (330-22000) were used to study rotation and internal motion of lignin in solution as a function of concentration and temperature.

INTRODUCTION:

Lignin Structure:

Lignin is the second most abundant natural polymer next to cellulose[1]. Its functions in the plant cell wall include structural stability, aid in water and nutrient transport and defence against attack by microorganisms[1]. It is found in hardwood and softwood trees and other non-woody sources such as grass[2]. Chemically, lignin is a phenylpropanoid

macromolecule formed by an enzymic dehydrogenative polymerization of lignin precursors *p*-coumaryl, coniferyl and sinapyl alcohols[2] (Figure 1). These monomers are joined by various linkages such as ether or carbon-carbon bonds to form the lignin macromolecule[3].

The structure of lignin has not been clearly elucidated. Furthermore, it would be impossible to determine a 'universal' lignin structure as lignin is different for each tree species and even between locations in a single tree[4]. Structural studies have involved techniques ranging from chemical tests for functional groups to spectroscopy[1,2,4].

Lignin in softwood, such as spruce, consists mainly of 4-hydroxy substituted phenylpropane units (guaiacyl-type). Approximately two-thirds of these units are joined together by ether type linkages and the rest by carbon-carbon bonds[5]. The most common linkage is the β-O-4 linkage (approximately 50% of total linkages)(Table 1)[5]. Other linkages which are shown in Figure 2 are α-O-4, β-5, 5-5, 4-O-5, β-1 and β-β[3,5,6]. Types of structural units in lignin are shown in Figure 3. Lignin functionality is dominated by oxygen containing groups which include methoxyl groups, hydroxyl groups and carbonyl groups[5].

Carbohydrates are bound to lignin[3]. Softwoods contain mainly galactoglucomannans, arabinoglucuronoxylan and a minor amount of arabinogalactan[5].

NMR Analysis:

The basics of NMR theory will not be covered in this thesis as there are several good books on the subject[7,8]. However, for the purpose of clarity some basic principles of

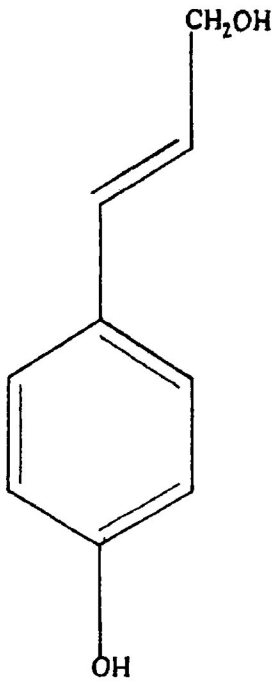

p-coumaryl alcohol

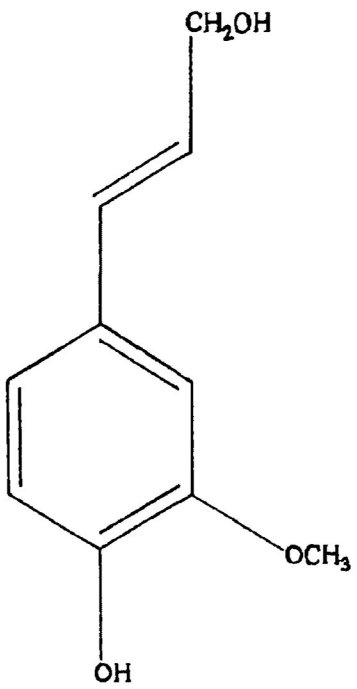

coniferyl alcohol

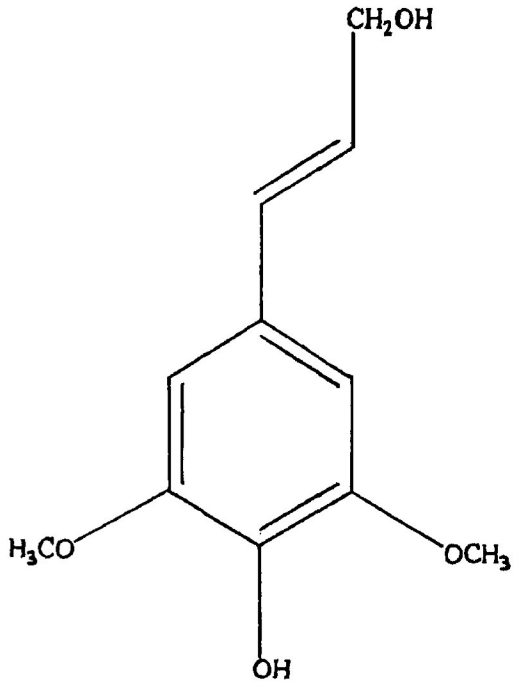

sinapyl alcohol

Figure 1 Lignin precursors[2]

Linkage	Structure	% of Total Linkages
β-O-4	arylglycerol-β-aryl ether	50
α-O-4	noncyclic benzyl aryl ether	0.2-8*
β-5	phenylcoumaran	9-12
5-5	biphenyl	10-11
4-O-5	diaryl ether	4
β-1	1,2-diarylpropane	7
β-β	linked through side chains	2

*Recent work by Ede and Kilpeläinen[72] (using 2-D NMR techniques) indicates that the percentage of non-cyclic benzyl aryl ethers (<0.3%) is not as high as previously reported[5]. It should be noted these results are non-quantitative and may be selective for the low-mass, slowly relaxing components.

Table 1 Percentages of lignin linkages in softwood[5]

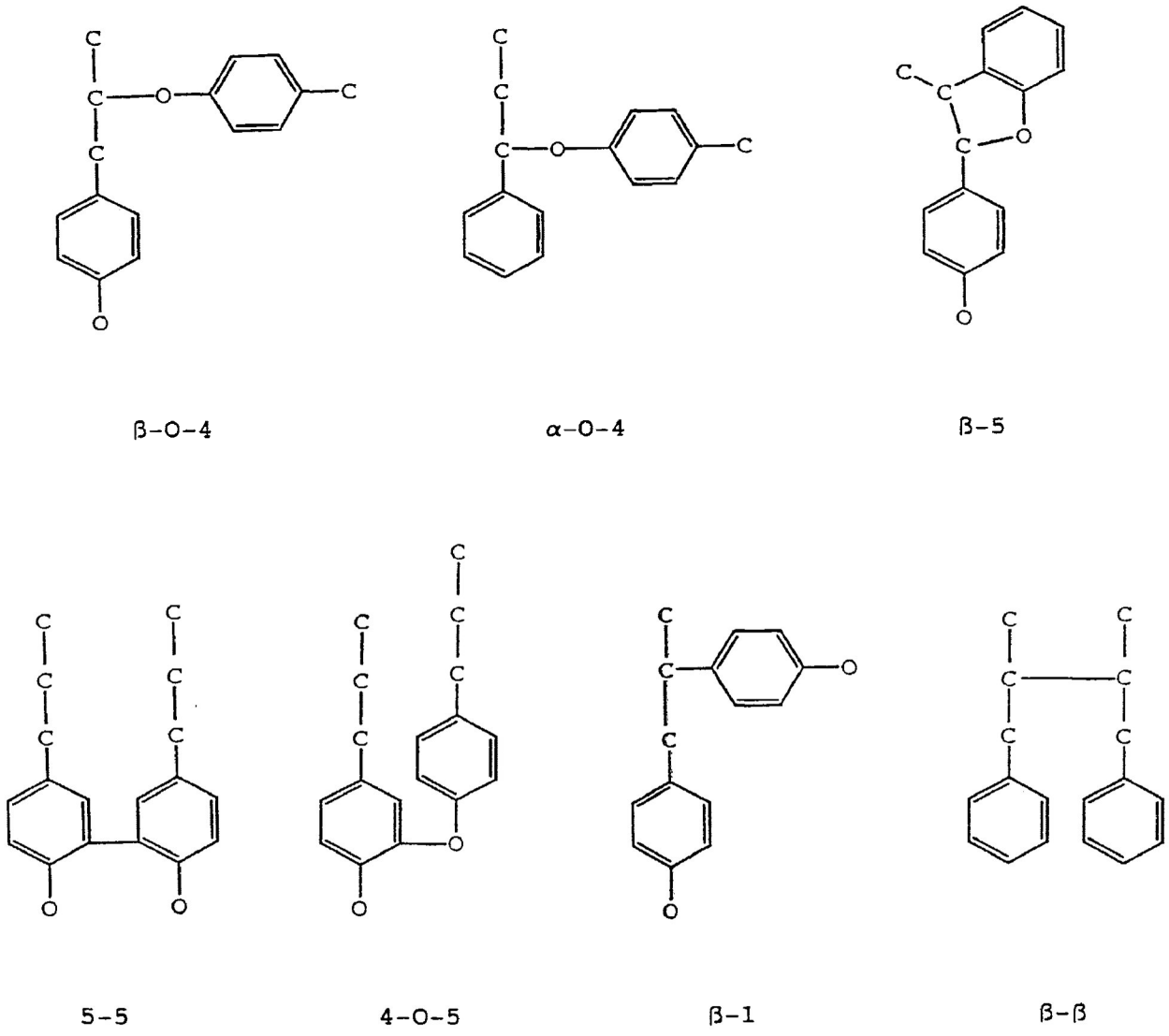

Figure 2 Linkages between phenylpropane units in lignin[3,6]

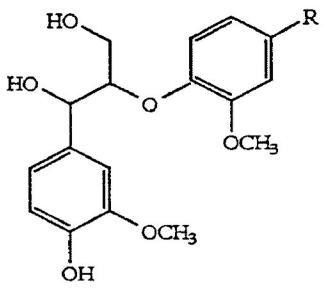

1a R = CHO
1b R = CH=CHCHO
1c R = $CHCH_2OH$

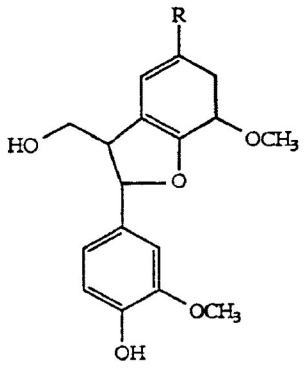

2a R = CH=CHCHO
2b R = $CH=CHCH_2OH$

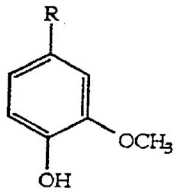

3a R = CHO
3b R = $CH_2CH_2CH_2OH$
3c R = CH=CHCHO
3d R = $CH=CHCH_2OH$

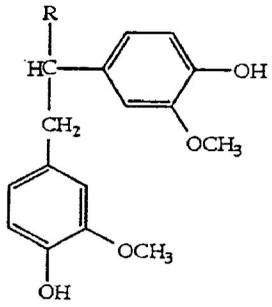

4a R = H
4b R = CH_2OH

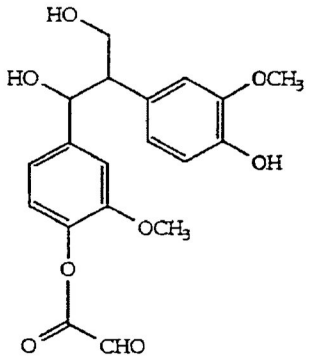

5

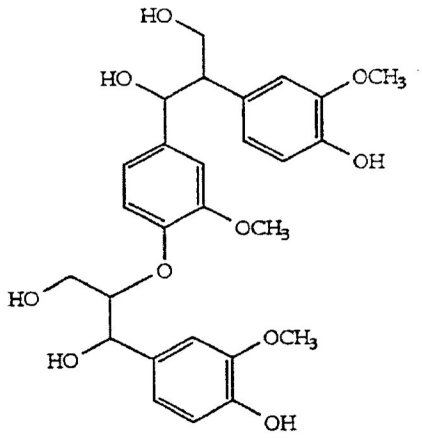

6

Figure 3 Structural units in spruce lignin and spruce wood[38,49]

spectrum interpretation will be mentioned along with a brief description of each experiment.

One-Dimensional NMR:

The most widely used experiment is the one-dimensional proton experiment which contains information regarding chemical shifts, multiplicities, integrations and coupling constants. The chemical shift depends on the electronic environment of the proton[8]. For lignin, aldehydic protons occur between 9.8-9.94 ppm, the aromatic region is between 6.5-8.0 ppm, methoxyl protons at 3.7-3.95 ppm, aromatic acetoxyl at 2.3 ppm and aliphatic acetoxyl at 2.1 ppm. Vinylic protons between 5.4-7.8 ppm may overlap with the aromatic region[1]. Multiplicity or peak splitting contains information concerning neighbouring protons which are responsible for splitting a signal into many peaks according to the n + 1 rule where n = number of neighbouring protons[8]. Integration provides a measure of the relative number of protons contributing to a specific peak or group of peaks. Coupling constants obtained by measuring the distance between peaks in a multiplet are used to confirm assignments and determine configuration.

A coupled carbon-13 spectrum contains the same type of information as a proton spectrum but with a chemical shift range of 200 ppm compared to 10 ppm for proton. A proton-decoupled carbon spectrum consists of single peaks each representing a carbon. Reference data for lignin model compounds have appeared in the literature[9,10,11].

Some of the interactions affecting NMR experiments are spin-spin or scalar coupling, dipolar and quadrupolar interactions.

The basic proton experiment described earlier provides information about spin-spin coupled protons. Experiments utilizing the nuclear Overhauser effect (NOE) provide information about dipolar interactions. One such experiment is the NOE difference experiment[12] where a specific nucleus is irradiated and the interacting nuclei are observed. This is possible because spin exchange from the nucleus affects the intensity of the observed signal from the other nucleus[13]. On the spectrum, the irradiated nucleus is represented by a negative peak while the nuclei to which it is coupled will have positive peaks or negative peaks. Proton pairs not experiencing a dipolar interaction will not have any peaks[13]. The NOE enhancement for two spins in the steady state is shown below[13].

$$\frac{M_H(\text{irrad})}{M_H^{\circ}} = 1 + \frac{6J_2(2\omega_H) - J_o(0)}{J_o(0) + 3J_1(\omega_H) + 6J_2(2\omega_H)} = 1 + \eta_{HH} \qquad (1)$$

η = NOE enhancement factor
J = spectral density
M = magnetization

Two-Dimensional NMR:

Experiments used for this project utilized either spin-spin or dipolar spin exchange. Two-dimensional experiments relying on spin-spin coupling were homonuclear correlated spectroscopy (COSY)[14,15], HMQC (^{1}H detected multiple-bond heteronuclear multiple quantum correlation)[16,17] and HMBC (^{1}H detected multiple-bond heteronuclear multiple quantum correlation)[17,18]. Experiments using exchange through dipolar

interactions were homonuclear NOE spectroscopy (NOESY)[13] and heteronuclear NOE spectroscopy (HOESY)[19,20,21].

The basic pulse sequence for a homonuclear two-dimensional experiment, shown below, is helpful for describing the NOESY and COSY experiments used.

$$P_1(\phi) - t_1 - P_2(\phi) - t_2 \text{ (acquisition)} \qquad (2)$$

For the COSY experiment, the first pulse (P_1) creates transverse magnetization which evolves due to chemical shift, T_2 relaxation and spin-spin coupling (coherent transfer) during the evolution time, t_1[17,22]. The result of the magnetization transfer for the COSY experiment is cross peaks representing scalar coupled protons on the COSY spectrum[7,8]. A COSY spectrum has proton spectra on both axes and on the diagonal. A cross peak is an off-diagonal peak at the intersection of the chemical shifts of the coupled protons.

Heteronuclear two-dimensional experiments are more complicated and involve spin exchange between nuclei of different elements. The HMQC experiment uses single quantum coherence to relate carbons to directly attached protons. One bond connectivities are favoured by adjusting the delay time in the pulse sequence for J_{CH} to 130-140 Hz. By doing this, interactions with smaller coupling constants will not be observed[23].

The HMBC experiment uses zero and double quantum coherences with a low pass J filter to emphasize long range coupling[24]. The J filter, to suppress the direct coupling, involves an additional time delay added at the beginning of the pulse sequence to allow the magnetization of the proton coupled to the heteronucleus to dephase. The added time

delay is based on the $^1J_{CH}$ coupling constant ($\frac{1}{2}(^1J_{CH})$ for simple experiments)[23,24]. Since direct one bond coupling constants are larger than long distance coupling constants a short time delay only allows long distance couplings to be observed[23].

The next set of experiments are based on the nuclear Overhauser effect. The NOESY[13] relates dipolar interacting protons and the HOESY[19,20,21] relates carbons and protons. Cross-relaxation between protons in the NOESY experiment and between carbons and protons in the HOESY experiment occurs during the mixing time[23], t_2 in equation (2). The intensity of the cross peaks in both experiments depends on the correlation and mixing times[22]. For the NOESY experiment, the intensity of the cross peak at τ_m is determined by

$$I_{AB}(\tau_m) = I_{BA}(\tau_m) = -\frac{M_o}{2}\frac{W_2^{AB} - W_o^{AB}}{|W_2^{AB} - W_o^{AB}|}[1 - e^{-R_c\tau_m}]\, e^{-R_L\tau_m} \qquad (3)$$

where R_c is the cross-relaxation rate, R_L is the other relevant T_1 rates, W_2 is double quantum transition probability and W_o is zero quantum transition probability[25].

In the slow motion limit, which is relevant to this study, the cross-peak intensity[25] may be simplified to

$$I_{AB}(\tau_m) = I_{BA}(\tau_m) = \frac{M_o}{2}[1 - \exp\{-2q_{AB}\tau_c\tau_m\}]\exp\{-R_1^{ext}\tau_m\} \qquad (4)$$

where $q_{AB} = \frac{1}{10}\gamma_A^2\gamma_B^2\hbar^2 r_{AB}^{-6}[\frac{\mu_o}{4\pi}]^2$, $R_L = R_1^{ext}$ and τ_c is the correlation time. With the initial rate approximation, the equation[25] further simplifies to

$$I_{AB}(\tau_m) \approx M_o q_{AB}\tau_c\tau_m(1 - R_1^{ext}\tau_m) \qquad (5)$$

PART ONE: MODEL COMPOUNDS

INTRODUCTION:

Lignin models contain functional groups, linkages and side chains believed to be present in the macromolecule. NMR spectra of lignin are very complicated due to the large number of nuclei present and the similarity of structural units. These spectra are further complicated by broad lines due to the 'polymeric nature of lignin'[26]. Solutions of smaller molecular weight model compounds do not have this problem and have well defined peaks. Since the spectra of model compounds are simple, they have played an important role in the structural studies of lignin.

The most common lignin models used for NMR studies so far have been monomers and dimers[9,10,27]. Several studies of trimers have appeared recently[28,29]. It is important to advance toward larger models because each new aromatic ring or side chain changes the environment of other rings or chains. This is especially true for NMR spectroscopy where the chemical shift of a nucleus may be perturbed by molecular structure. Also, larger model compounds more accurately represent lignin.

NMR spectroscopy was used in this study to characterize a model lignin trimer. Side chains were examined first using proton and COSY experiments followed by a 2D heteronuclear experiment to determine carbon-13 shifts. From here, aromatic protons were assigned based on their relationships to side chains as established by long-range 2D and NOE experiments. Among the difficulties encountered in establishing aromatic

proton chemical shifts was the change in the observed peak position due to the magnetic field strength in the tightly coupled aromatic region of the proton spectrum. Assignment of both the aliphatic and aromatic protons for the lignin model compound in this study allowed conformation about rotatable bonds to be identified.

Model Compound:

Acetoguaiacyl-dehydrodi-isoeugenol methyl ether or IIB is a model compound of lignin consisting of three aromatic rings joined together by different linkages. There is a vinylic side chain, four methoxyl groups and a carbonyl group. Figure 4 is a picture of IIB with nomenclature.

There are 19 different proton and 30 different carbon peaks expected. Of these, 7 protons and 7 carbons are aliphatic, one carbon is carbonyl, 4 protons and 4 carbons are methoxyl, 8 protons and 18 carbons are aromatic. The multiplicity expected for each proton signal was determined using the $m = 2nI + 1$ rule where

m = multiplicity
n = number of equivalent neighbour nuclei
I = spin, ½ for proton[8]

Multiplicities expected for IIB are listed in Table 2. For the most part, these were observed on the experimentally obtained proton spectrum except for protons 2 and 6 on rings A and B and any interactions with small coupling constants of approximately 2.0 Hz. It is useful to compare the experimentally observed signals with the expected signals to confirm assignments.

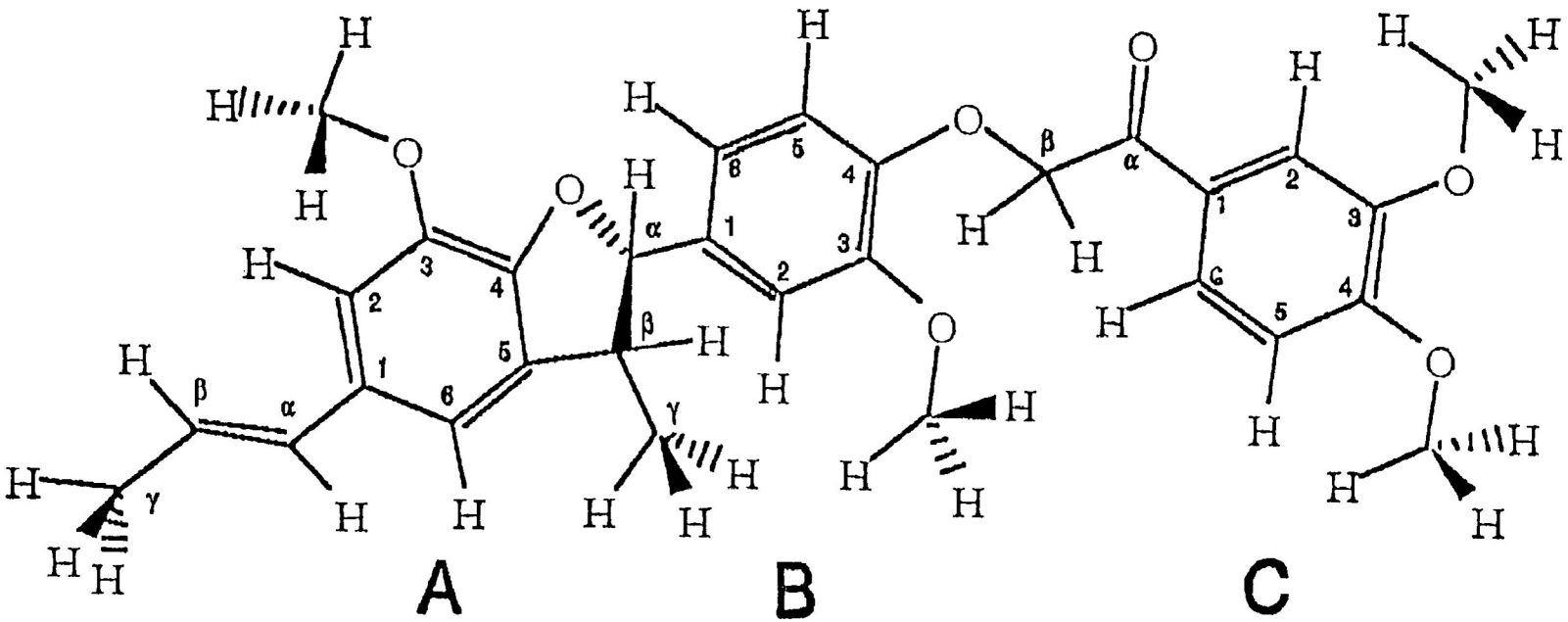

Figure 4 **Acetoguaiacyl-dehydrodi-isoeugenol methyl ether (IIB) with nomenclature**

Proton	Expected Multiplicity	Reasoning
γA	two doublets	$^3J_{\gamma A-\beta A'}$, $^4J_{\gamma A-\alpha A}$
βA	two quartets	$^3J_{\beta A-\gamma A'}$, $^3J_{\beta A-\alpha A}$
αA	two quartets	$^3J_{\alpha A-\beta A'}$, $^4J_{\alpha A-\gamma A}$
2A, 6A	doublet	*meta* coupling
γB	doublet	$^3J_{\gamma B-\beta B}$
βB	two quartets	$^3J_{\beta B-\alpha B'}$, $^3J_{\beta B-\gamma B}$
αB	doublet	$^3J_{\alpha B-\beta B}$
2B	two doublets	*meta* and *para* coupling
5B	two doublets	*ortho* and *para* coupling
6B	two doublets	*ortho* and *meta* coupling
βC	singlet	
2C	two doublets	*meta* and *para* coupling
5C	two doublets	*ortho* and *para* coupling
6C	two doublets	*ortho* and *meta* coupling

Table 2 Expected multiplicities for IIB[8]

RESULTS AND DISCUSSION:

Side Chains:

The side chains were assigned first. Coupling constants, multiplicity and chemical shifts from the proton spectrum were used to determine which protons were on the same side chain. Analysis of the COSY crosspeaks confirmed assignments. The methoxyl protons were not assigned at this point. Figure 5 shows the 500 MHz proton spectrum between 1.3 and 6.5 ppm along with integration values and Figure 6 is the COSY spectrum with side chain connectivities. As can be seen in Figure 5 and in Table 3 the chemical shifts at 6.35, 6.10 and 1.86 ppm have coupling constants in common which means these protons are most likely coupled. The COSY spectrum in Figure 6 confirms these coupling relationships. This set of protons is on side chain A (see Table 3 for assignments). Configuration about the double bond on side chain A (refer to Figure 4) was determined from the magnitude of the coupling constant at 6.35 and 6.10 ppm. According to the literature[8,30,31], the large coupling constant of 15.7 Hz indicates a *trans* configuration about the double bond. Side chain B was assigned in the same way as side chain A. Again, the coupling constants for the protons (5.10, 3.44, 1.37 ppm) were similar (Figure 5 or Table 3) and the connectivities were clear on the COSY spectrum.

The methylene protons on side chain C have a chemical shift of 5.28 ppm. They were the only protons with a singlet peak in the aliphatic region of the proton spectrum and no cross peaks on the COSY spectrum.

The assignments for the carbon shifts were obtained from the HMQC experiment (Table 4). A decoupled carbon-13 spectrum is shown in Figure 7.

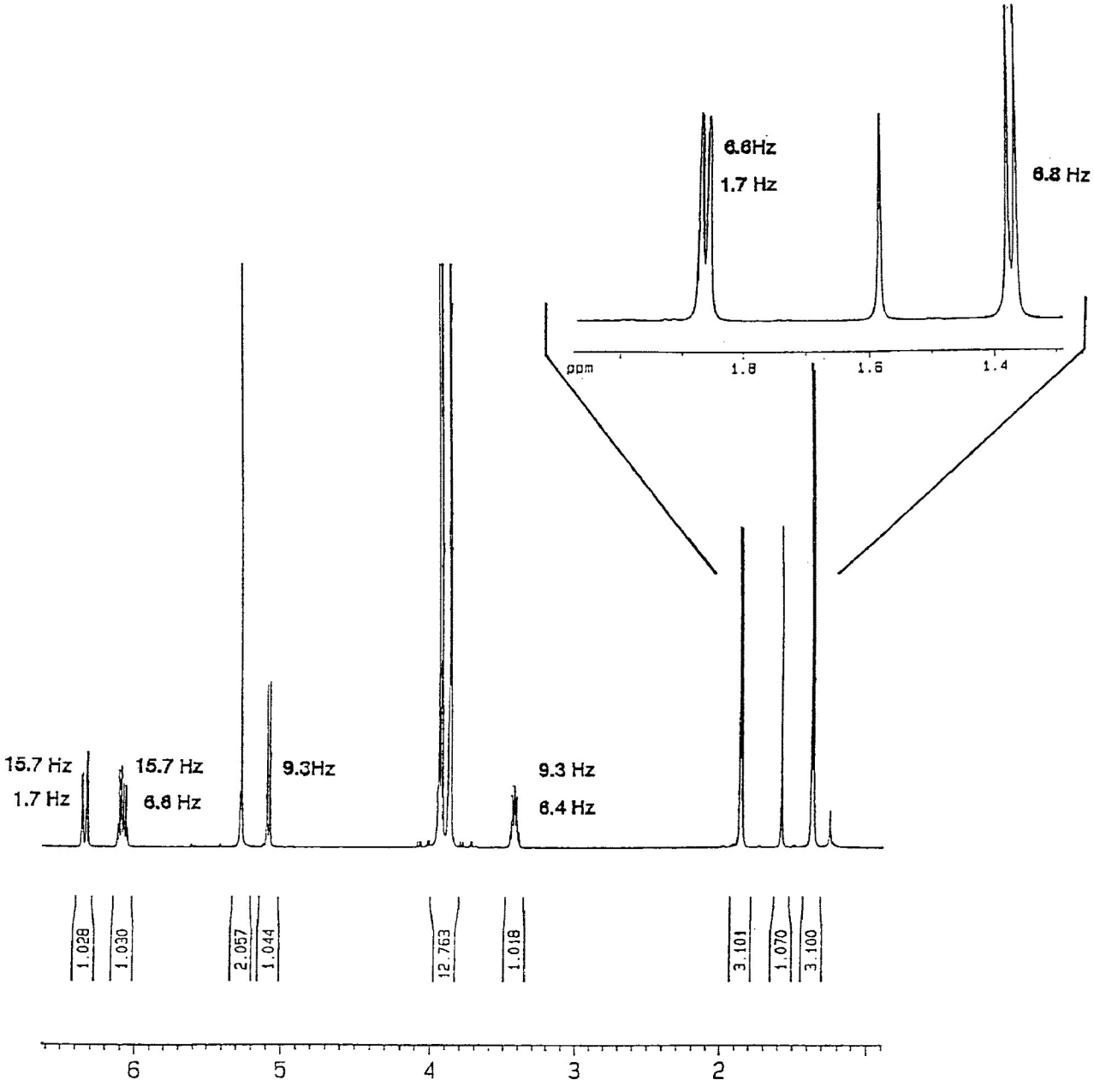

Figure 5 Aliphatic region on 500 MHz proton spectrum with coupling constants

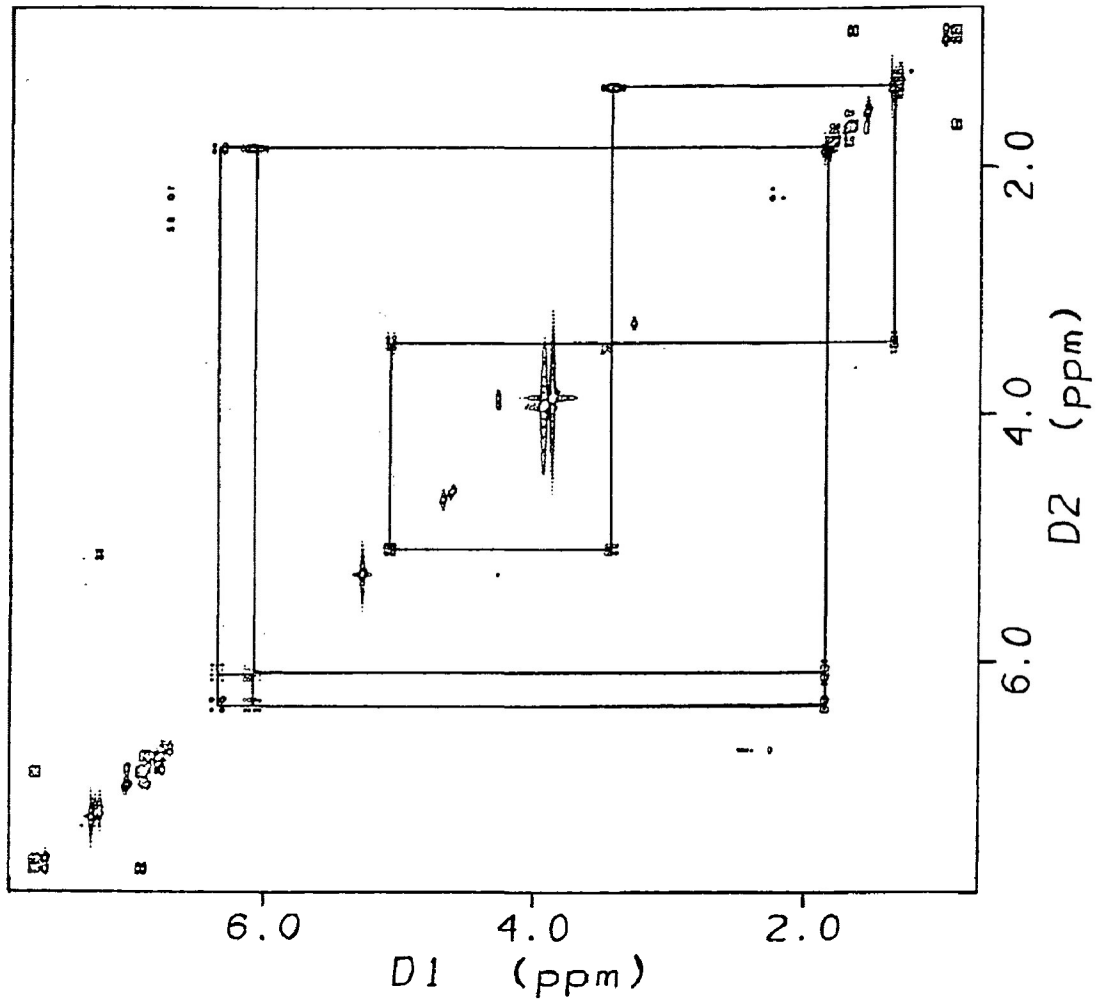

Figure 6 200 MHz COSY (Correlated Spectroscopy) with side chain connectivities

	PROTON (ppm)	CARBON-13 (ppm)	$^{1}J_{C-H}$ (Hz)	$^{3}J_{H-H}$ (Hz)		$^{4}J_{H-H}$ (Hz)	
6A	6.75	113.3					
5A		133.1					
4A		146.5					
3A		144.1					
2A	6.78	109.3	151.4				
1A		132.2					
γA	1.86	18.3	125.7	6.6	βA	1.7	αA
βA	6.10	123.5	153.8	15.7	αA		
				6.6	γA		
αA	6.35	130.9	148.9	15.7	βA	1.7	γA
OMe3A	3.89						
6B	6.88	119.0	157.4	8.2	5B	2.0	2B
5B	6.79	114.1	158.7	8.2	6B		
4B		147.6					
3B		149.8					
2B	7.00	110.3	158.7			2.0	6B
1B		134.2					
γB	1.37	17.7	127.0	6.8	βB		
βB	3.44	45.5	130.8	9.3	αB		
				6.6	γB		
αB	5.10	93.4	150.1	9.3	βB		
OMe3B	3.87						
6C	7.67	122.8	162.2	8.4	5C	2.0	2C
5C	6.90	110.2	161.1	8.5	6C		
4C		153.8					
3C		149.2					
2C	7.59	110.5	159.9	2.0	6C		
1C		127.8					
βC	5.28	72.0	143.8				
αC		193.1					
OMe3C	3.93						
OMe4C	3.95						

Table 3 Chemical shifts and coupling constants measured from 500 MHz proton spectrum and 200 MHz coupled carbon-13 spectrum

HMQC (ppm)		HOESY (ppm)		HMBC (ppm)	
7.67-122.8	6C	7.67-193.1	6C-αC	7.67-193.1	6C-αC
7.59-110.5	2C	7.67-127.8	6C-1C	7.67-153.8	6C-4C
7.00-110.3	2B	7.67-122.8	6C-6C	7.67-110.5	6C-2C
6.90-110.2	5C	7.59-193.1	2C-αC	7.59-193.1	2C-αC
6.88-119.0	6B	7.59-149.2	2C-3C	7.59-153.8	2C-4C
6.79-114.1	5B	7.59-127.8	2C-1C	7.59-149.2	2C-3C
6.78-109.3	2A	7.59-122.8	2C-6C	7.59-127.8	2C-1C
6.75-113.3	6A	7.59-110.5	2C-2C	7.59-122.8	2C-6C
6.35-130.9	αA	7.00-149.8	2B-3B	7.00-149.8	2B-3B
6.10-123.5	βA	7.00-134.2	2B-1B	7.00-147.6	2B-4B
5.28-72.0	βC	7.00-110.3	2B-2B	7.00-134.2	2B-1B
5.10-93.4	αB	6.89-110.2	5C-5C	7.00-119.0	2B-6B
3.44-45.5	βB	6.88-134.2	6B-1B	7.00-93.4	2B-αB
1.86-18.3	γA	6.79-147.6	5B-4B	6.90-153.8	5C-4C
1.37-17.1	γB	6.79-114.1	5B-5B	6.90-149.2	5C-3C
		6.78-144.1	2A-3A	6.90-127.8	5C-1C
		6.78-109.3	2A-2A	6.88-147.6	6B-4B
		6.75-133.1	6A-5A	6.88-110.3	6B-2B
		6.75-132.2	6A-1A	6.88-93.4	6B-αB
		6.75-123.5	6A-βA	6.79-149.8	5B-3B
		6.75-113.3	6A-6A	6.79-134.2	5B-1B
		6.35-130.9	αA-αA	6.78-146.5	2A-4A
		6.10-123.5	βA-βA	6.78-144.1	2A-3A
		5.28-193.1	βC-αC	6.78-130.9	2A-αA
		5.28-72.0	βC-βC	6.78-113.3	2A-6A
		5.10-134.2	αB-1B	6.75-146.5	6A-4A
		5.10-93.4	αB-αB	6.75-130.9	6A-αA
		3.95-110.2	OMe4C-5C	6.75-109.3	6A-2A
		3.93-110.5	OMe3C-2C	6.75-45.5	6A-βB
		3.89-109.3	OMe3A-2A	6.35-113.3	αA-6A
		3.87-110.3	OMe3B-2B	6.35-109.3	αA-2A
		3.44-133.1	βB-5A	6.35-18.3	αA-γA
		3.44-45.5	βB-βB	6.10-132.2	βA-1A
		1.86-18.3	γA-γA	6.10-18.3	βA-γA
		1.37-17.7	γB-γB	5.28-193.1	βC-αC
				5.28-147.6	βC-4B
				5.10-134.2	αB-1B
				5.10-119.0	αB-6B
				5.10-110.3	αB-2B
				3.95-153.8	OMe4C-4C
				3.93-149.2	OMe3C-3C
				3.89-144.1	OMe3A-3A
				3.87-149.8	OMe3B-3B
				3.44-146.5	βB-4A
				3.44-133.1	βB-5A
				3.44-113.3	βB-6A
				3.44-93.4	βB-αB

Table 4 Peak assignments from the 500 MHz HMQC, HOESY and HMBC experiments

Table 4 continued

HMBC (ppm)	
3.44-17.7	αB-γB
1.86-130.9	γA-αA
1.86-123.5	γA-βA
1.37-133.1	γB-5A
1.37-93.4	γB-αB
1.37-45.5	γB-βB

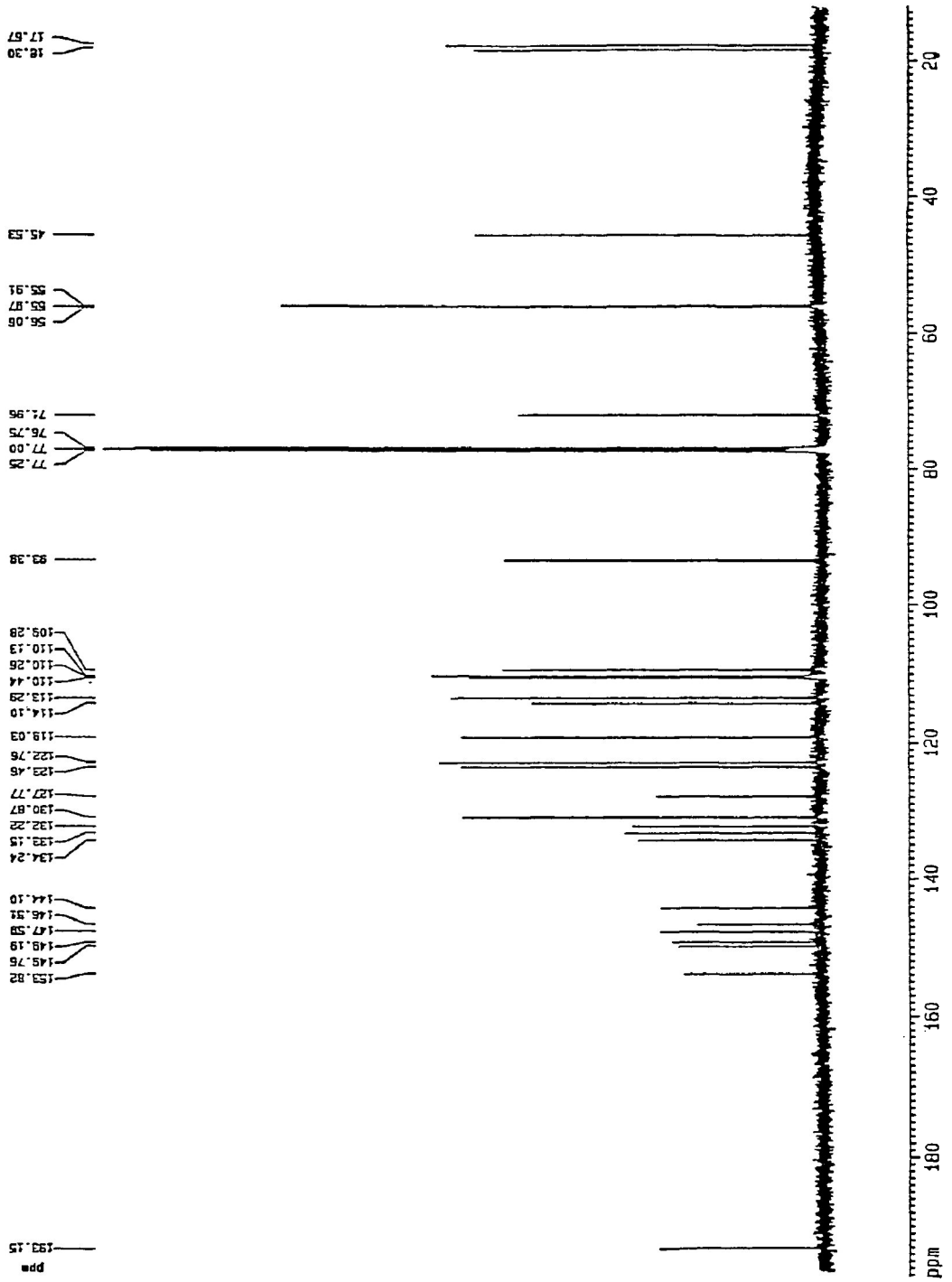

Figure 7 500 MHz decoupled carbon-13 spectrum of IIB

The assignment of the aliphatic protons was straightforward because of the well resolved peaks and extensive literature available[9-11,26-32].

Aromatics:

The first step in aromatic proton analysis was to determine multiplets from the overlapping peaks in the aromatic region. The peaks on the proton spectrum (Figure 8) at 7.67 (two doublets), 7.59 (doublet) and 7.00 (doublet) ppm were isolated from other peaks (no overlap) and the integration values indicated each multiplet belonged to a single proton. The remaining aromatic proton peaks between 6.75 and 6.95 ppm were overlapped and therefore not readily distinguishable. Integration of the region indicated five types of protons were in this region. Coupling constant and peak shape analysis along with Gaussian and Lorentzian linebroadening allowed the region to be resolved into five signals as seen in Figure 8. Confirmation of the multiplets came from the HMQC experiment where multiplets were visible so it was clear which peaks were coupled (Figure 9).

Next, COSY data (Table 5) and coupling constants (Table 3) determined which protons belonged on the same ring. From this data peaks centered at 7.67, 7.59 and 6.90 ppm were on the same ring and protons with shifts 7.00, 6.88 and 6.79 ppm were also together.

Protons were assigned to rings using a variety of long-range and nuclear Overhauser enhancement experiments. Consider the protons with chemical shifts of 7.67, 7.59 and 6.90 ppm. HMBC data (Table 4) showed connections from the carbonyl carbon (193.1 ppm) to 7.67 and 7.59 ppm. NOESY (Table 5) and NOE difference spectra (Figure 10

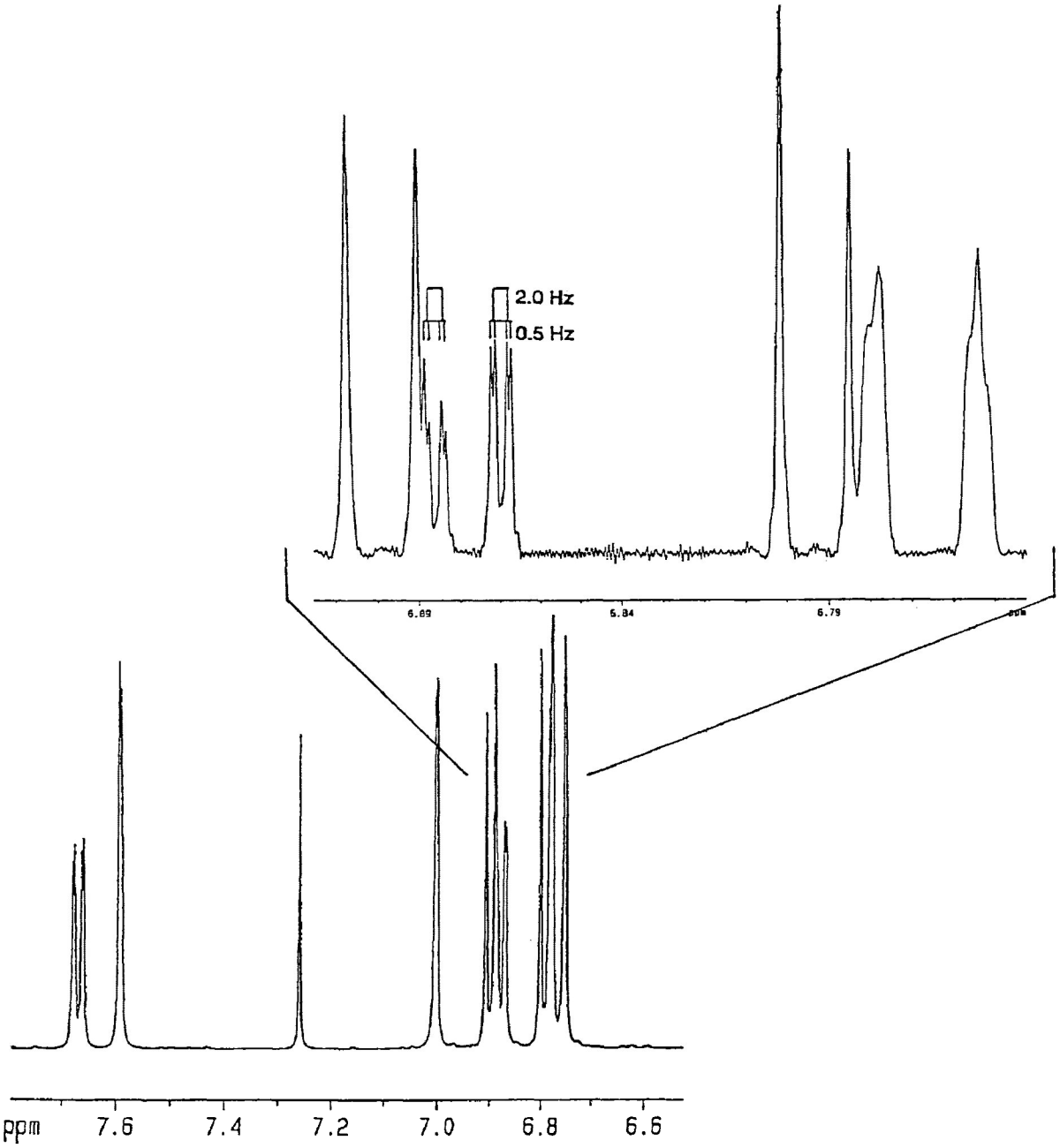

Figure 8 Aromatic region on 500 MHz proton spectrum

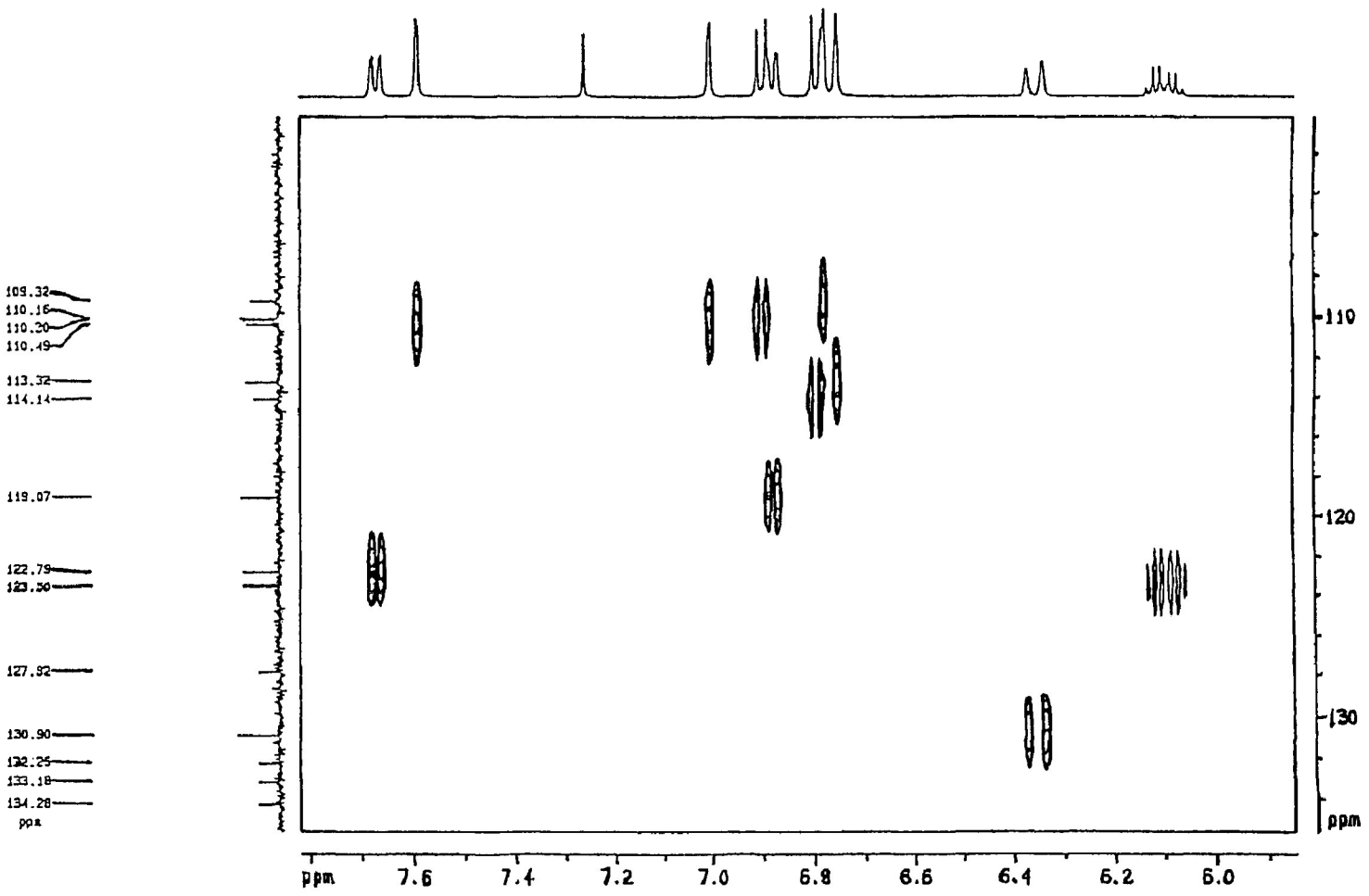

Figure 9 Aromatic and vinylic regions on the 500 MHz HMQC spectrum

COSY (ppm)		NOESY (ppm)	
7.67-7.59	6C-2C	7.67-7.59	6C-2C
7.67-6.90	6C-5C	7.67-6.90	6C-5C
7.00-6.90	2B-6B	7.67-5.28	6C-βC
7.00-6.79	2B-5B	7.59-6.90	2C-5C
6.88-6.79	6B-5B	7.59-5.28	2C-βC
6.78-6.75	2A-6A	7.59-3.93	2C-OMe3C
6.35-6.10	αA-βA	7.00-6.88	2B-6B
6.35-1.86	αA-γA	7.00-5.28	2B-βC
6.10-1.86	βA-γA	7.00-5.10	αB-βB
5.10-3.44	αB-βB	7.00-3.87	2B-OMe3B
3.44-1.37	βB-γB	7.00-3.44	2B-βB
		6.90-5.28	5C-βC
		6.90-3.95	5C-OMe4C
		6.88-6.79	6B-5B
		6.88-5.28	6B-βC
		6.88-5.10	6B-αB
		6.79-5.28	5B-βC
		6.78-6.75	2A-6A
		6.78-5.10	2A-αB
		6.78-3.89	2A-OMe3A
		6.75-6.35	6A-αA
		6.75-6.10	6A-βA
		6.75-1.86	6A-γA
		6.75-1.37	6A-γB
		6.35-6.10	αA-βA
		6.35-1.86	αA-γA
		6.10-1.86	βA-γA
		5.10-3.44	αB-βB
		5.10-1.37	αB-γB
		3.44-1.37	βB-γB

Table 5 Peak assignments from 200 MHz COSY and 500 MHz NOESY spectra

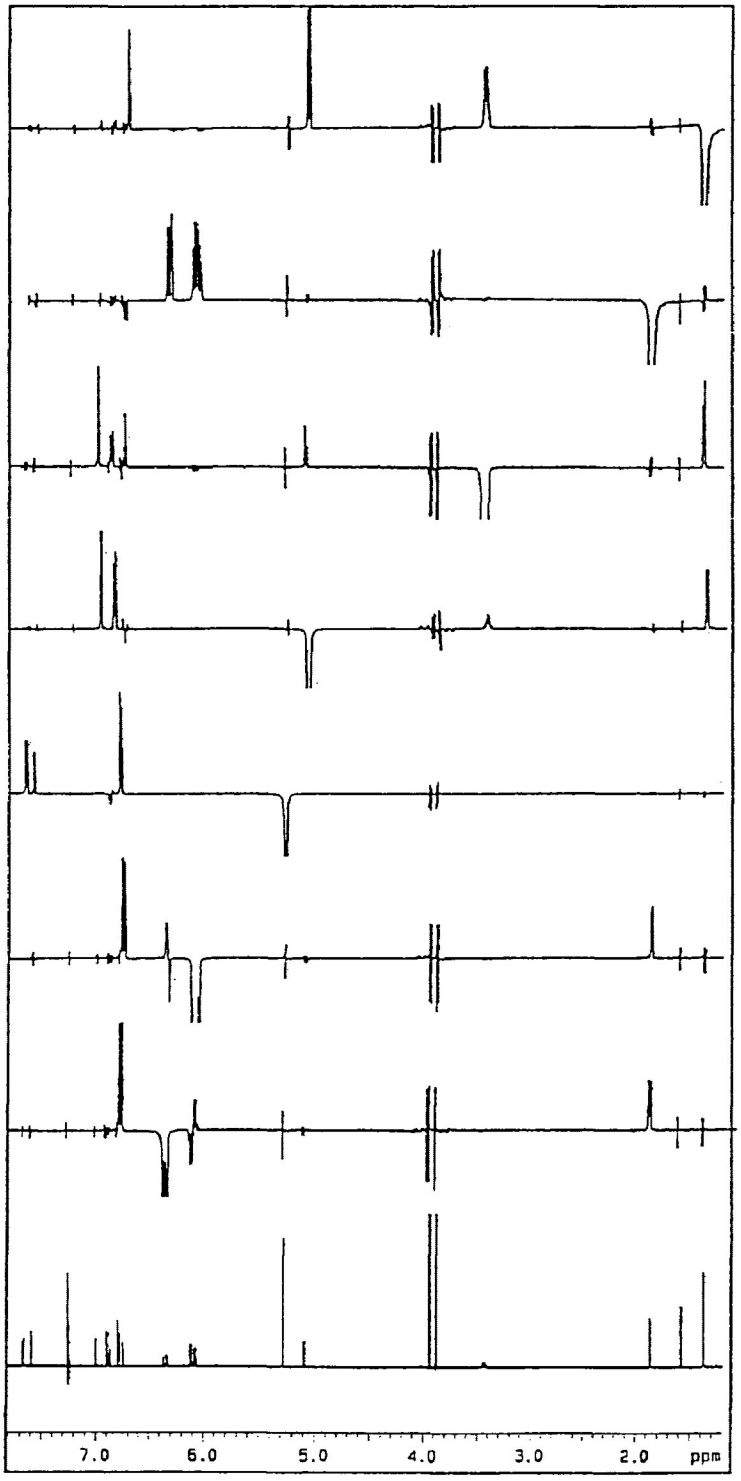

Figure 10 500 MHz NOE difference spectra

Irradiate		Observe		Integral	Distance
1.37	γB	3.44	βB	12.49	2.70
		5.10	αB	9.90	2.94
		6.75	6A	5.38	3.47(6A)
		6.78	2A		6.52(2A)
1.86	γA	6.10	βA	9.77	2.76
		6.35	αA	7.75	3.12
		6.75	6A	-0.99	5.42
3.44	βB	1.37	γB	4.64	2.70
		5.10	αB	1.96	3.02
		6.75	6A	1.96	3.04
		6.88	6B	2.64	3.30
		7.00	2B	4.33	3.49
3.87	OMe3B	6.78	2A	2.06	11.21
		7.00	2B	16.2	13.72
		7.59	2C	0.34	6.30
3.88	OMe3A	6.10	βA	-0.46	5.55
		6.35	αA	-0.50	6.94
		6.78	2A	12.41	3.86
		7.00	2B	2.56	7.19
		7.59	2C	0.19	11.08
3.93	OMe3C	6.90	5C	0.90	6.20
		7.00	2B	0.18	11.13
		7.59	2C	17.77	2.76
3.95	OMe4C	6.90	5C	14.31	2.75
		7.59	2C	1.13	6.20
		7.67	6C	-0.85	5.10
5.10	αB	1.37	γB	3.53	2.94
		3.44	βB	1.98	3.02
		6.88	6B	6.59	3.74
		7.00	2B	4.75	2.42
5.28	βC	6.79	5B	6.80	2.63
		6.88	6B	-0.66	5.06
		7.59	2C	2.29	4.40
		7.67	6C	6.37	2.47
6.10	βA	1.86	γA	6.48	2.76
		6.35	αA	3.03, -3.52	3.10
		6.75	6A	13.93	3.77(6A)
		6.78	2A		1.83(2A)
6.35	αA	1.86	γA	5.16	3.12
		6.10	βA	-0.55	3.10
		6.75	6A	12.05	5.42(6A)
		6.78	2A		4.44(2A)

Table 6 Assignments and internuclear distances obtained from 500 MHz NOE difference spectra and MOPAC program

and Table 6) both had peaks from $H_{\beta C}$ (5.28 ppm) to 7.67 and 7.59 ppm. The carbonyl carbon is adjacent to ring C therefore peaks at 7.67, 7.59 and 6.90 ppm are most likely on ring C. The positions of the ring protons were then deduced from coupling constants and confirmed by long-range experiments. Coupling between protons 7.67 and 6.90 ppm was larger (8.5 Hz) than the 2.0 Hz coupling between protons at 7.67 and 7.59 ppm (Table 3). No coupling was observed between 7.59 and 6.90 ppm. HMBC experiment detected coupling between the carbonyl carbon at 193.1 ppm and the protons at 7.67 and 7.59 but not to the proton at 6.90 ppm. Also there was no COSY peak at 7.59-6.90 ppm. From this evidence, 7.67 must be *ortho* to 6.90 and *meta* to 7.59 ppm. 6.90 must be *para* to 7.59 ppm. In conclusion, the ring C protons are 7.67 ppm is 6C, 7.59 ppm is 2C and 6.90 ppm is 5C. The same procedure for assigning ring C was used to assign rings A and B.

Carbon-13 chemical shifts were determined using two-dimensional heteronuclear experiments (HOESY and HMBC) with comparison to chemical shifts from lignin models reported in articles by Nimz[11] and Kringstad and Mörck[9,10].

Similarities in chemical shifts for certain ring positions were evident when IIB was compared to other model compounds[1,29,32] with similar side chain structures and ring substitution. Figure 11 shows the models which were compared and Table 7 lists the chemical shifts of interest. Rings with an adjacent carbonyl group consistently had chemical shifts between 7.5 and 7.85 ppm for protons at ring positions 2 and 6. The proton on the same ring at position 5 had a chemical shift of 6.90 ppm. For rings with a

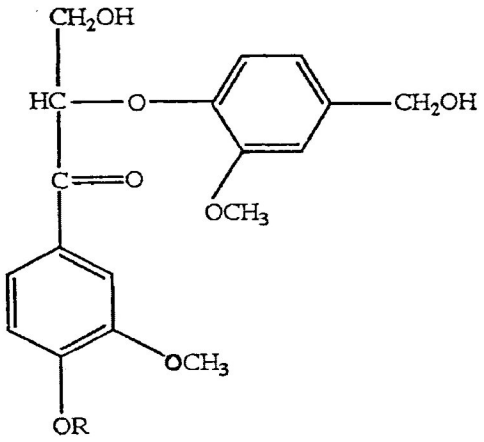

1

R = CH_3

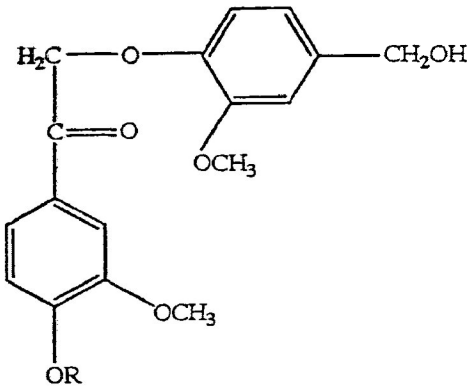

2

R = CH_3

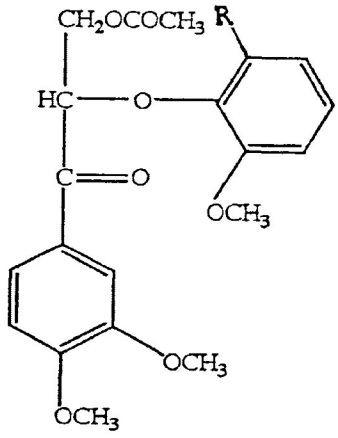

3

R = H, OCH_3

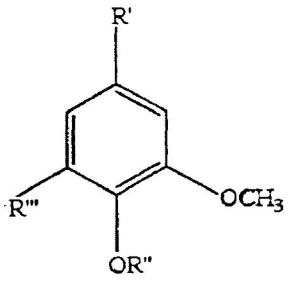

4

R' = R-CO-
R'' = H, CH_3
R''' = H

Figure 11 Models similar in structure to IIB[1,29,32]

Model	Chemical Shift (ring position) (ppm)		
Ring with α-C=O:			
IIB	7.59(2)	6.90(5)	7.67(6)
1	7.52(2)	6.92(5)	7.52(6)
2a, 2b	7.60(2)	6.90, 6.91(5)	7.58, 7.68(6)
3a, 3b	7.62, 7.63(2)	6.90(5)	7.76, 7.67(6)
4	7.68(2)	6.90(5)	7.85(6)
Ring with adjacent ether linkage:			
IIB	7.00(2)	6.79(5)	
2a, 2b	6.97, 6.95(2)	6.78, 6.79(5)	
3a, 3b	6.96, 6.94(2)	6.84, 6.82(5)	

Table 7 Chemical shifts for models similar in structure to IIB[1,29,32]

4-O-ether linkage (see Figure 11), the proton at position 2 had a chemical shift between 6.95 and 7.00 ppm and proton at position 5 had a chemical shift between 6.78 and 6.84 ppm. The chemical shifts appear to be consistent for each ring position even though the models change in size from a monomer to a trimer indicating that a trimer is not a large enough model for conformation to have an effect on chemical shifts.

Coupling constants calculated for IIB and monomer model number 4[29] (Figure 11) were also similar. The *ortho* coupling constant for IIB for positions 5 and 6 was 8.4 Hz (Table 3) and the *meta* coupling constant for positions 2 and 6 was 2.0 Hz. Both values agreed well with the monomer model which had an *ortho* coupling constant of 8.5 Hz and a *meta* coupling constant of 2.1 Hz[1].

Methoxyl Protons:

The peaks on the proton spectrum corresponding to the methoxyl protons consisted of four peaks of equal height. Since the methoxyl groups were not close enough to other protons for scalar coupling, there was no multiplicity. These factors combined with a small chemical shift range of 0.08 ppm made it difficult to distinguish among the four groups.

Experiments relying on long range interactions were necessary to assign the methoxyl protons. The HMBC spectrum was used to identify coupling between the methoxyl proton and the methoxyl substituted ring carbon. For example, the methoxyl group at the 3 position on ring C (3.93 ppm) had a peak at 3.93-C_{3C} (149.2 ppm) on the HMBC spectrum. The HOESY spectrum had a peak at 3.93 ppm to the carbon at position 2 (110.5 ppm). This indicates that spacially the methoxyl proton is closer to the

unsubstituted carbon adjacent to the methoxyl substituted carbon. The NOESY spectrum confirms this and shows a connection between the proton at position 2 (7.59 ppm) and 3.93 ppm. Figure 12 shows the methoxyl regions of the long-range experiments. The one-dimensional NOE difference spectra and the large NOE value from the NOESY experiment between 3.93 ppm and position 2 confirmed the location of this methoxyl group (Figure 10 and Table 6).

200 MHz versus 500 MHz:

Magnetic field strength affects spectral resolution[33] and the observed position of peak multiplets. In Figure 13, a portion of the aromatic regions from the 200 MHz and 500 MHz spectra is displayed. It is apparent the resolution changes with an increase in field strength. The peaks on the 500 MHz spectrum are sharper and better defined than the peaks on the 200 MHz spectrum (compare the multiplets centred at 6.89 ppm). The top spectrum in Figure 13 shows a multiplet with four peaks. If we refer back to Figure 8 (top) the same multiplet has eight peaks on the 500 MHz spectrum. More information can be obtained from the 500 MHz spectrum for this particular multiplet because three coupling constants can be calculated versus two coupling constants on the 200 MHz spectrum.

The dependence of peak position on magnetic field strength is also visible in Figure 13. The multiplets representing protons 5C and 6B overlap on the 200 MHz spectrum whereas the same two multiplets are side by side on the 500 MHz spectrum. Also, multiplets representing 5B, 2A and 6A are overlapped on the 200 MHz spectrum but not on the 500 MHz spectrum. A higher field results in a greater frequency difference

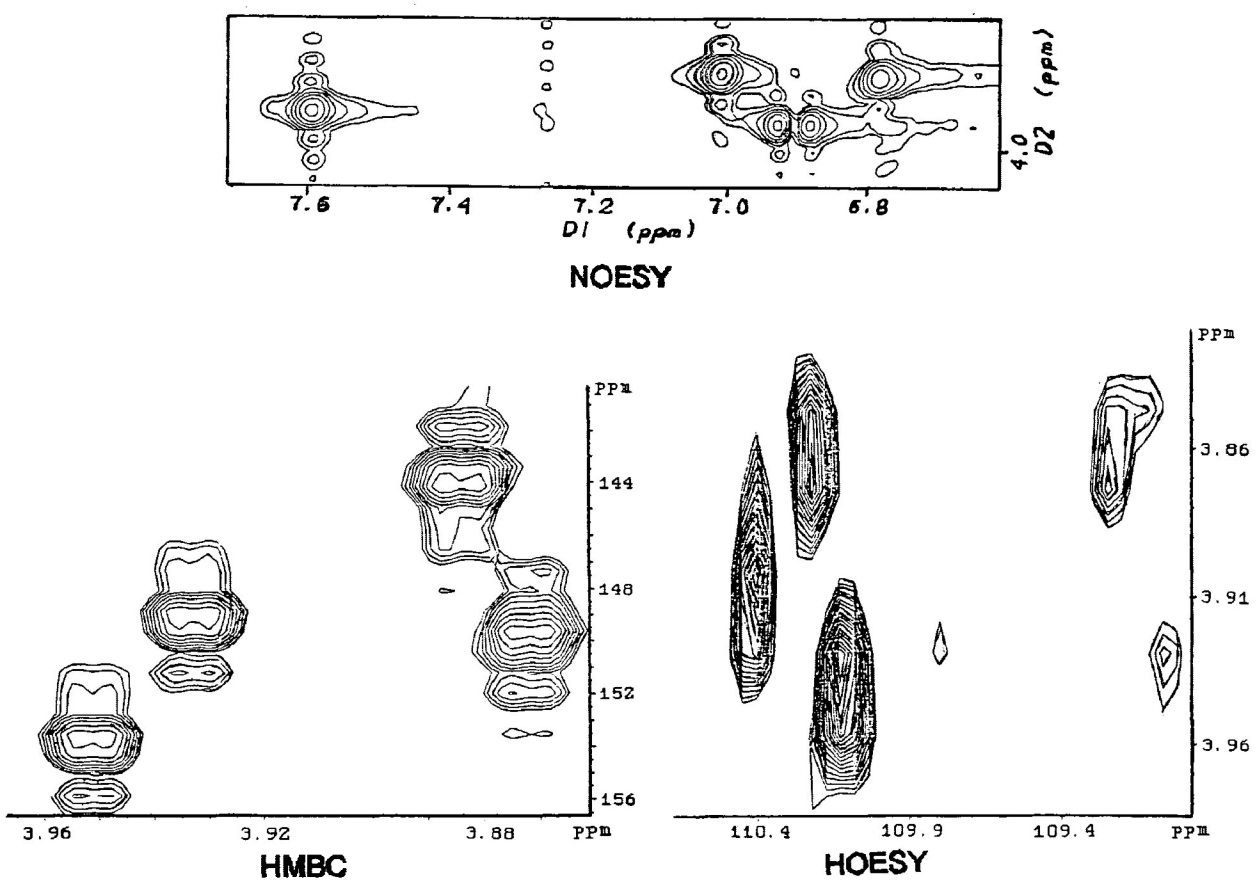

Figure 12 Methoxyl regions on various two-dimensional spectra

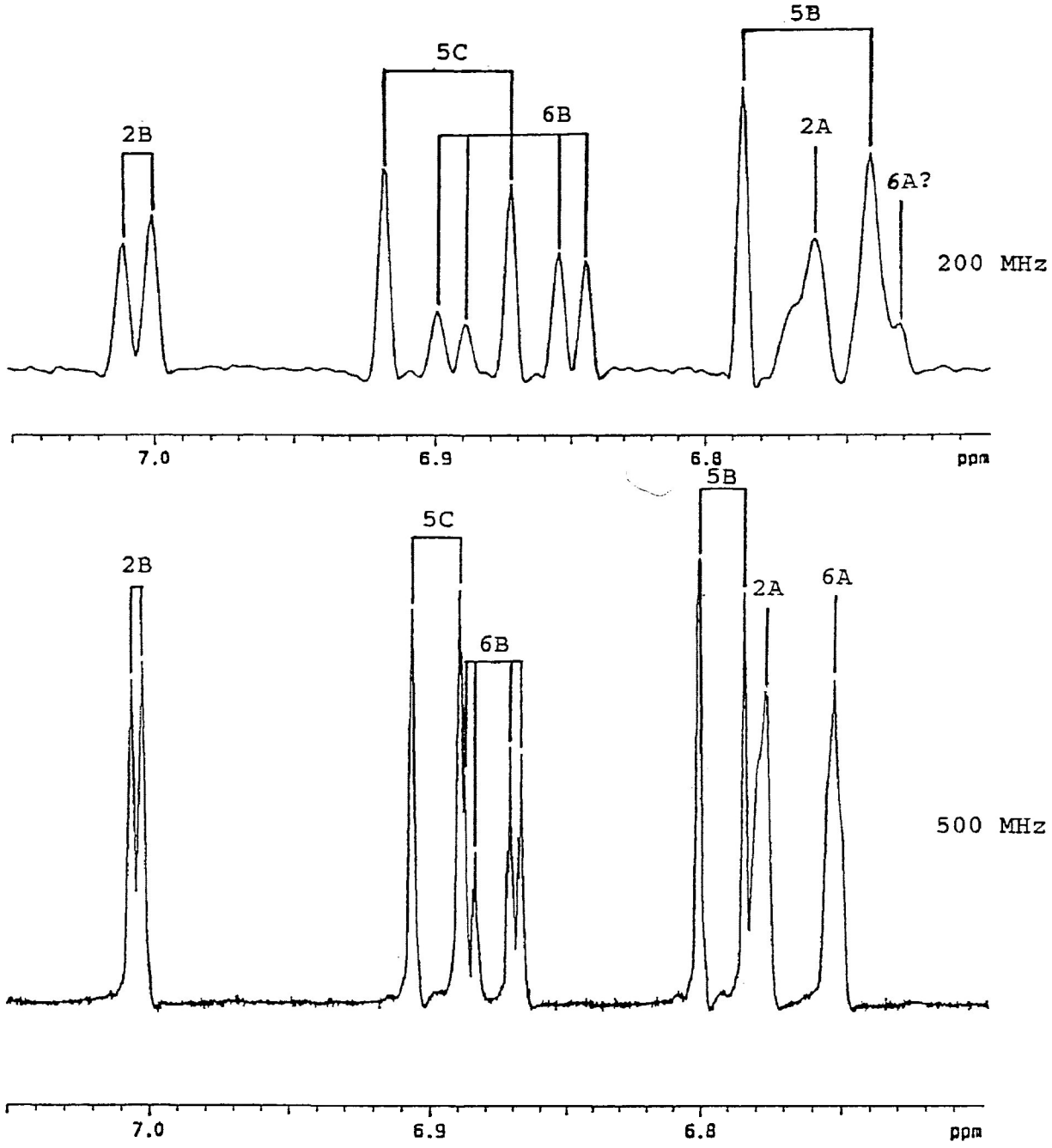

Figure 13 Chemical shift dependence on magnetic field strength 200 MHz versus 500 MHz

between groups of peaks which simplifies spin systems[34,35]. For IIB, the frequency difference between peaks for 2B and 6B is 0.12 ppm or 24 Hz on the 200 MHz spectrum and 61 Hz on the 500 MHz spectrum. This means in the tightly coupled aromatic region between 6.75 and 6.95 ppm the system is exhibiting more AB character on the 200 MHz spectrum and more AX character on the 500 MHz spectrum.

NOE and Conformation:

Nuclear Overhauser effect or NOE experiments are an effective way to evaluate spacial aspects of chemical structure[32]. For this project NOEs were used to determine the importance of different conformations as well as confirm chemical shift assignments.

Experiments used for conformational purposes were the 1-D NOE difference, 2-D NOESY and HOESY experiments. Steady-state NOE is obtained from the NOE difference experiment whereas NOEs from NOESY experiments are measured by transient effects[13,33]. Internuclear distances obtained from the 1-D experiment rely on the observation that rate of spin exchange through dipolar interactions is proportional to the inverse sixth power of the distance between dipolar coupled nuclei. Distances from NOESY experiments may be calculated from the initial buildup rates of the NOE[13,33].

The model compound IIB (Figure 4) can adopt different conformations due to rotatable bonds such as the single bonds of side chains A, B and C. Side chain A has a single bond between the α-position and ring A. NOEs from the NOE difference (Table 6) and NOESY experiments are similar in magnitude from side chain protons $H_{\alpha A}$ and $H_{\beta A}$ to the ring protons H_{2A} and H_{6A}. This implies that the C_1-C_α bond is free to rotate and

the side chain spends an equal amount of time in each position. For side chain B the distance (Table 6) calculated by semi-empirical methods showed that $H_{\alpha B}$-H_{6B} are farther apart than $H_{\alpha B}$-H_{2B} indicating that the dominant conformation is with $H_{\alpha B}$ and H_{2B} close together. The larger integral value measured from the NOESY experiments (Table 8) for $H_{\alpha B}$-H_{2B} agrees with this computational result. Since $H_{\alpha B}$ and H_{2B} are 'close together' then there is probably minimal rotation about the αB-ring B bond. Protons $H_{\beta C}$ interact with protons H_{2C} and H_{6C}. The distance calculated using MOPAC between $H_{\beta C}$ and H_{6C} is approximately half the distance between $H_{\beta C}$ and H_{2C} indicating the ring is apparently turned so $H_{\beta C}$ and H_{6C} are in close contact. The integrals obtained from NOESY experiments and from the NOE difference experiments agree with this result (Table 6 and Table 8).

The methoxyl groups at ring position 3 appear to be oriented toward ring position 2 as evidenced by NOESY peaks (Table 5) between methoxyl protons and ring protons at position 2 and HOESY peaks (Table 4) between methoxyl protons and ring carbons at position 2 but not position 4. This orientation was found by Ede and Brunow[36] and is also supported by distances calculated using MOPAC (Figure 14).

NOESY Peak (ppm)	Mixing Time	Intensity 100 ms	200 ms	400ms
1.37-3.44	γB-βB	4.79	4.55	4.19
3.87-7.00	OMe3B-2B	1.98	3.58	6.39
3.89-6.78	OMe3A-2A	1.72	3.08	5.24
3.93-7.59	OMe3C-2C	1.84	3.19	5.70
3.95-6.90	OMe4C-5C	2.22	3.73	6.62
5.10-3.44	αB-βB	3.06	1.42	1.25
5.10-6.88	αB-6B	0.81	1.62	2.87
5.10-7.00	αB-2B	0.53	1.03	1.92
5.28-6.79	βC-5B	1.98	3.40	5.47
5.28-7.59	βC-2C	0.37	0.70	1.26
5.28-7.67	βC-6C	1.29	2.47	4.19
6.10-1.86	βA-γA	3.18	3.99	4.03
7.67-6.90	6C-5C	8.04	4.70	3.39

Table 8 NOESY initial rates from peak intensities

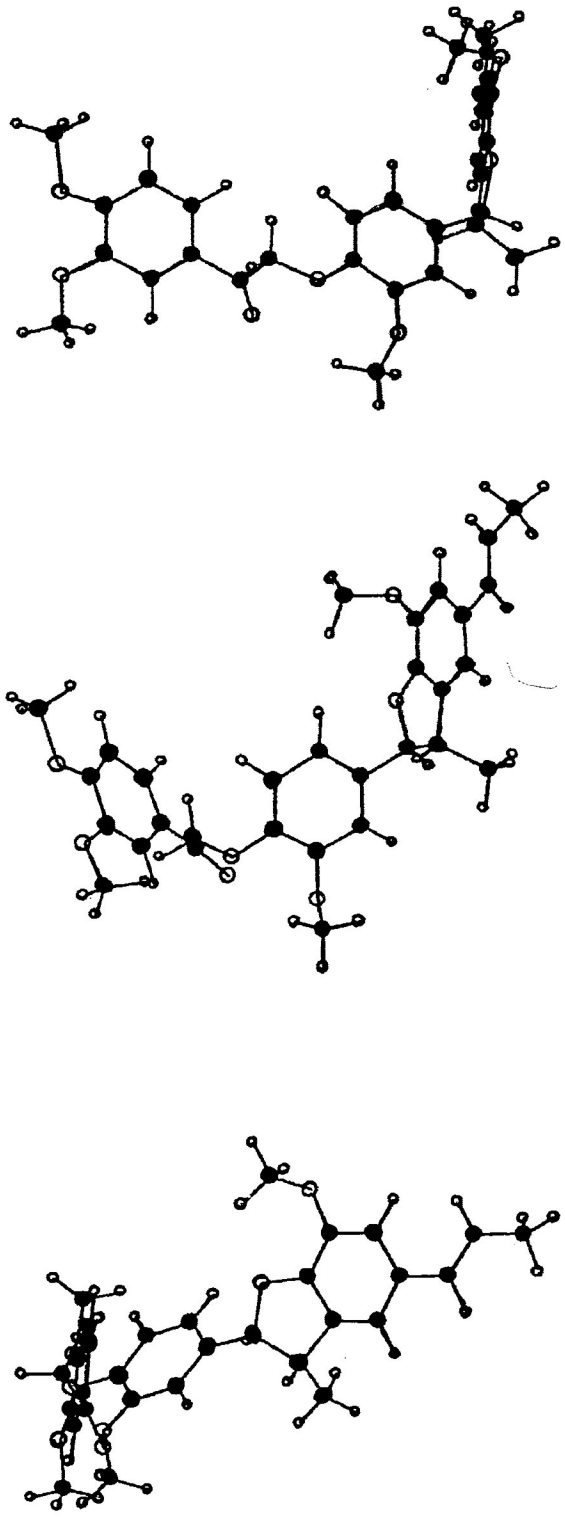

Figure 14 Three views of IIB showing conformation

PART TWO: EFFLUENTS

INTRODUCTION and BACKGROUND INFORMATION:

Hydrogen peroxide has proved effective in environmentally bleaching mechanical and chemimechanical pulps[37]. Hydrogen peroxide reacts primarily through nucleophilic attack of the hydroperoxyl anion on the carbonyl carbons on unetherified phenolic units in mechanical pulps[38,39,40]. The chromophoric groups in mechanical pulps primarily quinones, phenolic alpha-carbonyl and cinnamaldehyde units are altered but not removed by peroxide bleaching[4]. These chromophores decrease pulp brightness, increase yellowness and reduce the photostability of pulps if they are left unchanged[37]. Peroxide treatment of chemimechanical pulps results in lignin removal[37].

It is important to know the structures of the wood components before and after peroxide bleaching to gain an understanding of what changes are occurring in the bleaching process and how these changes can be used to improve the efficiency of the process. In this study, a series of effluents obtained from successive bleaching treatments was characterized using proton, phosphorus-31 and COSY NMR.

Hydrogen peroxide:

Peroxide behaves as a lignin-retaining bleaching agent. The bleaching action of hydrogen peroxide is due to the hydroperoxyl anion (HO_2^-)[37].

$$H_2O_2 + OH^- \leftrightarrow H_2O + HO_2^-$$

The pKa of hydrogen peroxide is 11.6. High pH tends to decrease peroxide stability[37]. Agnemo and Gellerstedt[40] found the maximum rate of decomposition of hydrogen peroxide occurred when the pH of the solution equalled the pKa value (11.6) for hydrogen peroxide[40]. Under alkaline conditions hydrogen peroxide decomposes into water, oxygen, hydroxy radicals, superoxide ions and singlet oxygen[41]. The oxygen may be responsible for producing and stabilizing chromophoric groups. To prevent peroxide decomposition buffers and stabilizers are added where the most common are sodium metasilicate, magnesium sulfate and a chelating agent such as Na_5DTPA (sodium diethylenetriaminepentaacetate)[37,40,41]. The buffers and stabilizers maintain the pH of the solution and stabilize the peroxide by adsorbing trace metal catalysts which cause decomposition[37].

α-Ketones and α,β-Unsaturated Aldehydes:

Peroxide oxidation of α-ketones proceeds via the Dakin reaction. A Dakin reaction transforms an aromatic ketone or aldehyde with an *ortho* or *para* hydroxyl group into the corresponding hydroquinone[42] (Figure 15).

Cinnamaldehyde type structures are oxidized by alkaline hydrogen peroxide to produce aryl-α-carbonyl structures (Figure 16). Reeves and Pearl have postulated a mechanism where the reaction starts with the formation of an intermediate peroxide, this is followed by epoxide formation, and side chain loss to form an aromatic aldehyde and a carboxylic acid[42,43]. The aromatic aldehydes can be further oxidized by peroxide to form

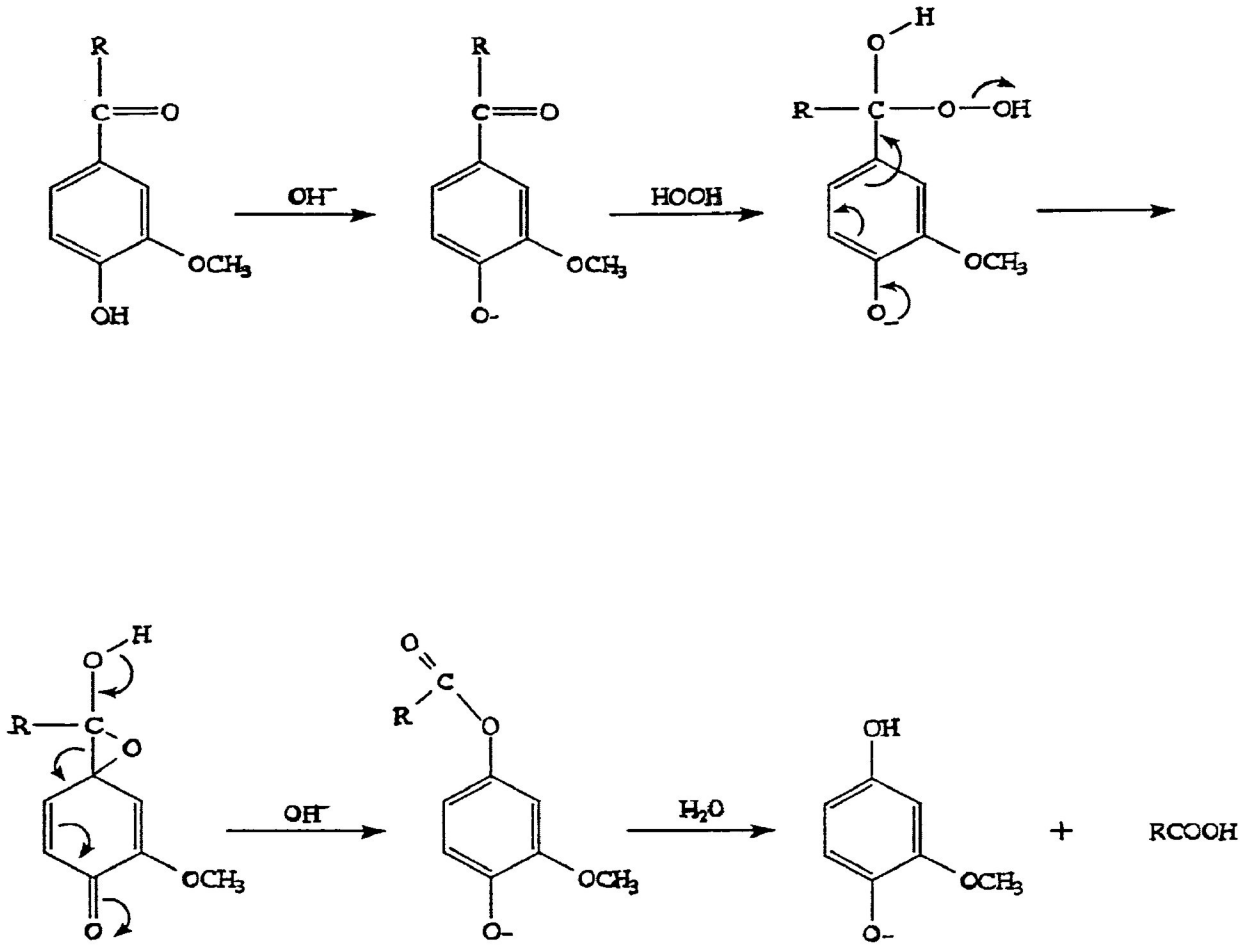

Figure 15 Peroxide oxidation of α-ketones[42]

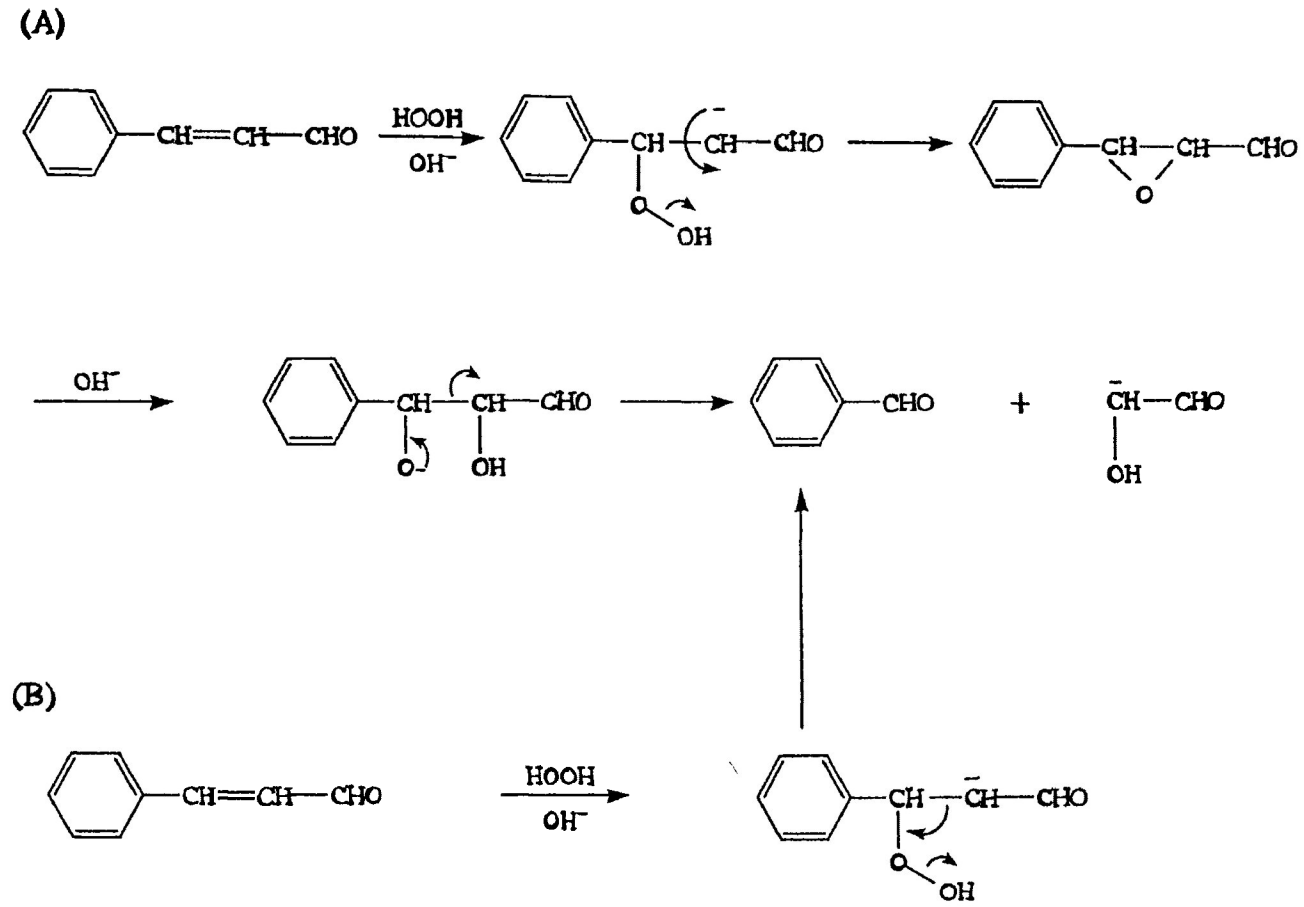

Figure 16 Peroxide oxidation of α,β-unsaturated aldehydes[42]

hydroquinones[43] (Figure 15). Oxidation of hydroquinones by oxygen leads to quinones which readily react with peroxide to form dicarboxylic acids[44]. The rate constant[43] for oxidation of cinnamaldehyde structures with stabilized peroxide at pH=10.5 and 30°C was 52.4 x 10^{-3} min^{-1} (Table 9).

Reactions of Phenolic Structures:

Non-carbonyl phenolic structures may be degraded by unstabilized hydrogen peroxide but stabilized peroxide had no effect on phenolic structures[40,45]. The reaction of phenols with an unstabilized peroxide solution at pH=10.5 and 45°C has been described as a four part sequence according to a model compound study on α-methylvanillyl alcohol (Figure 17). The four parts are "oxidation to acetoguaiacone followed by a Dakin reaction (A), 'Dakin-like' reaction (B), oxidative demethylation (C) and oxidative ring rupture and fragmentation of intermediates" (D)[45]. The final products are aliphatic acids.
Of the three competing reactions A, B, C, in Figure 17 it appears that reaction B is more important than A and reaction C competes favourably with reactions A and B[45]. The rate constant[40] for the decomposition of model α-methylsyringyl alcohol by stabilized hydrogen peroxide at pH=10.5 and 30°C was 0.53 x 10^{-3} min^{-1} (Table 9).

Reactions of Beta-O-4 Structures:

Oxidation of a β-O-4 model compound, guaiacylglycerol-β-guaiacyl ether (Figure 18) with unstabilized alkaline hydrogen peroxide at pH=10.5 and 45°C appears to proceed mainly by a 'Dakin-like' reaction involving a side chain displacement[46] but the details of this reaction are unclear. Phenolic and carbonyl groups liberated by this reaction may

Model Compound	pH	Temperature (°C)	Rate Constant ($kmin^{-1}$)
cinnamaldehyde	10.5	30	52.4×10^{-3}
α-methylsyringyl alcohol	10.5	30	0.53×10^{-3}
1,2-diarylpropane-1,3-diol	11.0	30	0

Table 9 Rate constants for the reaction of selected model compounds with peroxide[40,43,48]

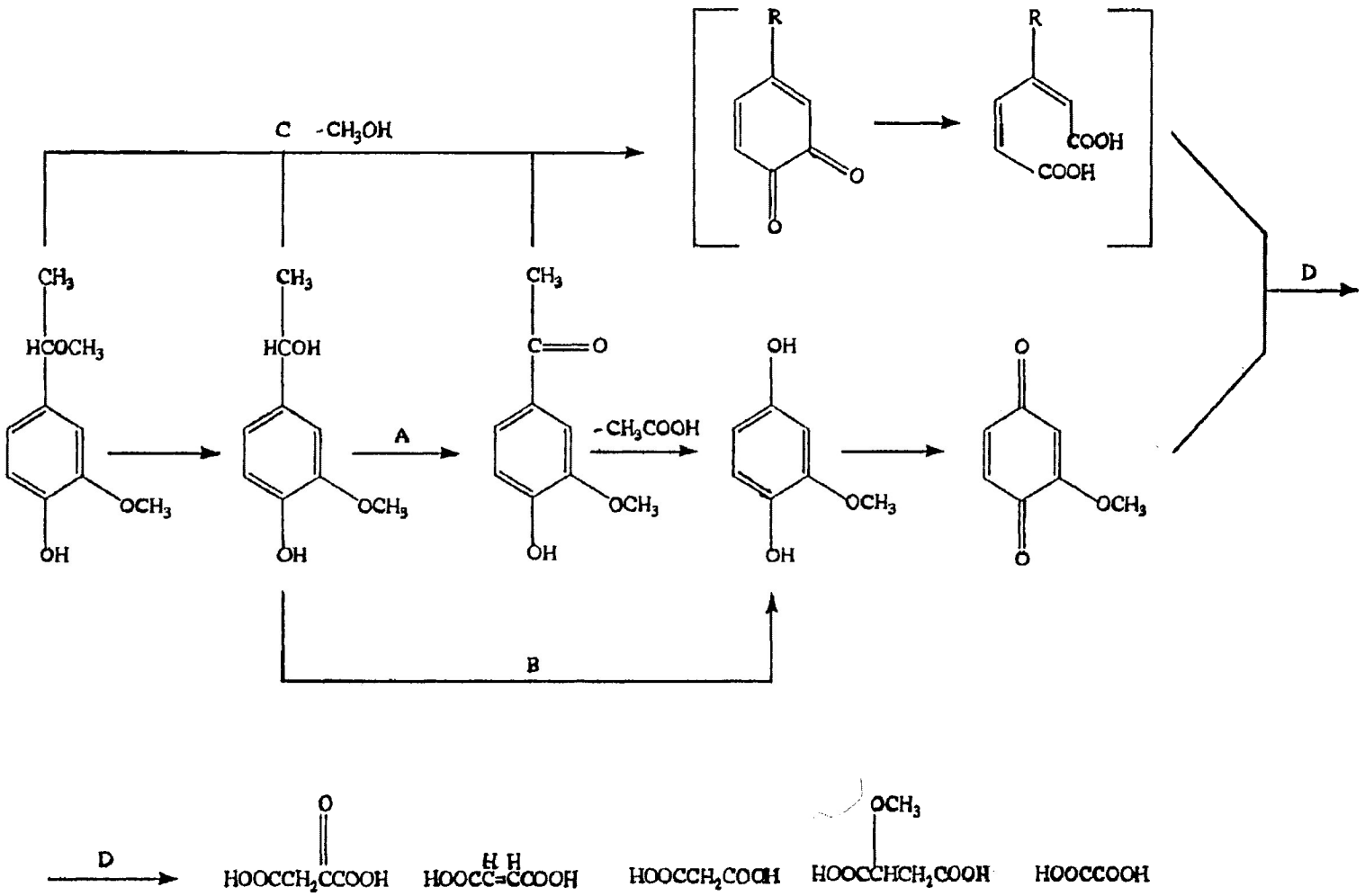

Figure 17 Decomposition of α-methylvanillyl alcohol with peroxide[45]

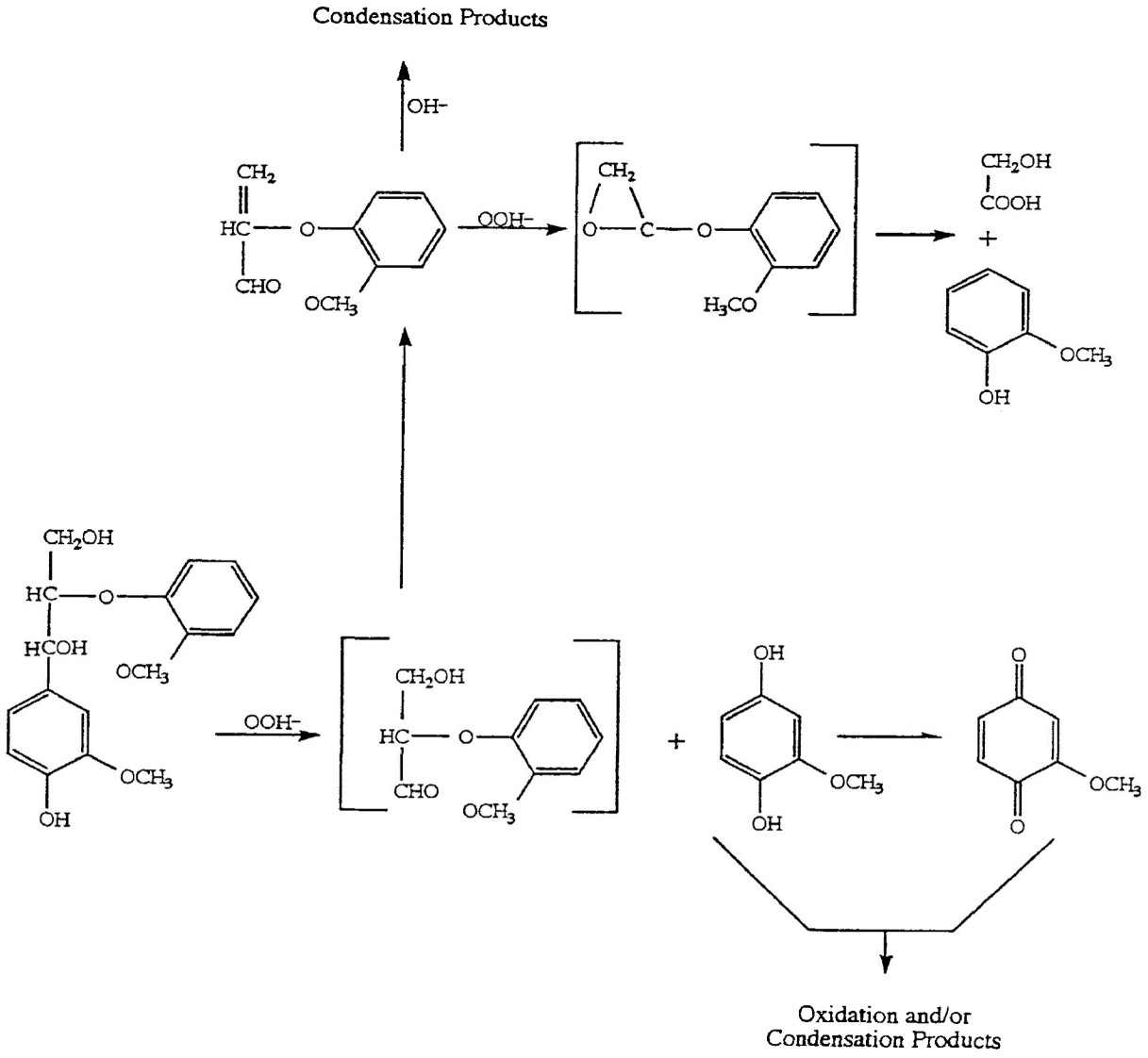

Figure 18 **Major route for peroxide oxidation of β-O-4 model compound guaiacylglycerol-β-guaiacyl ether**[46]

react further with peroxide. The β-O-4 units in the model compound and in lignin were virtually unreactive toward peroxide stabilized by Na_5DTPA or silicate[38,46]. It is important to determine how β-O-4 structures react to peroxide because they are the major linkage in lignin[38] (see Table 1).

Reactions of Beta-1 Structures:

The main reactions of 1,2-diarylpropane models with stabilized alkaline hydrogen peroxide at pH=10.5 were nucleophilic attack of hydroperoxide anion on a quinonemethide (Figure 19) and oxidation of stilbenes both initially formed by reactions with alkali[47]. The β-1 diol model was more reactive (69% reacted) toward unstabilized peroxide than toward peroxide/Na_5DTPA (30% of model reacted)[47]. Stilbenes are leucochromophores which can be converted into quinones upon exposure to oxygen[47,48] (Figure 20). A study on bleached spruce groundwood showed a decrease in diarylpropane structures and an increase in diguaiacyl stilbene structures[49]. The rate constant for decomposition of a 1,2-diarylpropane-1,3-diol model into stilbenes with stabilized peroxide at 30°C and pH=11.0 is approximately zero[48] (Table 9).

RESULTS AND DISCUSSION:

Overview:

Beta-O-4, beta-1 and coniferaldehyde structures were among several lignin structures found in effluents from four bleaching stages. Integration of the proton spectra was used to determine the relative amounts of each structure in each effluent to get an idea of the importance of certain bleaching reactions at each stage.

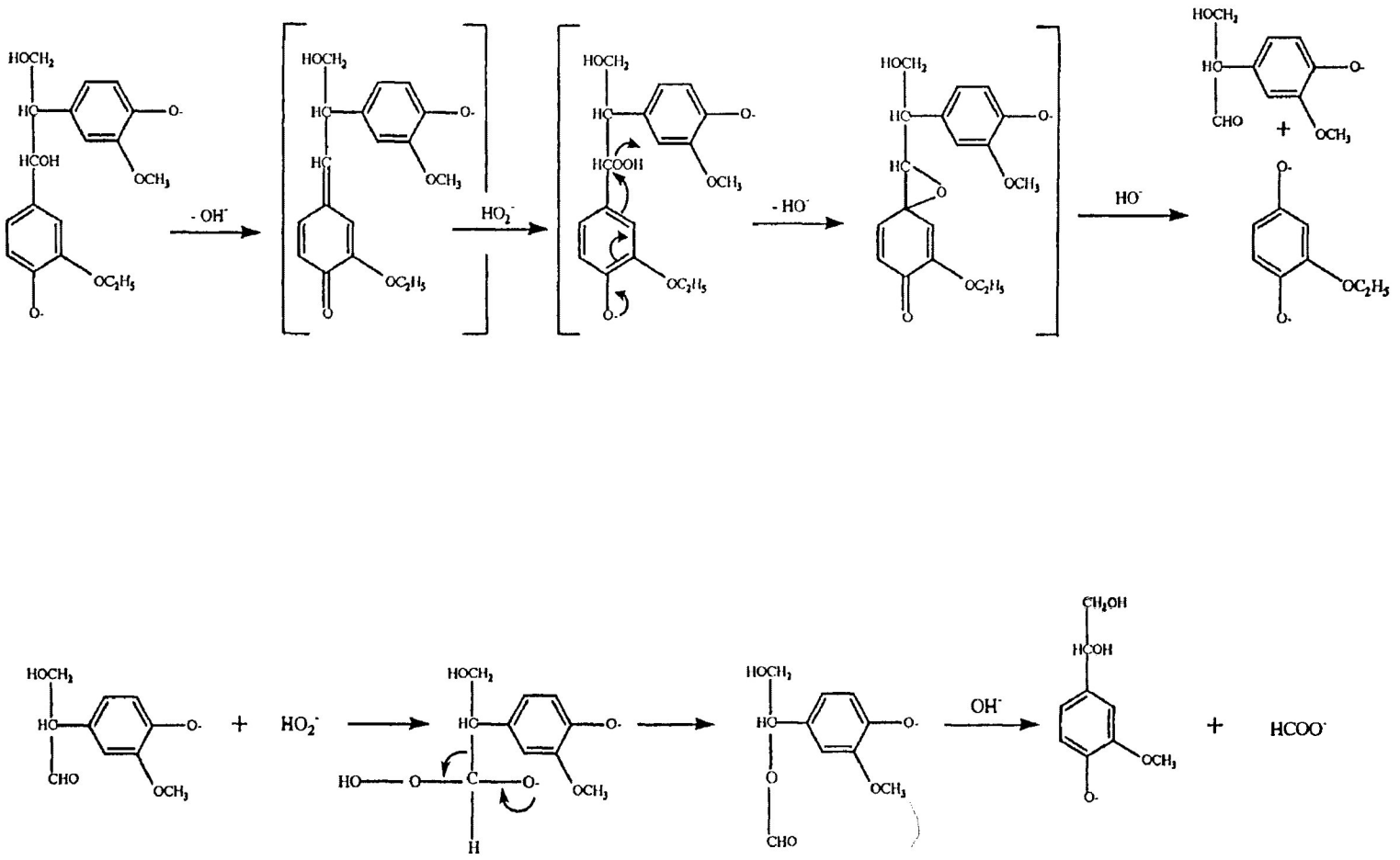

Figure 19 Reaction of peroxide with a β-1 model compound[47]

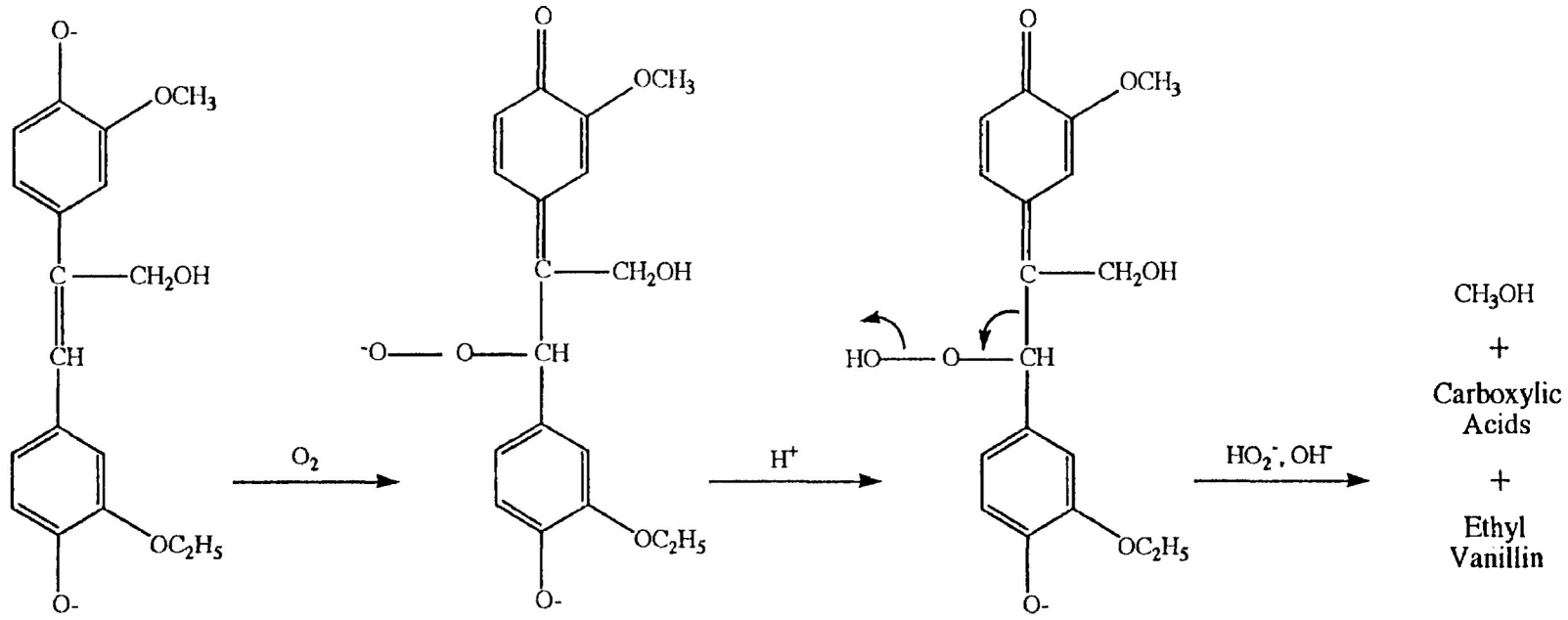

Figure 20 **Major route for conversion of a stilbene into a quinone by reaction with oxygen[47].**

A two-dimensional COSY experiment helped to identify lignin structures and confirm the assignments made from the proton experiments. Phosphorus-31 experiments were also helpful in this way. Many attempts to obtain a carbon-13 spectrum were unsuccessful due to a low signal to noise ratio caused by very broad peaks.

Variation of Structural Elements:

Beta-O-4 Units:

Proton spectra of the effluents had peaks at 6.06, 4.69 and 4.40 ppm (Figure 21 and Table 10) indicating α, β and γ protons respectively in β-O-4 structures. Cross peaks on the COSY spectra (Figure 22 and Table 11) at 6.06-4.69 and 4.69-4.40 ppm confirmed the presence of β-O-4 structures. Hydroxyl protons from arylglycerol-β-aryl units were present on the phosphorus-31 spectra (Figure 23 and Table 12).

Approximately 50% of the total linkages in softwood lignin are believed to be β-O-4 linkages[5] (Figure 2). A large majority of these linkages are part of arylglycerol-β-aryl ether structures (structure 1 in Figure 3). These structures represent approximately 30-50% of the side chains in spruce lignin[50].

Peaks on the proton spectra of the effluents from the four bleaching stages were integrated using a Lorentzian fit program (see Experimental Section) and various ratios were calculated using the measured frequencies of the different groups. A plot of the relative frequency of β-O-4 units measured from the 6.06 ppm peak versus bleaching stage is shown in Figure 24. There is a decrease in β-O-4 structures relative to methoxyl groups with increasing bleaching stage. Beta-O-4 structures were present in the effluents

Figure 21 200 MHz proton spectra of the effluents from the four bleaching stages (From top to bottom: first, second, third and fourth stages)

Proton Chemical Shift (ppm)	Interpretation
9.84	formyl protons in benzaldehyde units
7.57	aromatic protons adjacent to carbonyl groups
7.40	aromatic protons in benzaldehyde units and vinyl protons on the carbon atoms adjacent to aromatic rings in cinnamaldehyde units
6.92	aromatic protons and certain vinyl protons
6.06	H_α in β-O-4 and β-1 structures
4.69	H_β in β-O-4 structures
3.82	protons in methoxyl groups
2.30	aromatic acetate
2.09	aliphatic acetate

Table 10 Peak list for 200 MHz proton spectra of the effluents[50]

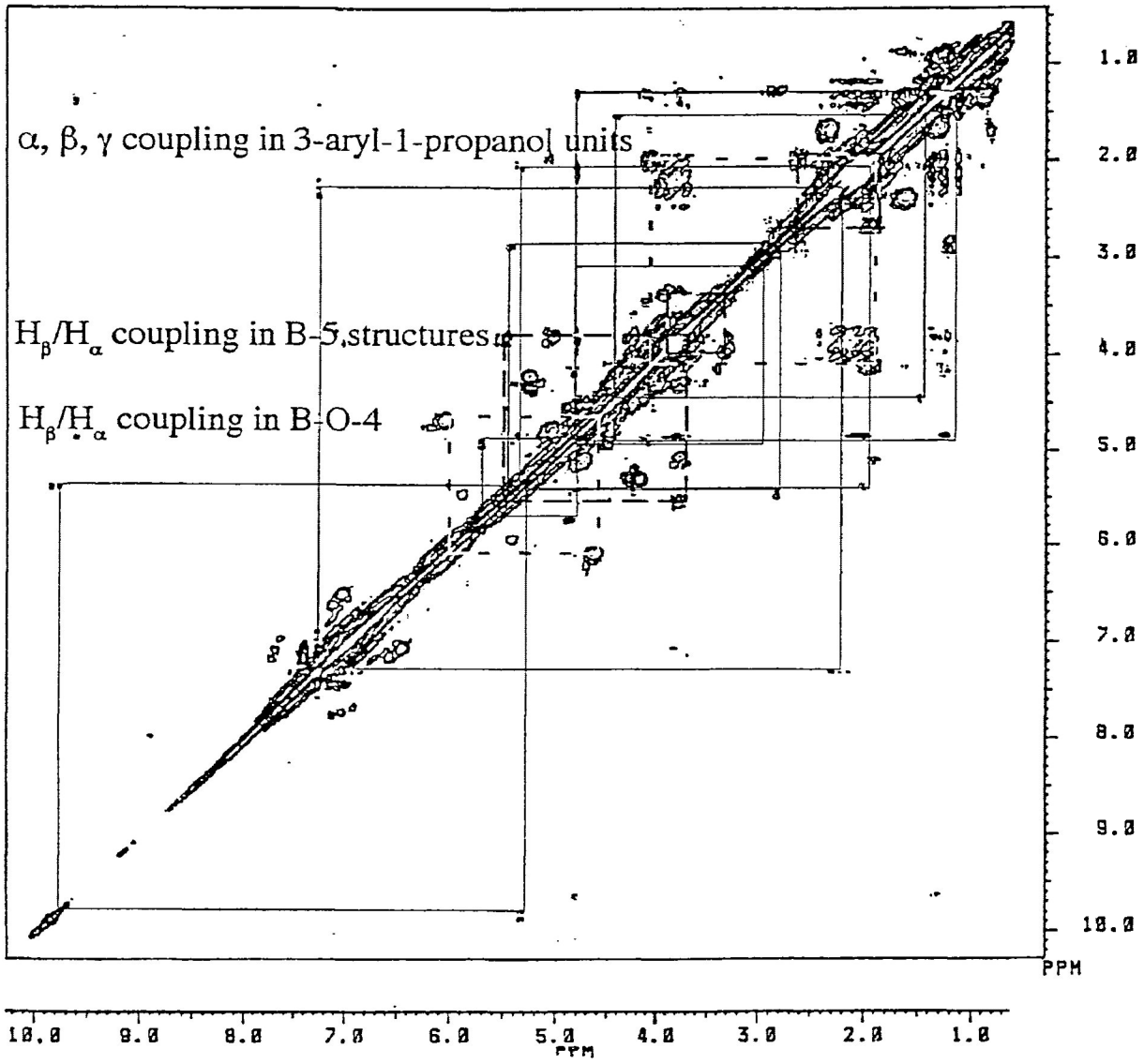

Figure 22 200 MHz COSY spectrum of acetylated effluent from the fourth bleaching stage

Chemical shift (ppm)	Interpretation
9.70-6.61	γ,α in coniferaldehyde
7.42-6.61	β,α in coniferaldehyde
7.54-7.41	aromatic protons in benzaldehyde
6.60-6.13	α,β vinylic protons in coniferyl alcohol
6.06-4.69	α,β in β-O-4 units
4.69-4.40	β,γ in β-O-4 units
5.54-3.79	α,β of β-5 linkage of phenylcoumaran
4.52-3.73	γ,β of β-5 linkage of phenylcoumaran
5.07-3.65	α,β of structure similar to side chain B of IIB (Figure 5)
3.65-1.38	β,γ of structure similar to side chain B of IIB (Figure 5)
4.08-1.90	γ,β of 3-aryl-1 propanol side chain
2.67-1.95	α,β of 3-aryl-1 propanol side chain

Table 11 Peak assignments for the COSY spectrum of the effluent from the fourth bleaching stage[1,27,36,50,52,53]

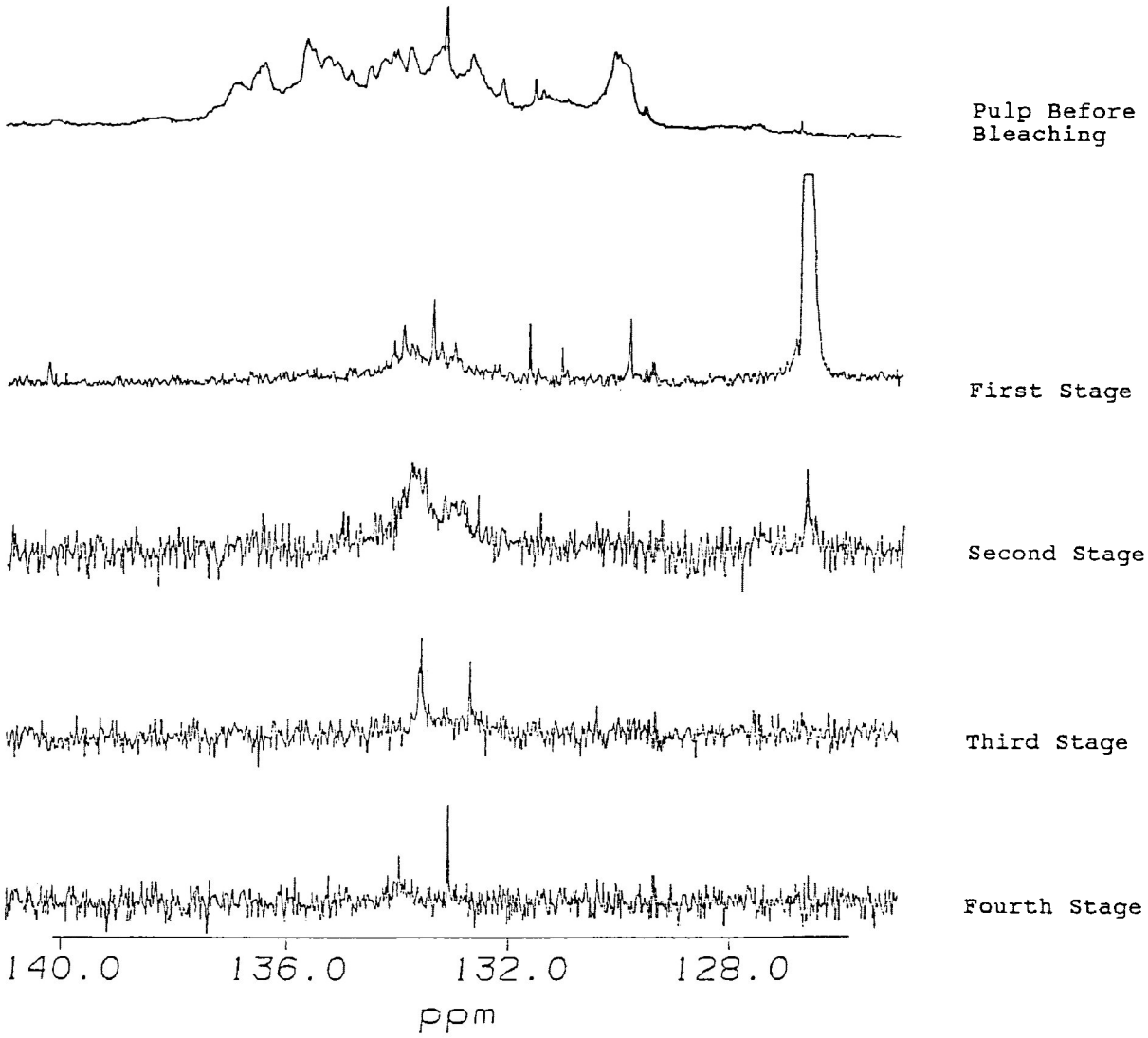

Figure 23 200 MHz phosphorus-31 spectra of the effluents from the four bleaching stages

Bleaching Stage 1	2	3	4	P-31 Peak (ppm)	Interpretation
✓	✓	no	no	135.2	*alpha*-hydroxyls in aryl-glycerol ß-guaiacyl units and LCC
✓	✓	no	✓	133.8	*gamma* hydroxyls in *alpha*-carbonyl containing units, cinnamyl alcohol, LCC
✓	✓	✓	✓	133.3	*gamma* hydroxyls in arylglycerol-ß-aryl units
✓	no	✓	no	132.5	primary aliphatic hydroxyls
✓	✓	no	no	131.5	phenolic hydroxyls in biphenyl units, and cinnamic aldehydes
✓	no	no	no	130.1	phenolic hydroxyls in guaiacyl structures
✓	no	no	✓	129.3	phenolic hydroxyls in guaiacyl and catechol structures
✓	✓	no	no	126.7	carboxylic acid hydroxyls

no = not observed
LCC = lignin carbohydrate complexes

Table 12 Peak assignments for phosphorus-31 NMR of effluents[54]

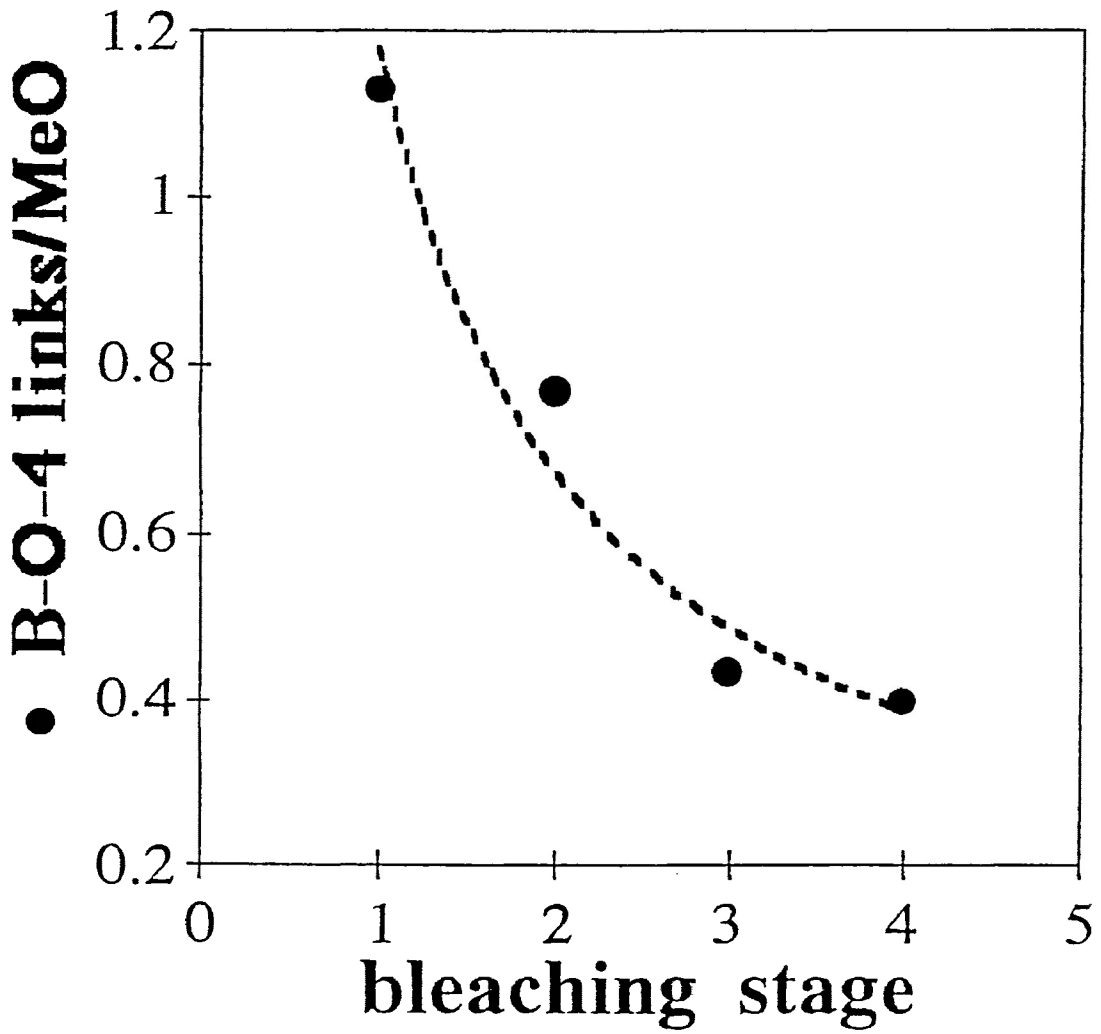

Figure 24 Ratios of β-O-4 units to methoxyl groups versus bleaching stage

from each bleaching stage indicating that some delignification must have occurred. The structural moieties cleaved during delignification have not been identified. However, these results indicating the stability of β-O-4 structures to peroxide bleaching agree with previous reports[38,46,51].

Phenolic Structures:

The relative frequency of phenols was determined by integration of the aromatic acetoxyl peak (2.30 ppm)[50] on the proton spectra. The relative proportion of phenolic hydroxyls decreased with increasing bleaching stage (Figure 25). The phosphorus-31 spectra (Figure 23, Table 12) also showed a decrease in phenolic units. This may suggest that phenolic units that were more susceptible to peroxide bleaching (unetherified which are more reactive toward unstabilized peroxide versus etherified) were removed in the earlier bleaching stages.

The decline in phenolic units in conjunction with the decline in β-O-4 units with increasing bleaching stage may suggest that β-O-4 linkages are not broken during bleaching. This is important because under conditions where hydrogen peroxide is unstable β-O-4 linkages may be destroyed generating phenolic hydroxyl containing moieties which may be susceptible to further degradation[46]. Since intact β-O-4 units were detected in the effluents and both the phenolic hydroxyl and β-O-4 contents decreased with bleaching stage, the phenolic units in the effluents must be directly from the pulp or from some other reaction.

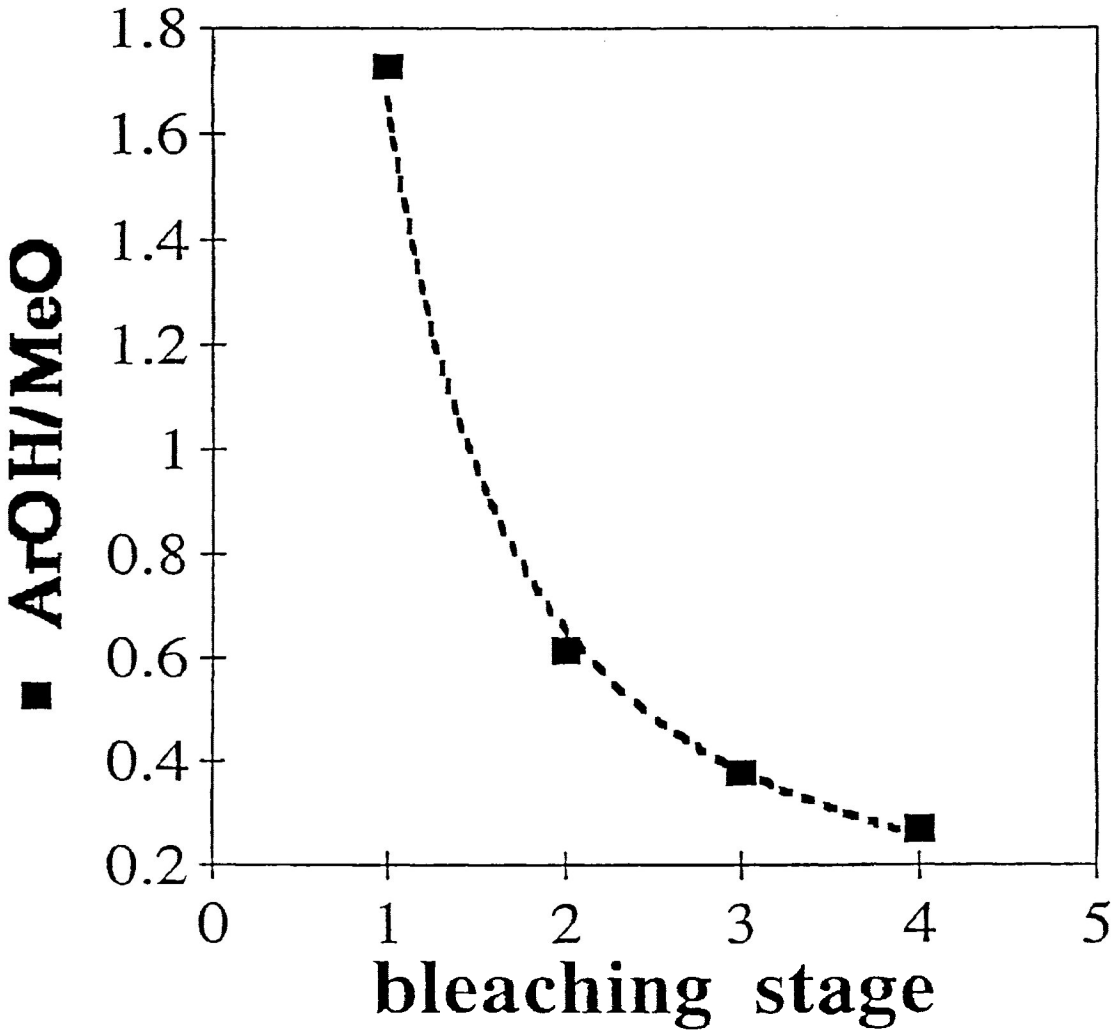

Figure 25 Ratios of phenolic hydroxyls to methoxyl groups versus bleaching stage

3-Aryl-1-Propanol Units:

It is believed there are only a small amount of 3-aryl-1-propanol units (structure 3b in Figure 3) present in lignin[52]. Side chain couplings were detected on the COSY spectrum at 1.95-2.67 (α-β) and 1.90-4.08 ppm (β-γ)[52]. These peaks were not visible on the proton spectra.

Beta-5 Units:

Cross peaks on the COSY spectra show α-β (5.54-3.79 ppm)[52] and β-γ (3.73-4.52 ppm)[36] couplings for the side chain of a β-5 unit.

Phenylcoumaran type structures (structure 2 in Figure 3) contain the β-5 linkage (Figure 2) which constitutes approximately 9-12% of all softwood linkages[5]. Phenylcoumaran structures are not attacked by unstabilized peroxide[42] nor by stabilized peroxide[49].

Aldehydes:

Carbonyl groups are one of the characteristic functional groups on lignin formed and destroyed by peroxide bleaching when they are on phenolic groups. There are approximately 10-15 carbonyl groups for every 100 phenylpropane units[5].

The proton and COSY spectra contained peaks attributable to both coniferaldehyde/cinnamaldehyde and benzaldehyde units (Table 10 and Table 11). Side chain protons in coniferaldehyde units occurred at 6.60, 7.49 and 9.70 ppm[53]. The formyl proton for coniferaldehyde (9.70 ppm) was not detected on the proton spectra but it did

appear on the COSY spectra. The formyl proton (9.84 ppm) for benzaldehyde was evident on the proton spectra.

The relative frequency of benzaldehyde hydroxyls increased with increasing bleaching stage (Figure 26) which suggests more of the cinnamaldehyde type structures are attacked by peroxide in the later stages. This result corresponds to the result of Reeves and Pearl[42] who demonstrated peroxide oxidation of a cinnamaldehyde model compound resulted in benzaldehyde and benzoic acid. In terms of the expected relative rate constant (Table 9), oxidation of cinnamaldehyde should be rapid compared to oxidation of phenolic α-carbonyl structures.

Carboxylic Acids:

NMR difference spectra of acetylated and acetylated/methylated effluents from the first bleaching stage show the presence of carboxylic acids at approximately 3.9 ppm (Figure 27). The amount of carboxylic acids present in comparison with methoxyl group content is approximately 7%. Peaks indicating carboxylic acids were evident on the phosphorus-31 spectra of the effluents at 126.7 ppm[54] (Figure 23 and Table 12). As can be seen in Figure 23, the carboxylic content decreases with increasing bleaching stage. Carboxyl group content is believed to increase at the expense of carbonyl groups[55]. The carboxyl groups may be formed by hydrolysis of polysaccharides or lignin[5]. The carbonyl groups appear to be removed more in the early bleaching stages.

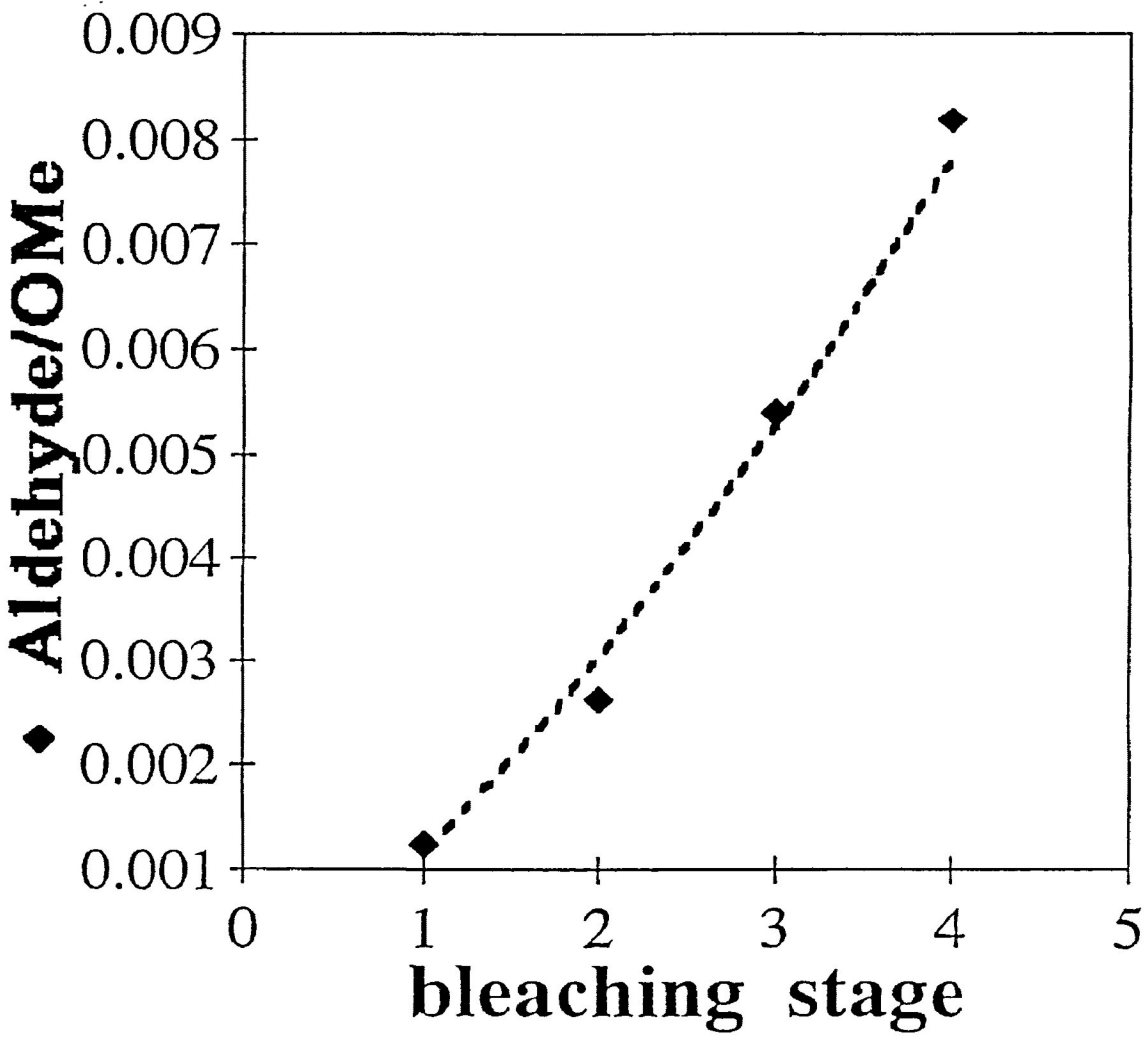

Figure 26 Ratios of formyl groups in benzaldehyde units to methoxyl groups versus bleaching stage

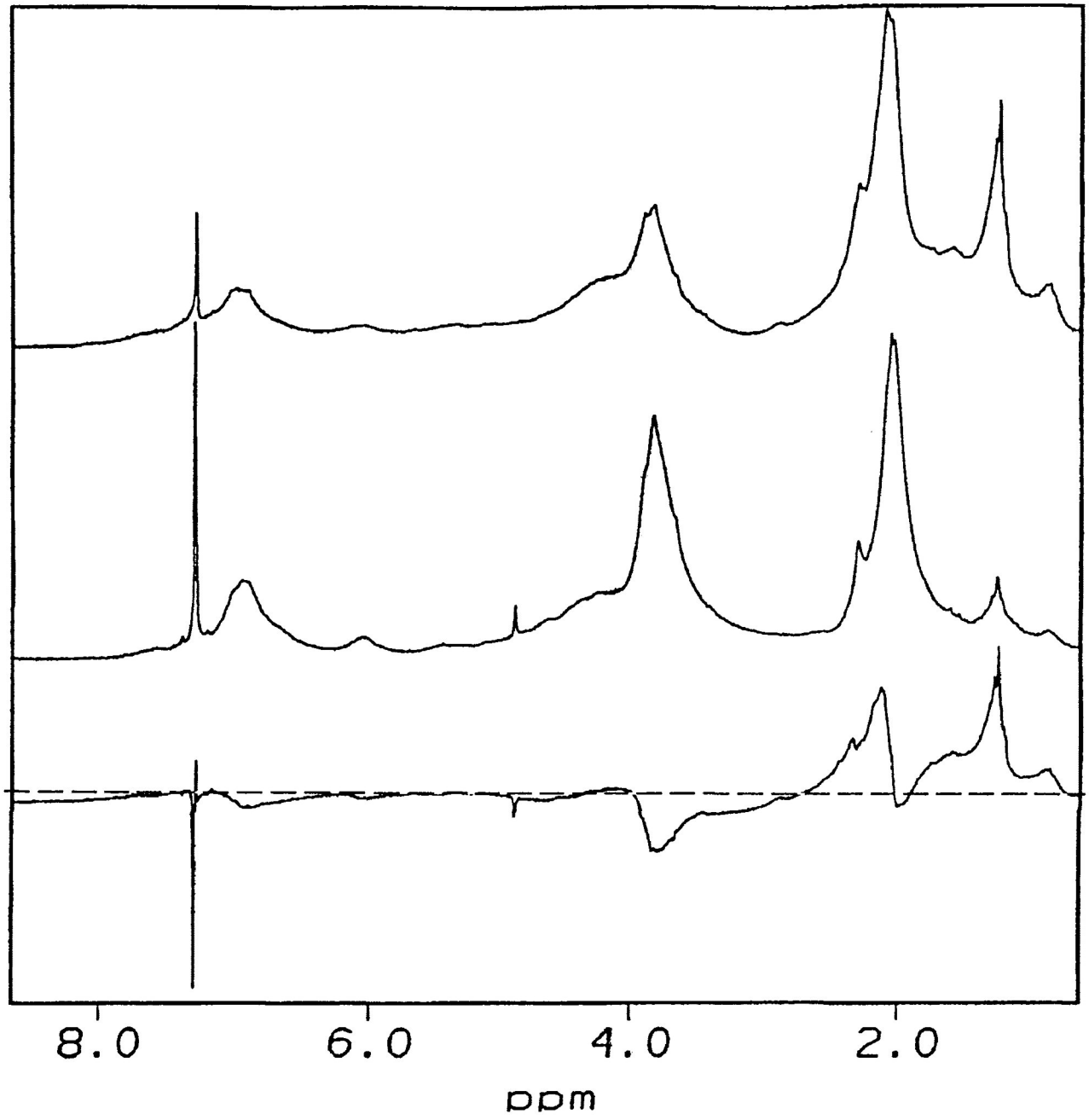

Figure 27 Difference spectrum (bottom) of acetylated (top) and acetylated/methylated (middle) effluent from the first bleaching stage showing the presence of carboxylic acids at 3.8 ppm

Aromatic Protons Adjacent to Carbonyl Groups:

COSY spectrum had a peak at 7.57-7.40 ppm indicating coupling between aromatic protons at positions 2 and 6 on a ring adjacent to a carbonyl group. The relative frequency of alpha carbonyl groups decreases with increasing bleaching stage (Figure 28) suggesting carbonyl groups in general are attacked by peroxide in the earlier bleaching stages. The decline in alpha carbonyl groups in conjunction with the decline in carboxylic acid groups with increasing bleaching stage agrees with the results of Bailey and Dence[45] who found that carboxylic acid groups are formed when carbonyl groups are attacked by peroxide.

Carbohydrates:

Proton spectra of the effluents indicated the presence of carbohydrates at 5.34, 5.04 and 4.69 ppm[56] (Figure 29). Phosphorus-31 spectra also had peaks indicating carbohydrates and carboxylic acids which may have been produced by the hydrolysis of polysaccharides and lignin[5]. The carbohydrates appeared to be more prevalent in the later bleaching stages (Figure 30) suggesting that the bonds between lignin and carbohydrates are resistant to peroxide bleaching. Further analysis of carbohydrates conducted in this lab involved derivatization to alditol acetates followed by gas chromatography.

Other Structures:

A broad peak characteristic of pinoresinol (β-β) structures was found on the proton spectrum (5.83 ppm) of the effluent from the fourth bleaching stage[1]. Since only this

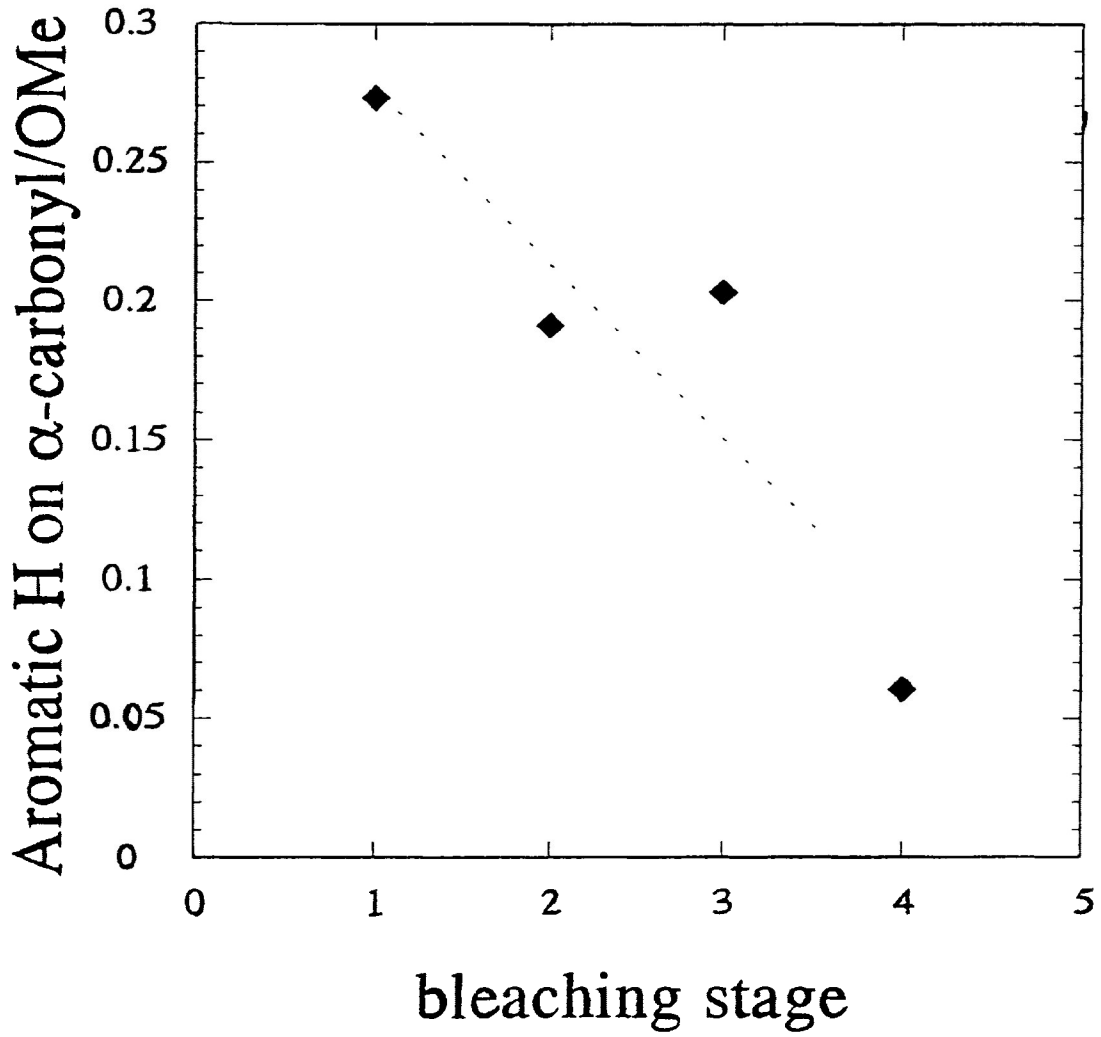

Figure 28 Ratios of aromatic protons with alpha carbonyl groups to methoxyl groups versus bleaching stage

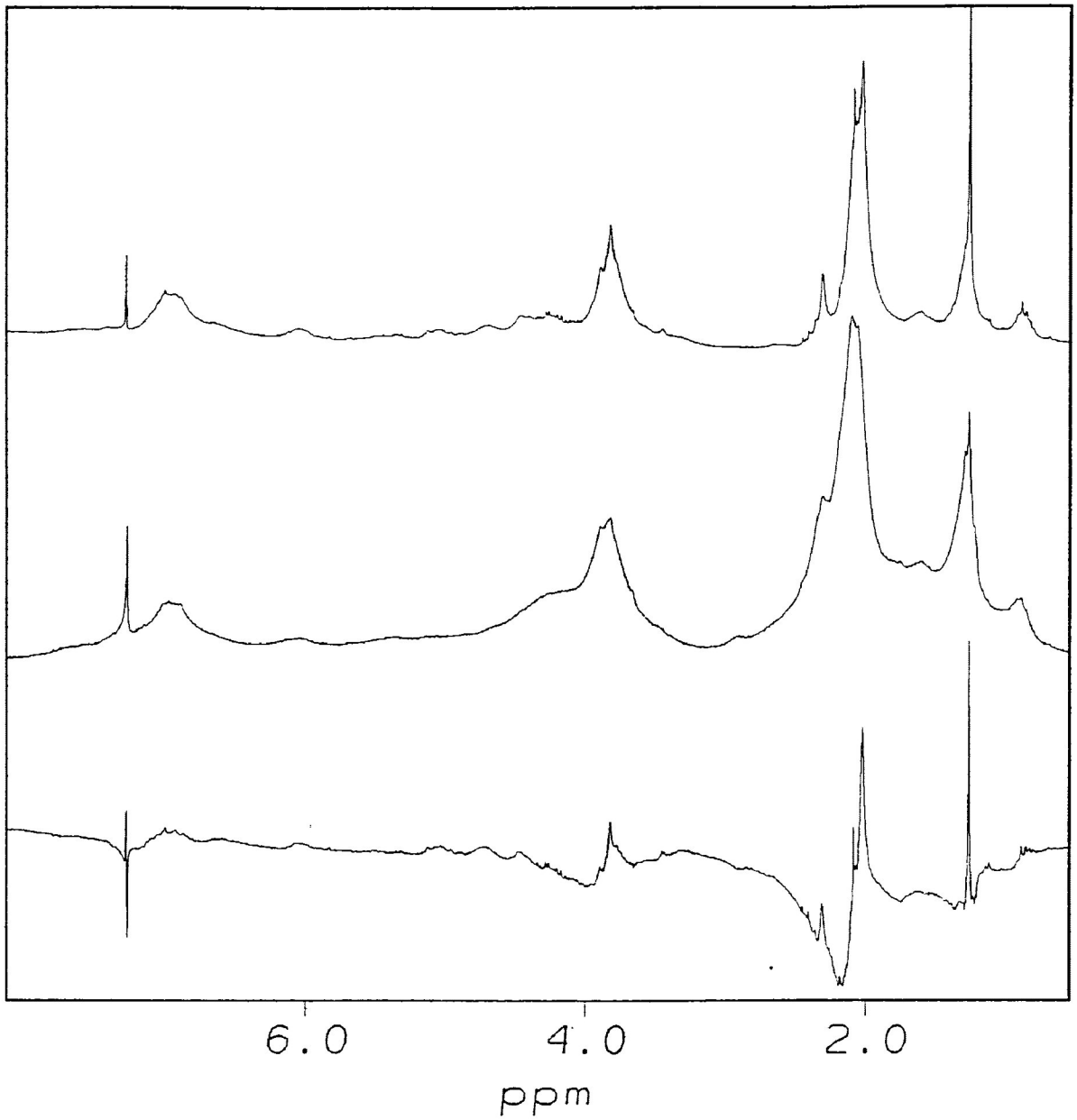

Figure 29 Difference spectrum (bottom) of effluent from the fourth bleaching stage (top) and first bleaching stage (middle) showing the presence of carbohydrates between approximately 4.0-5.5 ppm.

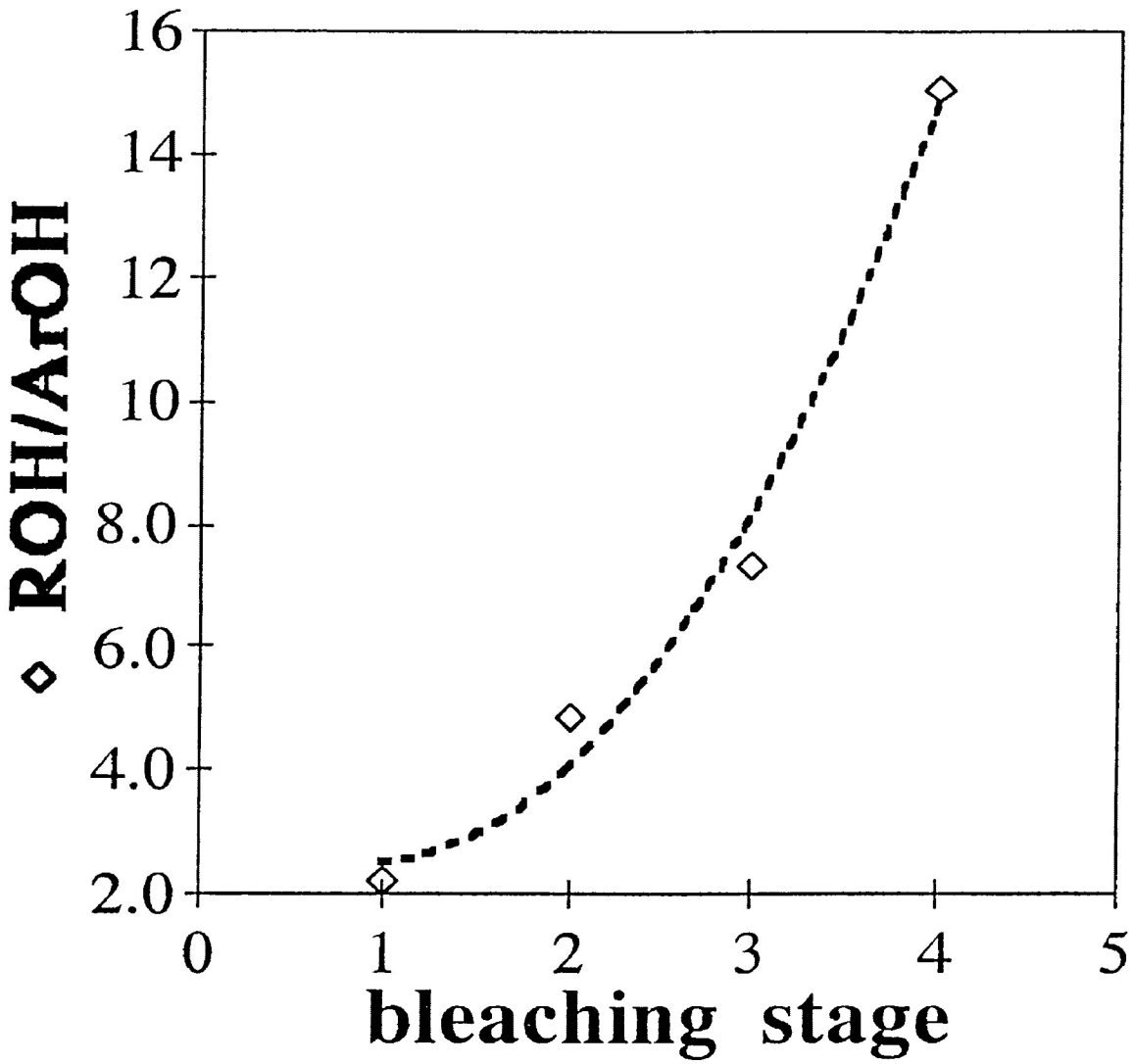

Figure 30 Ratios of aliphatic hydroxyl to aromatic hydroxyl groups versus bleaching stage

peak and none of the other peaks were found it is questionable whether this structure is really present.

Coniferyl alcohol (see Figure 1) had a COSY peak at 6.60-6.13 ppm representing α and β vinylic protons in a *trans* configuration[1]. Coniferyl alcohol end-groups are stable during peroxide bleaching[49].

The COSY spectrum had two cross peaks at 3.65-1.38 and 3.65-5.07 ppm which suggests β-γ and β-α couplings[1] for structures similar to side chain B of IIB (Figure 5).

CONCLUSION:

Lignin fragments representing the major components in lignin such as β-O-4 units and phenols as well as degradation products such as benzaldehyde units and methoxyl groups are present in the effluents suggesting some delignification or lignin degradation occurs during peroxide bleaching. Carbohydrates are more prevalent in the later bleaching stages while lignin components are found more in the early stages. Carboxyl components with a high proportion of phenolic hydroxyl groups were more easily removed by bleaching than structures with low phenolic hydroxyl content. An increase in aldehyde groups with bleaching stage was unexpected since these groups are supposed to be removed during the bleaching process.

PART THREE: ANALYSIS OF NMR RELAXATION OF DEUTERIUM LABELLED KRAFT LIGNIN FRACTIONS

INTRODUCTION:

The high molecular weight of lignin is a problem for the lignin NMR spectroscopist who must contend with a large number of broad peaks in a small chemical shift range[57]. Spin-exchange in many two-dimensional experiments is further obscured by short relaxation times and spin diffusion[33]. The relaxation times are shorter than the evolution times in two-dimensional correlation experiments so it is not possible to resolve crowded peaks. In NOE based experiments long correlation times lead to spin diffusion[33].

In this study, deuterium relaxation times were calculated for samples obtained by fractionating spruce kraft lignin using size exclusion chromatography.

Deuterium Relaxation:

Most NMR relaxation processes are governed by the motions of the molecule[34]. Molecular motion is characterized by a correlation time which is the average time a molecule spends in any given position. The effective correlation time or correlation time which contributes the greatest to the spectral density is the most important to relaxation processes[34]. The efficiency of relaxation and spin exchange is determined by the spectral density[34]. The spectral density, $J(\omega)$, is obtained from the Fourier transform of the auto-correlation function[58].

$$G(\tau_1,\tau_2) = \overline{f(t_1)f^*(t_2)} \qquad (6)$$

$$J(\omega) = 2\int_0^\infty G(\tau)\cos(\omega\tau)d\tau = \int_{-\infty}^{\infty} G(\tau)e^{-i\omega\tau}d\tau \qquad (7)$$

Deuterium relaxation NMR may be used to evaluate effective correlation times because a simple quadrupolar relaxation mechanism dominates[59]. Also, deuterium can be substituted for protons with minimal structural modification[60]. Substituting certain protons for deuterium simplifies a proton spectrum because multiple peaks due to spin-spin coupling are reduced into less complicated multiplets or single peaks[61]. Deuterium relaxation times are relatively easy to interpret because deuterium relaxes almost exclusively by quadrupolar mechanism so other relaxation mechanisms can be ignored[59,61].

Deuterium relaxes predominantly by quadrupolar relaxation which is "interaction of an electric quadrupole moment with an electric field gradient"[34]. The electric field gradient is modulated by molecular motions[59]. The relaxation rates for spin 1 nuclei due to quadrupolar relaxation are shown below[58].

$$\frac{1}{T_1} = \frac{3}{80}\left(1 + \frac{\eta^2}{3}\right)\left(\frac{eQ}{\hbar}\frac{\delta^2 v}{\delta^2 z}\right)^2 \{J(\omega_o) + 4J(2\omega_o)\} \qquad (8)$$

$$\frac{1}{T_2} = \frac{1}{160}\left(1 + \frac{\eta^2}{3}\right)\left(\frac{eQ}{\hbar}\frac{\delta^2 v}{\delta^2 z}\right)^2 \{9J(O) + 15J(\omega_o) + 6J(2\omega_o)\} \qquad (9)$$

η = asymmetry parameter
J = spectral density

and $$J(\omega) = \frac{2\tau_c}{1 + \omega^2\tau_c^2} \qquad (10)$$

where ω_o = 30.7 MHz (192.9 rad/s) for deuterium

$$J(0) = 2\tau_c \qquad J(\omega) = \frac{2\tau_c}{1 + \omega^2\tau_c^2} \qquad J(2\omega) = \frac{2\tau_c}{1 + 4\omega^2\tau_c^2}$$

Dividing $1/T_2$ by $1/T_1$ leads to

$$\frac{T_1}{T_2} = \frac{1}{6}\frac{9J(\omega_o) + 15J(\omega_o) + 6J(2\omega_o)}{J(\omega_o) + 4J(2\omega_o)} \qquad (11)$$

Correlation Times:

Macromolecular structure of lignin in solution is largely unknown. For the purposes of relaxation time analysis, lignin will be considered as a sphere undergoing isotropic motions[62]. The correlation time under these circumstances may be described as a function of radius and viscosity[62].

$$\tau_c = \frac{4\pi\eta a^3}{3kT} \qquad (12)$$

k = Boltzmann constant
T = temperature in Kelvin
a = radius of molecule
η = viscosity of solvent

Also, since relaxation of quadrupolar nuclei is mainly due to rotational reorientation of the bond attached to the quadrupolar nucleus it is the rotational correlation time which is of particular interest[63].

RESULTS AND DISCUSSION:

Relaxation Times:

Concentration and Molecular Weight Dependence:

Samples from kraft lignin were obtained during size-exclusion chromatography. The UV absorbance of the size-exclusion profile is shown in Figure 31. Several samples collected from this experiment were chosen for the relaxation studies. Molecular weights were estimated by comparison to a similar Superose column calibrated with ultracentrifuge experiments.

Spin-lattice relaxation times, T_1, increased with increasing concentration for all molecular weights. Figure 32 shows this for molecular weights 2300 (····) and 480 (----)(Tables 13 and 14). Spin-spin relaxation times, T_2, decreased with increasing concentration for all samples except molecular weight 480 which appeared to be stable (Figure 33 and Table 15). The decrease in T_2 was more pronounced for higher molecular weight samples. A plot of calculated T_1/T_2 versus concentration was stable for molecular weight 480 but increased sharply for molecular weight 2300 (Figure 34).

Correlation times increased with increasing concentration for all samples (Figure 35) and also increased with molecular weight (Figure 36). The range of correlation times was 2.7×10^{-8} s to 8.1×10^{-10} s.

Temperature Dependence:

T_1 values for representative samples with molecular weights 480 and 2800 increased with temperature suggesting that the average T_1 value determined by a correlation time is faster than the T1 minimum correlation time. T_1 for molecular weight 480 increased

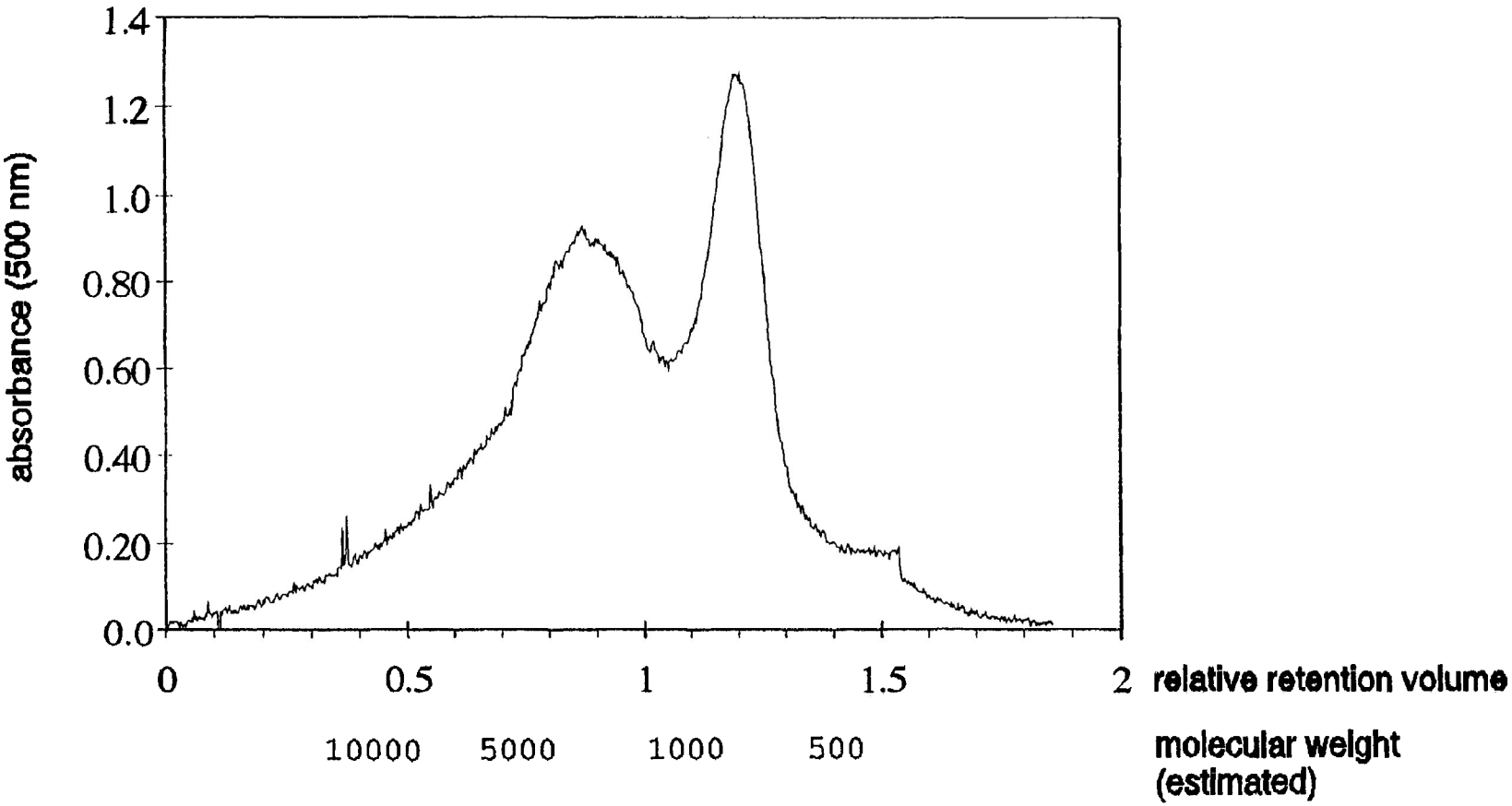

Figure 31 UV spectrum of spruce Kraft lignin with estimated molecular weights for the fractions

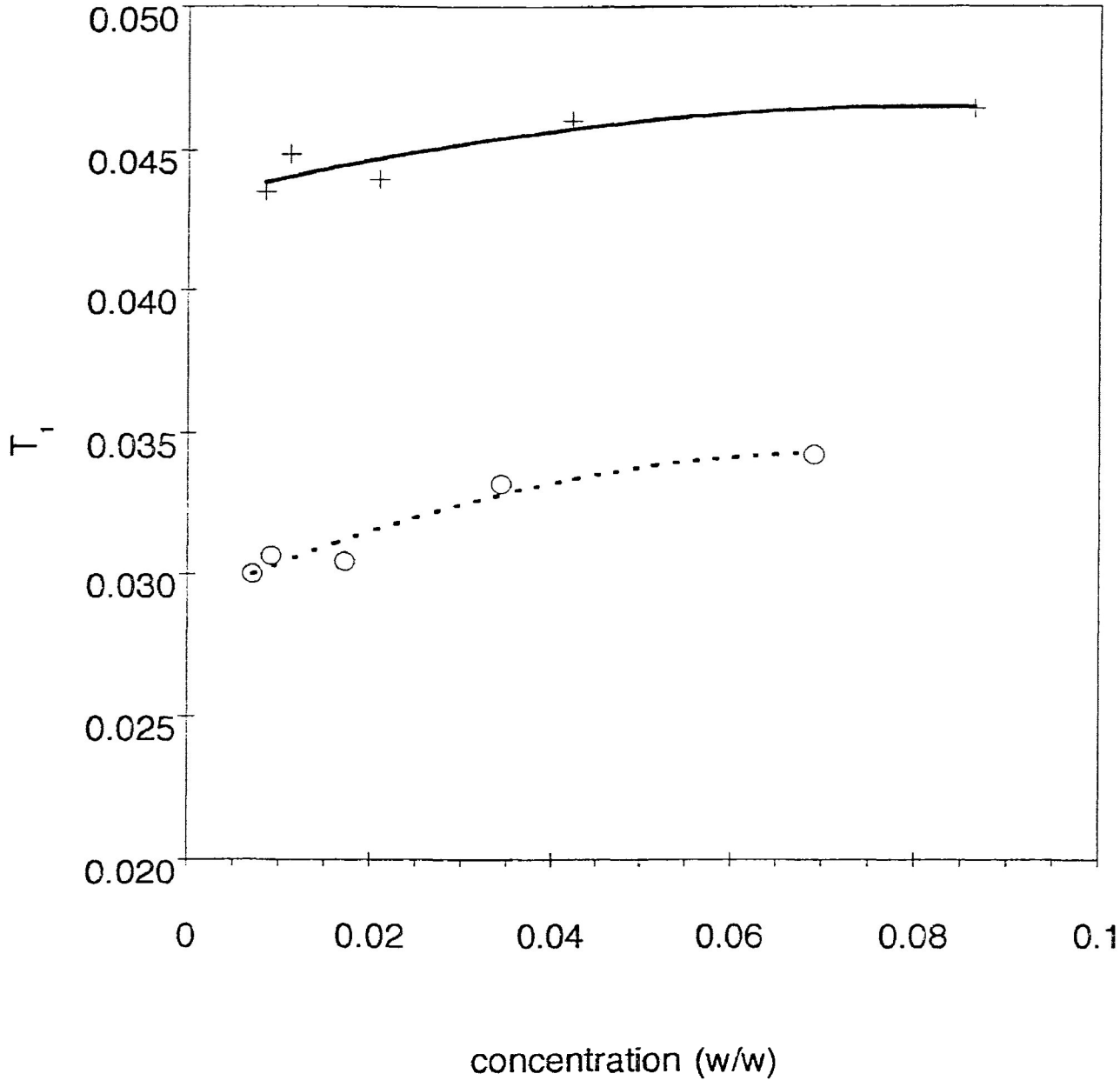

Figure 32 **Spin-lattice relaxation time versus concentration for molecular weights 2300 (····) and 480 (——)**

Molar Mass	Concentration (w/w)	$T_{1integral}$ (ms)	$T_{1height}$ (ms)	T_{1h}/T_{1i}(avg)
22 000	0.0175	43.5	46.7	
	0.00930	44.9	45.9	
	0.00459	40.8	45.5	1.16
	0.00243	37.1	56.7	
	0.00181	26.4	29.7	
12 500	0.0374	46.6	46.7	
	0.0186	42.9	56.7	
	0.0102	40.4	47.1	1.16
	0.00523	39.5	45.3	
	0.00391	40.2	47.3	
4000	0.0199	38.8	45.0	
	0.00996	35.1	46.4	
	0.00496	37.7	46.7	1.32
	0.00265	29.0	44.9	
	0.00200	38.6	53.3	
2800	0.0192	38.2	44.2	
	0.0102	32.9	43.5	
	0.00528	29.0	37.5	1.53
	0.00286	30.7	46.5	
	0.00216	25.3	67.1	
2300	0.0691	34.3	40.7	
	0.0344	33.2	40.0	
	0.0172	30.4	38.9	1.26
	0.00919	30.7	40.3	
	0.00711	30.0	39.8	
1700	0.0254	39.4	45.5	
	0.0125	38.9	47.9	
	0.00621	37.2	47.0	1.26
	0.00328	29.4	38.6	
	0.00246	28.9	39.6	
480	0.0863	46.5	56.7	
	0.0423	46.0	56.7	
	0.0210	43.9	55.5	1.28
	0.0111	44.9	58.5	
	0.00844	43.5	59.8	
330	0.0111	62.6	71.6	
	0.00548	55.7	71.1	
	0.00275	56.6	69.3	1.33
	0.00149	52.7	99.2	
	0.00112	60.5	73.4	

Table 13 Spin-lattice relaxation times for lignin fractions at various concentrations

Molar Mass	Concentration (w/w)	T_1 major (ms)	T_1 minor (ms)	Percentage of T_1 major
22 000	0.0175	49.3	17.6	86.0
	0.00930	61.2	8.83	81.7
	0.00459	44.9	44.9	72.6
	0.00243	44.8	1.12	89.2
	0.00181	40.9	15.6	54.7
12 500	0.0374	58.5	58.6	58.9
	0.0186	46.5	3.84e-5	95.0
	0.0102	43.7	43.8	57.0
	0.00523	43.9	43.9	92.7
	0.00391	43.9	43.9	63.1
4000	0.0199	40.6	40.7	44.2
	0.00496	53.9	1.43	87.4
	0.00200	38.5	38.5	84.6
2800	0.0192	566	27.1	16.2
	0.0102	33.0	33.0	54.6
	0.00528	30.5	30.5	54.4
	0.00286	54.3	0.741	76.8
	0.00216	23.7	23.7	52.8
2300	0.0691	39.7	28.6	49.4
	0.0344	50.9	24.3	41.2
	0.0172	39.8	17.5	65.4
	0.00919	37.3	4.00e-5	91.2
	0.00711	29.3	5.73	84.9
1700	0.0254	47.2	9.30	87.1
	0.0125	108	29.9	21.4
	0.00621	44.9	0.902	91.0
	0.00328	38.9	2.59e-5	88.2
	0.00246	41.9	1.18e-5	85.0
480	0.0863	195	40.6	11.4
	0.0423	225	41.8	8.34
	0.0210	132	42.2	5.34
	0.0111	54.1	1.75e-5	91.4
	0.00844	96.1	23.4	43.7
330	0.0111	72.5	5.71	91.4
	0.00548	159	39.2	28.0
	0.00275	103	103	33.3
	0.00112	182	28.8	39.0

Table 14 Spin-lattice relaxation times for lignin fractions at various concentrations (double exponential fit)

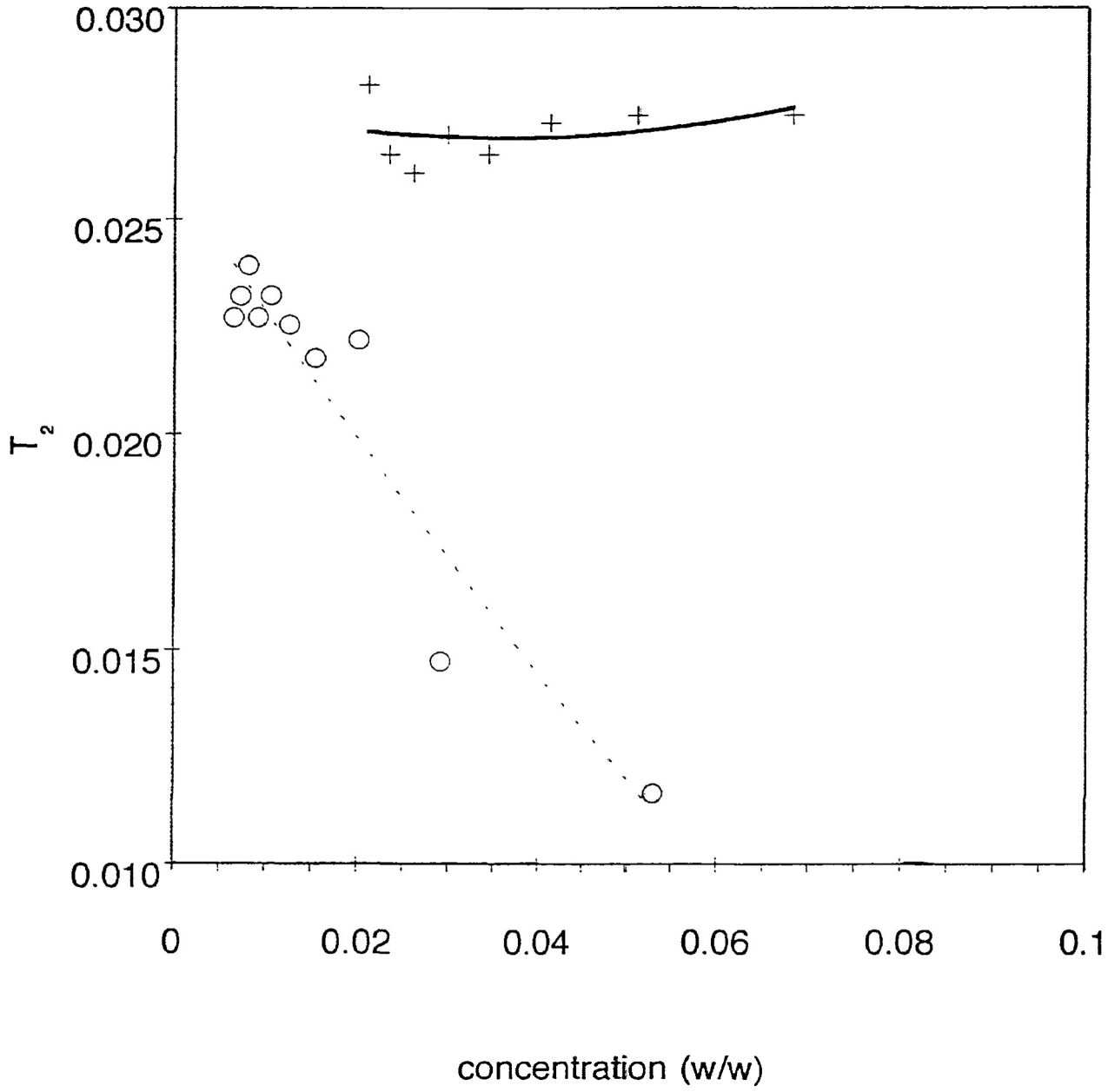

Figure 33 Spin-spin relaxation time versus concentration for molecular weights 2300 (····) and 480 (——)

Molar Mass	Concentration (w/w)	T_2 calculated (ms)
4000	0.0117	10.5
	0.00649	17.7
	0.00448	22.3
	0.00342	18.9
	0.00280	24.9
	0.00235	22.9
	0.00204	21.6
	0.00179	23.5
	0.00160	25.4
	0.00145	25.0
2300	0.0530	11.6
	0.0292	14.7
	0.0201	22.2
	0.0154	21.8
	0.0126	22.6
	0.0105	23.3
	0.00919	22.7
	0.00806	23.9
	0.00723	23.2
	0.00652	22.7
1700	0.0340	14.0
	0.0170	21.5
	0.0116	24.1
	0.00866	24.6
	0.00691	23.9
	0.00577	24.4
	0.00494	26.0
	0.00438	24.2
	0.00390	25.6
	0.00351	25.0
480	0.206	14.3
	0.102	20.5
	0.0682	27.4
	0.0512	27.4
	0.0412	27.2
	0.0344	26.5
	0.0298	27.0
	0.0261	26.1
	0.0234	26.5
	0.0211	28.2

Table 15 Spin-spin relaxation times calculated from line widths for fractionated lignin samples

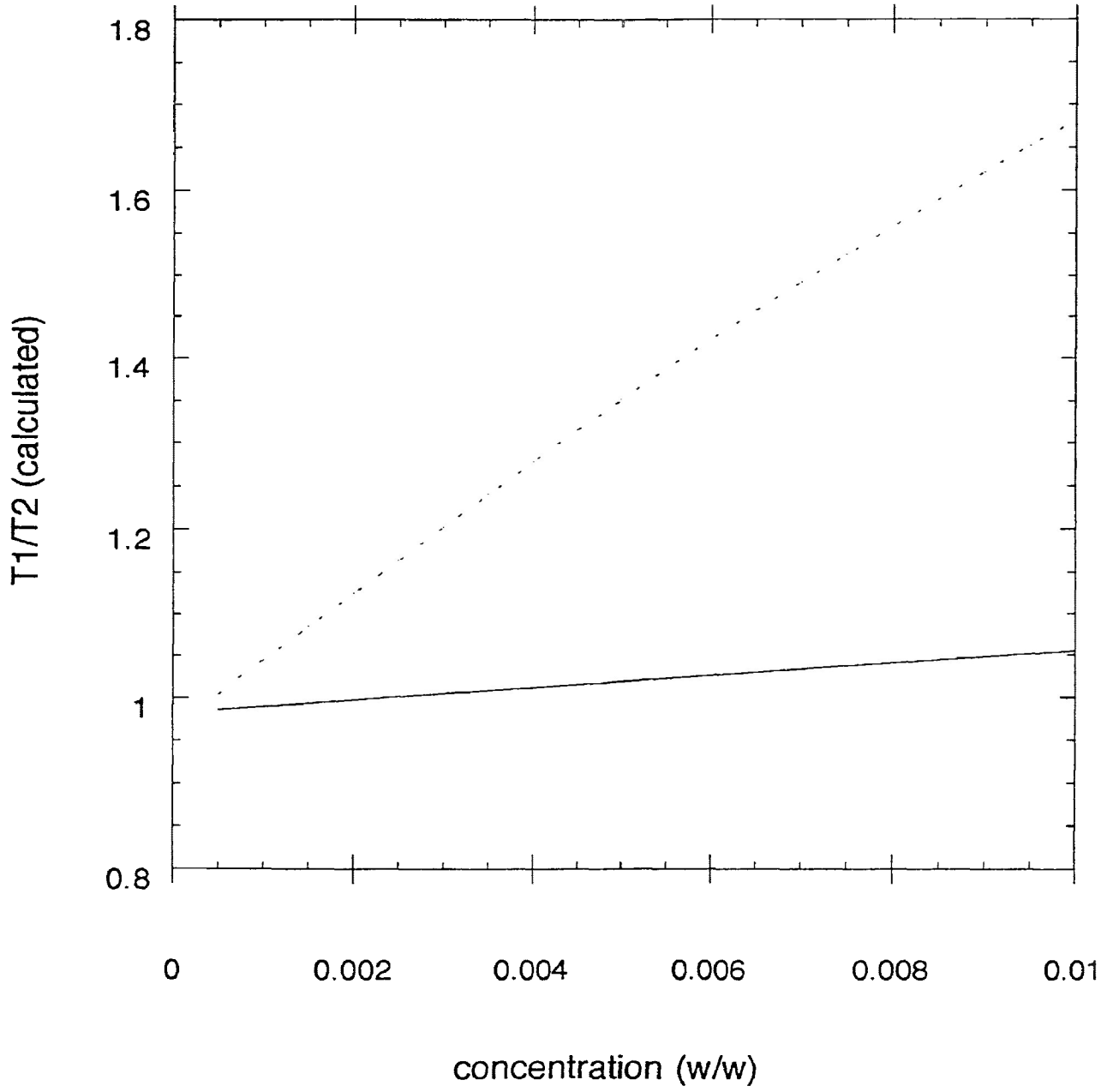

Figure 34 Ratio of T_1/T_2 versus concentration for molecular weights 2300 (····) and 480 (——)

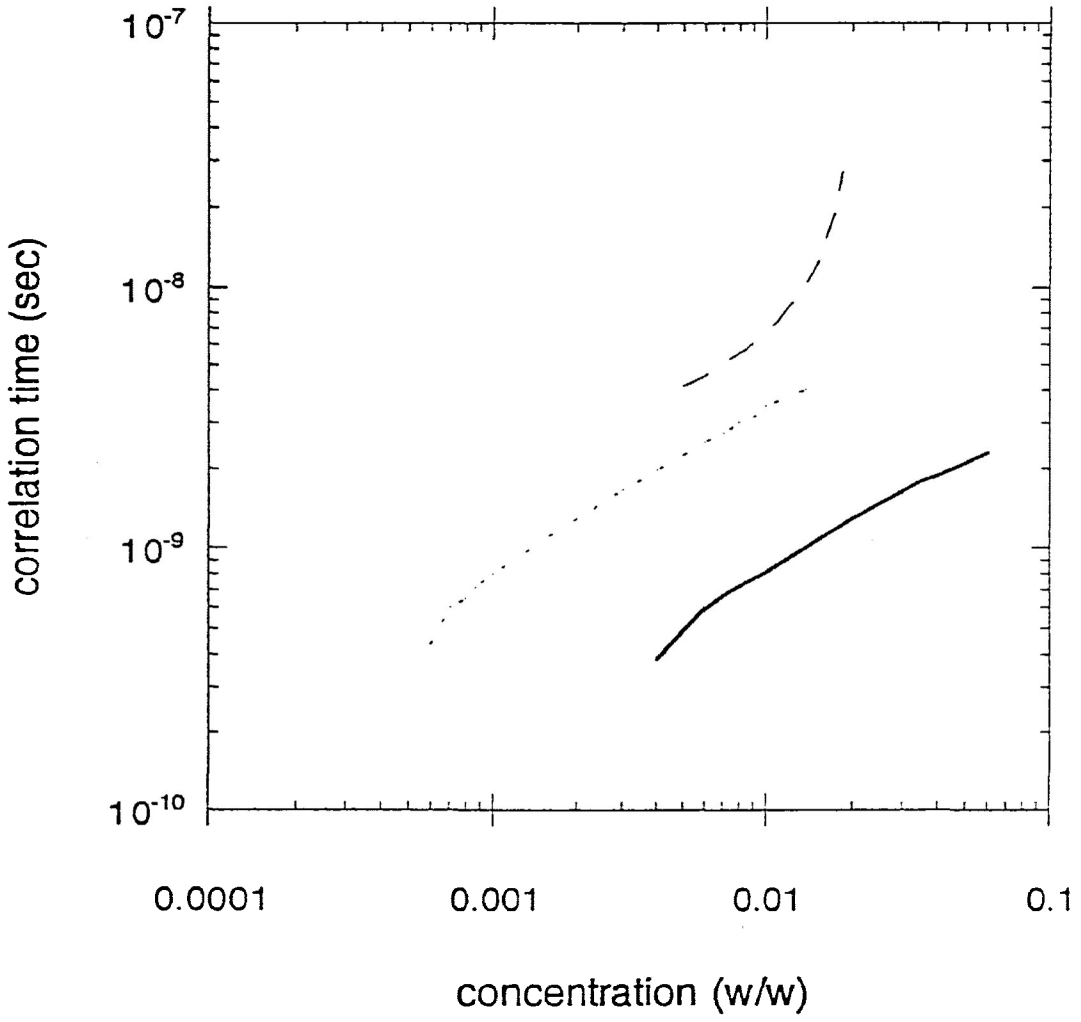

Figure 35 Rotational correlation time versus concentration for molecular weights 4000 (----), 2300 (····) and 480 (——)

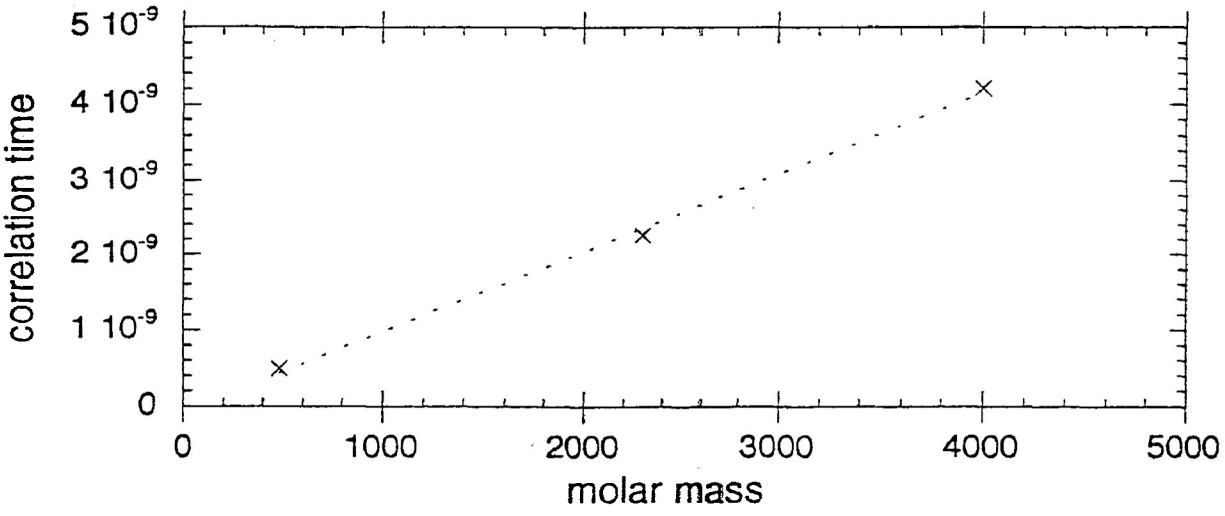

Figure 36 Rotational correlation time versus molar mass

more rapidly with temperature than T_1 for 2800 (Figure 37). The high molecular weight sample (2800) is probably near the "T_1 minimum" of a relaxation rate versus correlation time curve[34] where the T_1 value is not expected to change much. The polydispersity of a sample may increase the breadth of the T_1 minimum. The T_2 values also increased with temperature for the two samples but at approximately the same rate (Figure 38).

A plot of correlation time/viscosity*temperature versus temperature (Figure 39) does not have a linear shape which suggests that viscosity is not the sole cause of the variation in T_1 and T_2 with temperature.

A sudden change in T_1 and line shape indicates the start of new motions[64]. In this study it is difficult to say what is happening due to the different types of deuterium nuclei (both aromatic and aliphatic) contributing to the spectra. Future work should involve selectively labelling aromatic or aliphatic species with deuterium to separate their effects on the relaxation times.

The different rates of increase of T_1 with temperature may suggest different types of motion in the samples, as suggested by protein studies[64].

CONCLUSION:

NMR analysis of lignin provides a challenge to the NMR spectroscopist. In this study several lignin samples ranging in size from a lignin model trimer to lignin fractions with a molecular weight over 20 000 were analyzed using NMR spectroscopy.

The NMR study of a lignin model trimer led to a systematic approach to the structural analysis of lignin. Complete assignment of aliphatic and aromatic proton and carbon-13 chemical shifts were made. These chemical shifts were similar to the published chemical

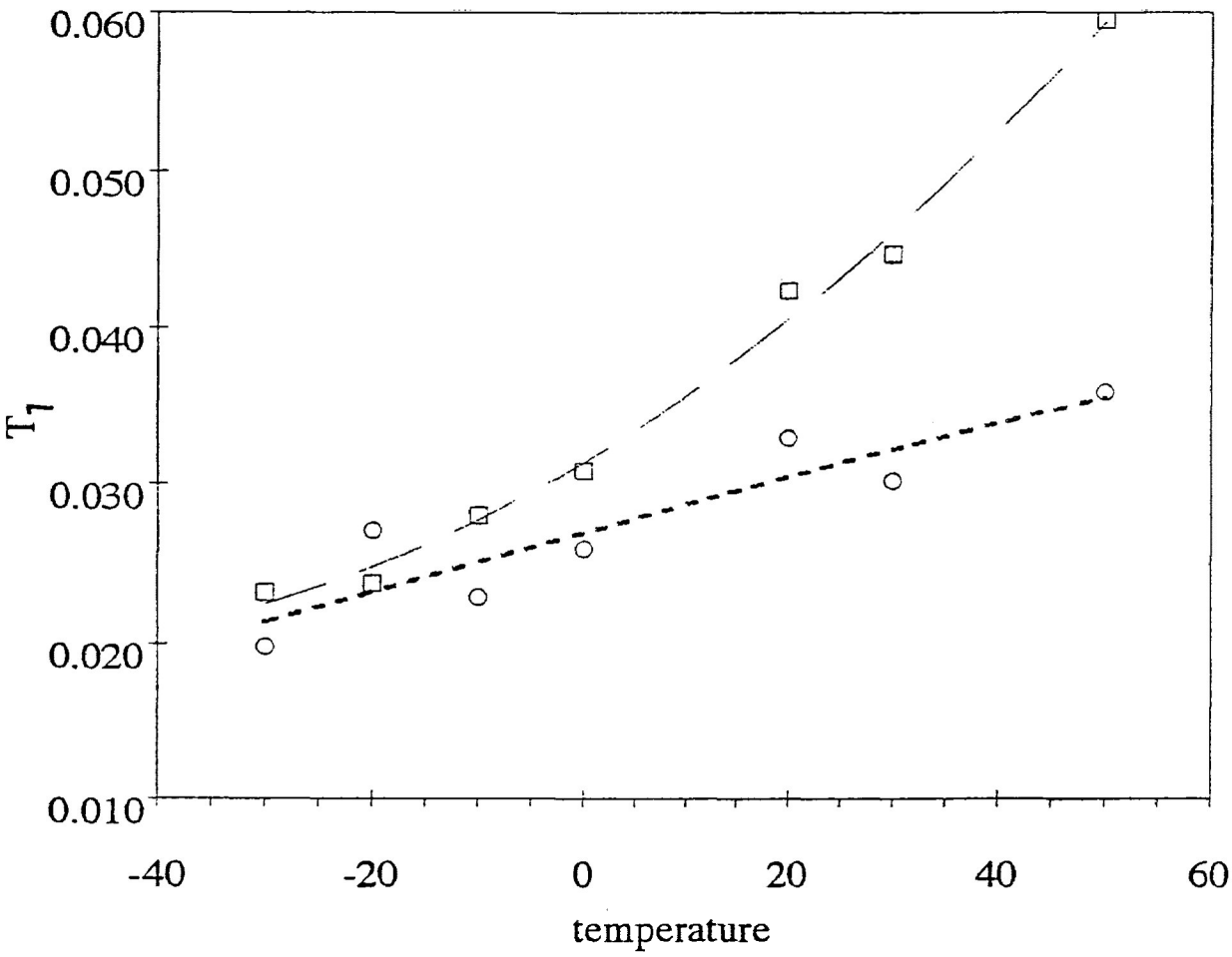

Figure 37 **Spin-lattice relaxation time versus temperature for molecular weights 2800 (····) and 480 (----)**

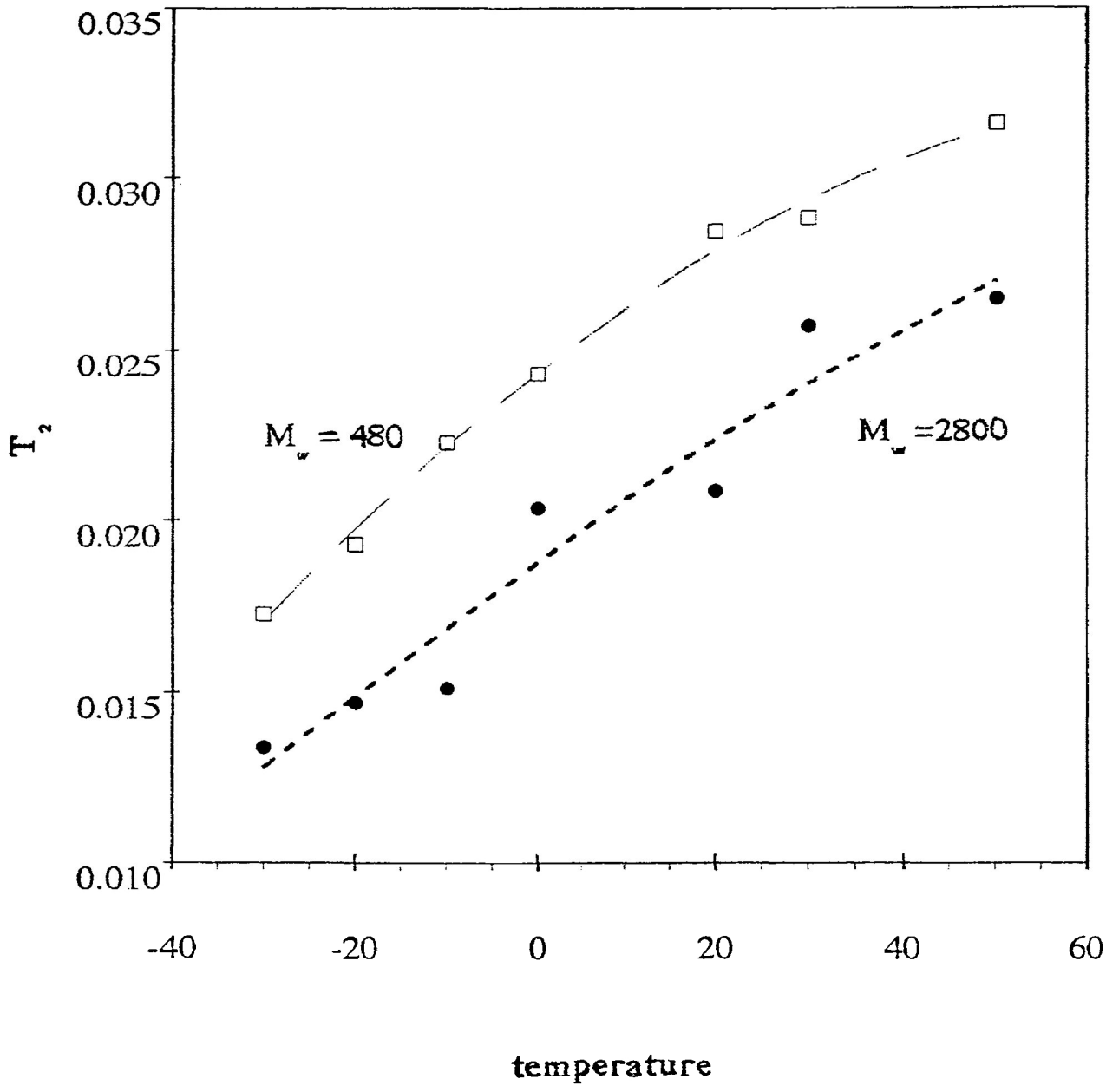

Figure 38 Spin-spin relaxation time versus temperature for molecular weights 2800 (····) and 480 (----)

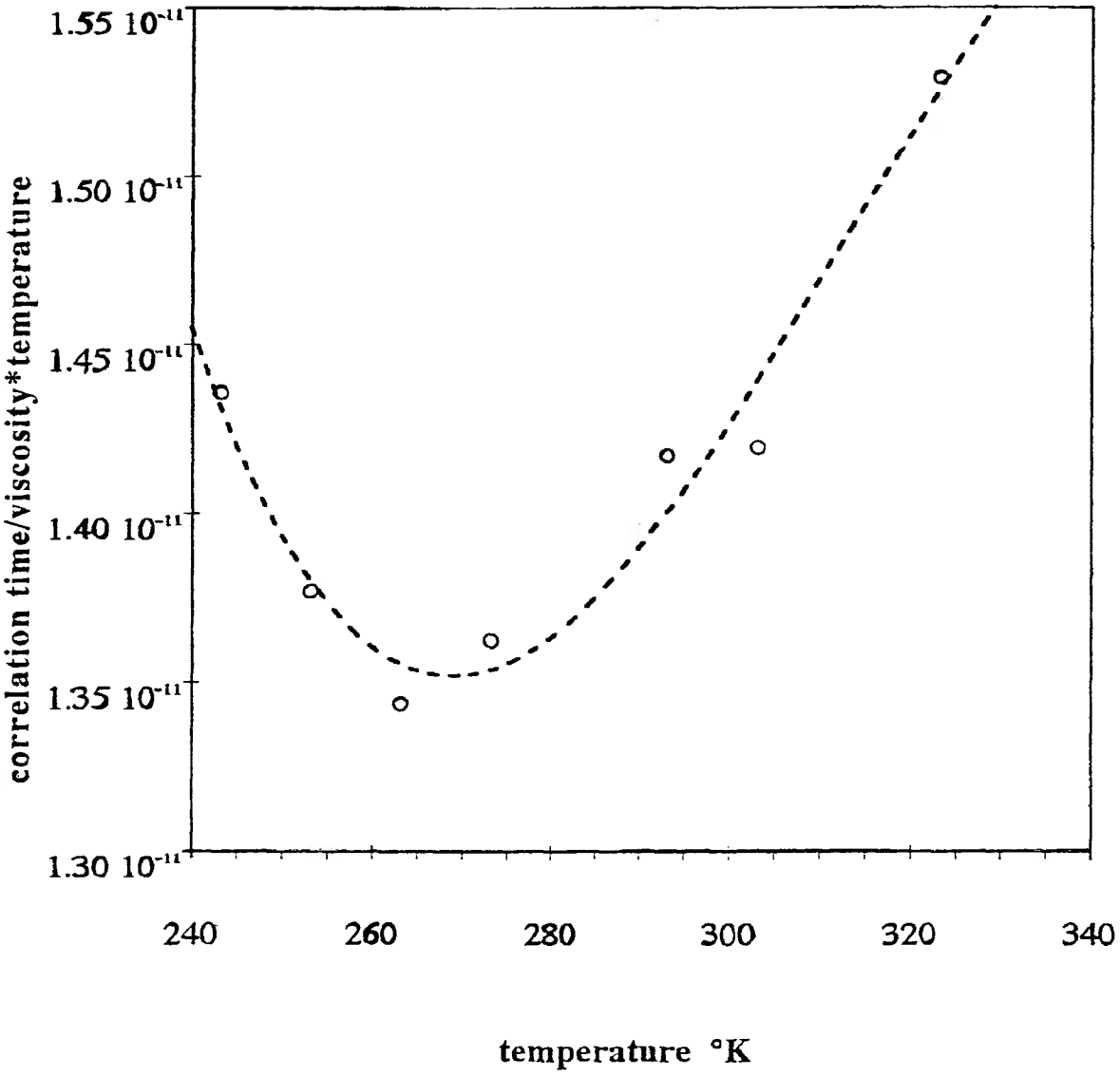

Figure 39 Correlation time/viscosity*temperature versus temperature for lignin fractions

shifts of lignin monomers and dimers indicating that a lignin trimer is not large enough for conformation to affect chemical shifts. Larger models should be analyzed to determine at what chain length conformation changes chemical shifts. Future studies should also include the determination of conformation in aqueous solution as a function of pH.

Structural elements present in effluents from the peroxide bleaching of spruce ground wood were identified using proton, phosphorus-31 and COSY NMR. A carbon-13 spectrum was not obtained. Integration of the proton spectra provided a measure of the relative frequencies of structural elements for each bleaching stage. From this data the time dependence of each element could be determined. The presence of β-O-4 units, phenolic structures and β-5 units in the effluents indicated they were resistant to bleaching. Carbohydrates in the lignin may have prevented reactions between these structures and peroxide. Further studies may help to decide whether bleaching stops when hydroquinones are formed or when carboxylic acids are formed.

Deuterium labelled kraft lignin fractions were used in an empirical and theoretical study of relaxation and correlation times as functions of concentration and temperature. Correlation times for acetylated kraft lignin fractions varied between 2.7×10^{-8} s and 8.1×10^{-10} s when temperature, molecular weight and concentration were changed. A sharp increase in T_1 values for some samples suggested the onset of new molecular motion. It was not possible to determine the relative contributions of aliphatic and aromatic protons to the relaxation time because the deuteration technique was not selective. Future work

should involve labelling either the aliphatic or aromatic structures to determine whether backbone or side chain motion is affecting the relaxation values. Selective labelling and varying the solvent conditions may also aid in determining the shape of lignin molecules in solution.

EXPERIMENTAL SECTION:

Model Compound:

Acetoguaiacyl-dehydrodi-isoeugenol methyl ether[65] was donated by Dr. Jerzy Arct at Lakehead University in Thunder Bay, Ontario. Solvent used for NMR studies was chloroform-d (99.8%, Cambridge Isotope Laboratories) with tetramethylsilane (99.9%, Cambridge Isotope Laboratories) as internal standard. The spectrometer at Lakehead University was a Bruker AC-E spectrometer operating at a proton frequency of 200 MHz and the spectrometer at the Prairie Regional NMR Center in Winnipeg, Manitoba was an AMX500 with a proton frequency of 500 MHz. The spectrometer in Winnipeg was operated by Kirk Marat.

The analysis of the model compound IIB is as outlined in Scheme I (page 89). Descriptions of the NMR experiments are in "NMR Analysis" (pre Part One) and experimental parameters are in "NMR Experiments" (Experimental Section).

Preparation of Kraft Lignin Samples for Deuterium Experiments:

Samples for deuterium relaxation experiments were prepared according to Scheme II (page 90).

Preparation of Effluent Samples:

Effluents were prepared according to the Experimental section in reference 66 and Scheme III (page 91).

Preparation of Spruce Kraft Lignin (Scheme IV page 92):

Spruce wood chips were steamed for 10 minutes before white liquor with 15.6 % effective alkali and 25 % sulfidity was added. The liquor to wood ratio was 4:1. During

Scheme I
Model Compounds

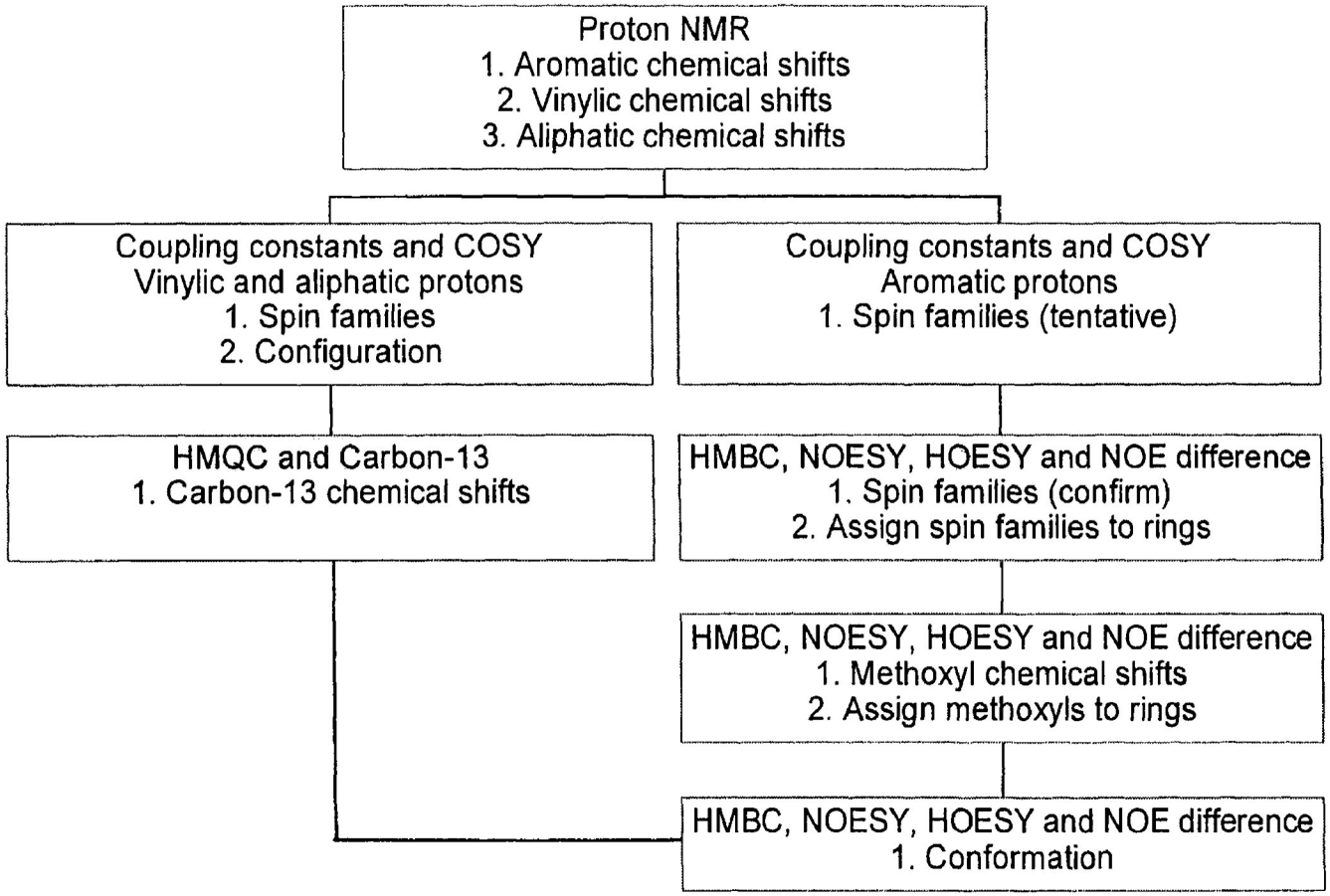

Scheme II
Deuterium Relaxation

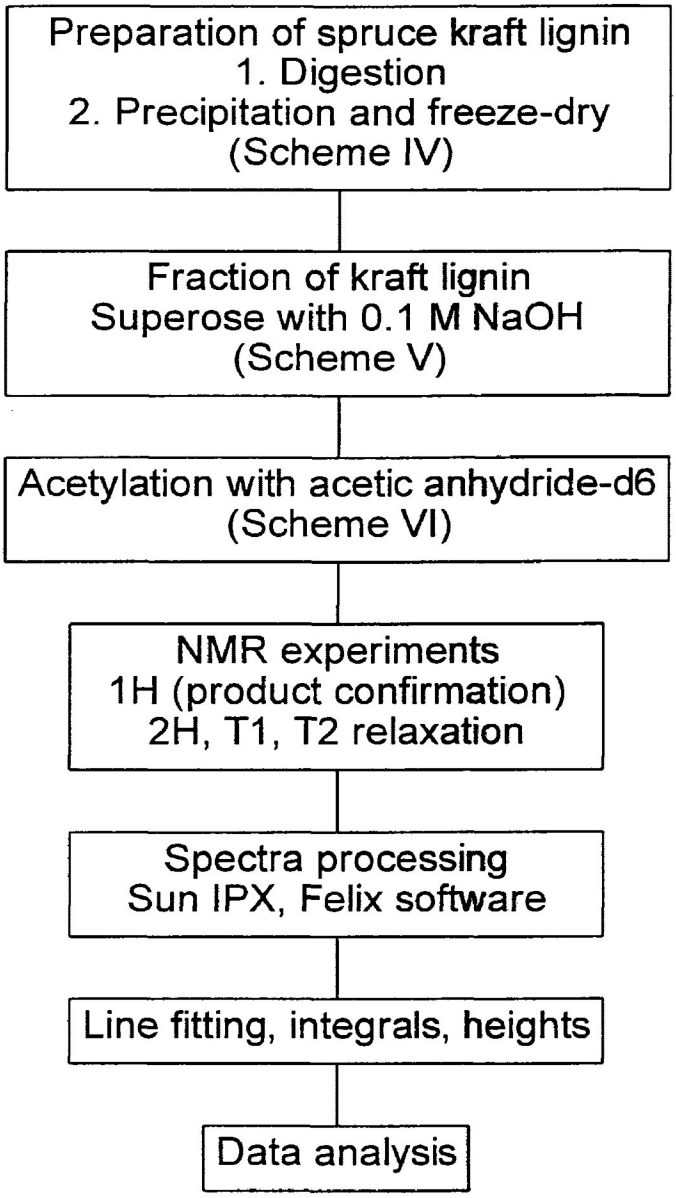

Scheme III
Preparation of Effluent Samples

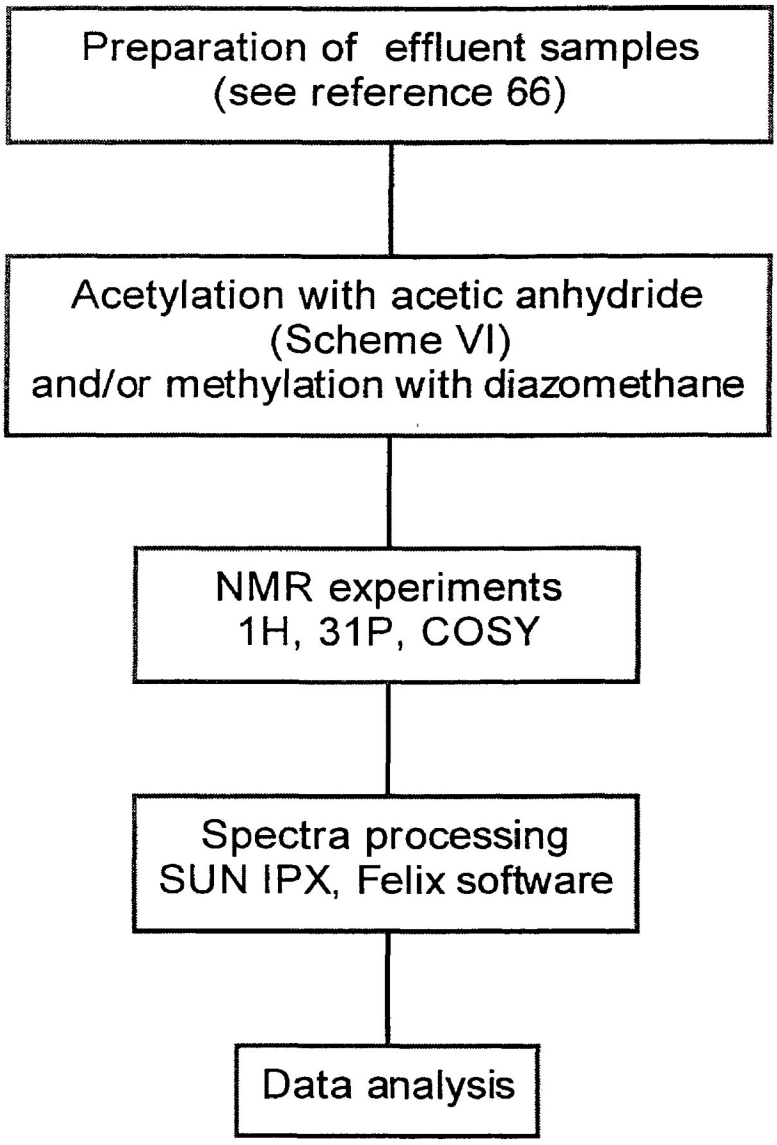

Scheme IV
Preparation of Spruce Kraft LIgnin

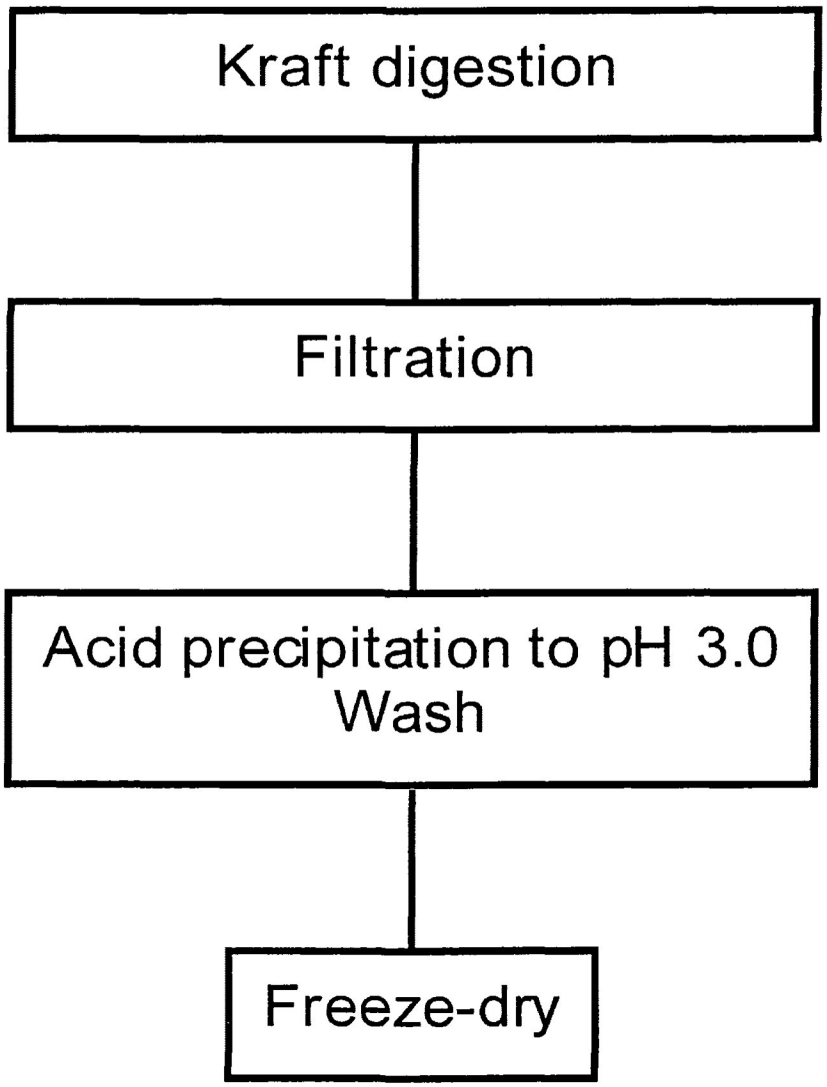

2.5 hours the chips were heated to 167 °C and then held at that temperature for 4 hours. When the kraft cook was over, the pulp was filtered and the black liquor was collected. The black liquor was diluted with distilled deionized water and the pH of the mixture was reduced to 3.0 by adding sulfuric acid dropwise with stirring. The mixture was centrifuged and the supernatant poured off. The lignin precipitate was washed with pH=3.0 sulfuric acid. The pH of the lignin was raised to 11.0 then dropped to 3.0 and the mixture was centrifuged again. The washing procedure (pH=11, pH=3, centrifuge) was repeated three times. The sample was freeze-dried. The calculated H factor was 1540 and the pulp kappa number was 21.5.

Fractionation of Kraft lignin (Scheme V page 94):

600 mg spruce kraft lignin was dissolved in 2.5 mL of 1.0 M NaOH and the weight of the sample was made up to 4.0 g with distilled deionized water. Sample was loaded onto a size-exclusion chromatography column containing Superose 12 gel (prep grade) with carbonate free 0.1 M NaOH as eluent and a spectrum was recorded at a wavelength of 500 nm. 18.0 mL fractions of the lignin were collected, neutralized with HCl and freeze-dried. Samples were dissolved in water, placed in a cellulose ester membrane with a MWCO = 500 and dialyzed for one hour in 0.01% mass/volume EDTA and three times for one hour each time in distilled deionized water. After freeze-drying the samples were acetylated.

Acetylation (Scheme VI page 95):

Approximately 1 tsp. of freshly ground barium oxide was added to approximately 300 mL of pyridine. Boiling chips were also added. The pyridine was distilled and the

Scheme V
Fraction of Kraft Lignin

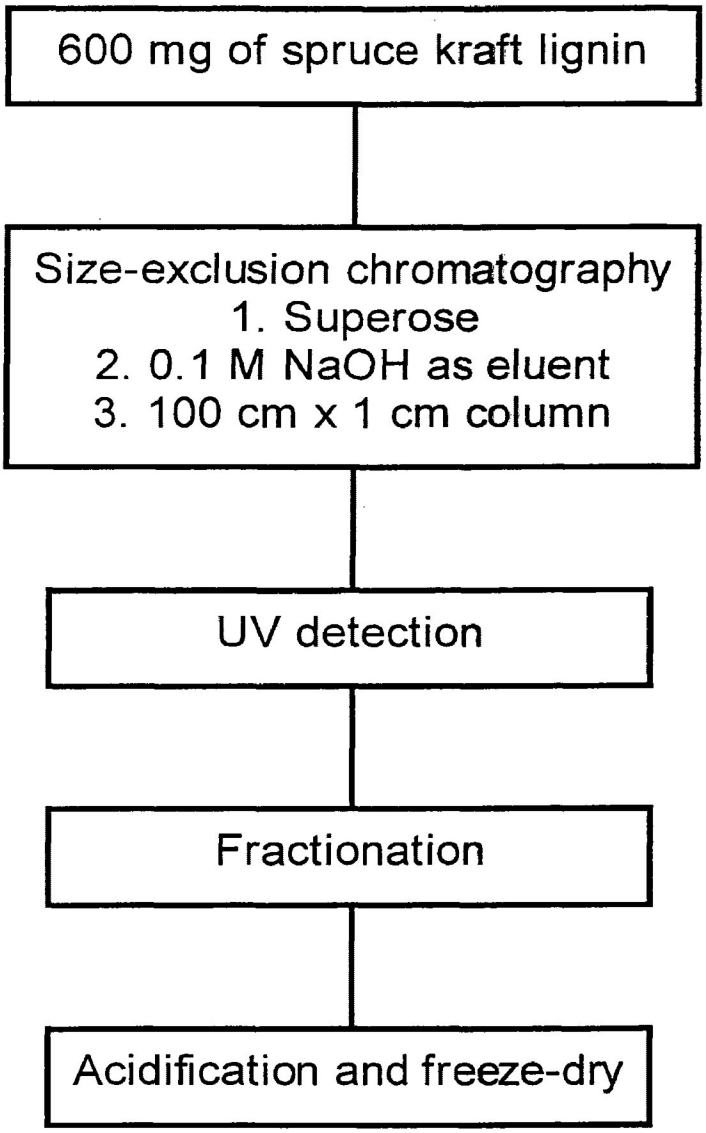

Scheme VI
Acetylation

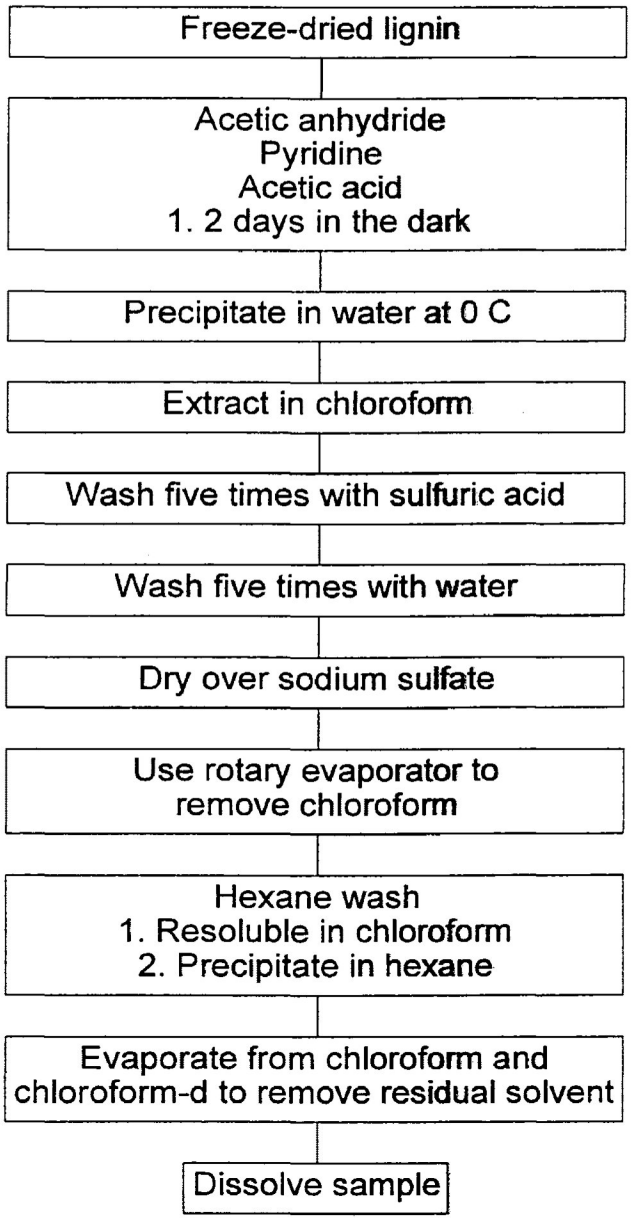

fraction boiling at 114-116°C was collected. The collected fraction was redistilled using a one-piece distillation apparatus with a Vigreux distilling column. Phosphorus pentoxide was added to approximately 300 mL of acetic anhydride in a 500 mL round-bottomed flask and allowed to sit overnight. The acetic anhydride was decanted into a 1000 mL round-bottomed flask containing boiling chips. The acetic anhydride was distilled and the fraction boiling at 136-138°C was collected. The acetic anhydride that was collected was redistilled using the one-piece distillation apparatus. Approximately 15 g of potassium permanganate was added to approximately 300 mL of glacial acetic acid. The acetic acid was distilled and the fraction boiling at 115°C was collected.

The amount of sample that was acetylated varied. The pyridine:acetic anhydride:acetic acid ratio was 51:28:1. A small amount of water was sometimes added first to dissolve the sample. The samples were swirled, flushed with nitrogen and placed in the dark for 48 hours.

Acetylation Work-up:

A solution of 150 mL distilled deionized water and 10 mL pyridine was cooled to 0°C. The acetylated sample was added and allowed to stand for one half hour. The mixture was extracted three times with 50 mL chloroform. The chloroform layer was washed five times with 50 mL 1M sulphuric acid and five times with 50 mL distilled deionized water. Chloroform layer was dried over anhydrous sodium sulphate. The chloroform was evaporated on a rotary evaporator (Yamato Scientific Co. Model RE-47).

Hexane Purification:

10 mL hexane was added to the sample, swirled around and discarded. Then, 10 mL chloroform was added, swirled around and evaporated. The above procedure was repeated five times. Chloroform was then added and evaporated three times to remove residual hexane.

Methylation:

Diazomethane Preparation:

Set up the apparatus in Diazald^{R} Kit (Diazomethane Generator). Measured 20 g potassium hydroxide and 20 mL distilled deionized water into a 500 mL round-bottomed flask with a Teflon-coated stirring bar. Pre-heated a water bath to 75°C and then raised the water bath to heat the flask. Added 20 mL of distilled 2(2-ethoxyethoxy)ethanol to the flask through a separatory funnel. Added 20 mL chloroform through separatory funnel. Dissolved 5 g Diazald (*N*-methyl-*N*-nitroso-*p*-toluenesulfonamide) in 50 mL chloroform. Excess diazomethane was collected via Teflon tubing with a glass tube extension which was submersed in ice cooled chloroform.

Sample Preparation:

50 mL hexane was added to sample, swirled and removed. Sample was dissolved in chloroform. Added diazomethane and mixed. Sample was extracted two times with chloroform and five times with distilled deionized water.

Phosphorus-31 NMR:

Phosphorus-31 NMR has recently been adapted for use by Argyropoulos[67]. The phosphorus is introduced onto the lignin by a phosphitylation reaction involving 1,3,2-dioxaphospholanyl chloride.

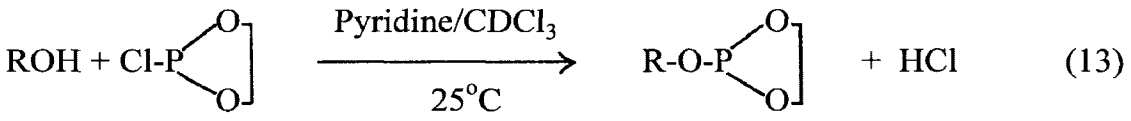

(13)

Labile hydrogens found on alcohols, aldehydes and carboxylic acids for example, are replaced by a phosphorus containing functionality[67]. The phosphorus compound 1,3,2-dioxaphospholanyl chloride has a chemical shift at 167.3 ppm. A product of the phosphorus compound and water has a chemical shift of 121.1 ppm.

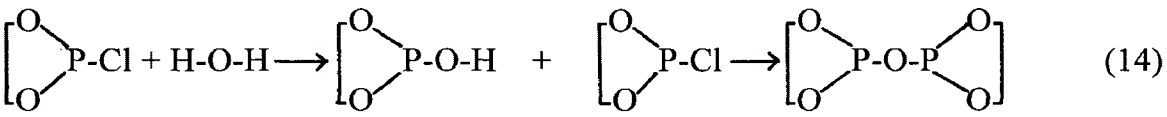

(14)

Since this product is independent of experimental conditions it can be used as a reference signal. A decoupled P-31 spectrum consists of single lines representing each type of phosphorus atom[67].

Preparation of 1,3,2-Dioxaphospholanyl Chloride[68]:

The apparatus consisted of a 250 mL 3-necked flask equipped with a 150 mL dropping funnel and large condenser capped with a $CaCl_2$ drying tube. Phosphorus trichloride (22

mL) and methylene chloride (50 mL) were poured into the flask. Ethylene glycol (14 mL) was slowly added via the dropping funnel while the mixture was stirred using a magnetic stirring plate. After refluxing the reaction was allowed to proceed for one half hour. The apparatus was adapted for distillation under reduced pressure. Nitrogen gas was constantly bubbled through the mixture to prevent air or moisture from entering. Residual methylene chloride was collected and discarded. The through distillation product was collected. P-31 NMR spectrum of the product had two peaks, one at 121.1 ppm representing a product formed by the reaction of the phosphorus reagent and water and another at 167 ppm indicating a pure and clean product[67].

Labelling with 1,3,2-Dioxaphospholanyl Chloride:

The procedure of Archipov et al[67] was followed for the labelling of samples with phosphorus. Freshly distilled pyridine (400 μL) and deuterated chloroform (500 μL) was added to 15 mg of sample. Carefully added 50 μL 1,3,2-dioxaphospholanyl chloride. The whole procedure was conducted under nitrogen gas with stirring[67].

Deuterium Labelling Methods:

1. Base Catalyzed: Refluxed 0.2 g vanillin dissolved in 10 mL deuterium oxide and 0.092 mL triethylamine for 4.5 hours[69]. Sample was freeze-dried.

2. Base Catalyzed: 0.1 g vanillin, 0.04 g potassium t-butoxide and 1.0 mL deuterium oxide were placed into a glass tube under nitrogen atmosphere. The tube was sealed and heated in an oven at 100°C for 72 hours[69]. The tube was cracked open and enough water was added to the sample to measure pH. The pH was lowered to 6.0 and sample was

extracted with chloroform.

3. 0.092 g vanillin was dissolved in 3.0 mL of 40 wt% solution of sodium deuteroxide in D_2O. Sample was poured into a 10 cm quartz UV cell and placed 11 cm from a mercury lamp[70]. Samples were taken after one hour and five hours of irradiation.

4. Weighed 0.5 g ground milled spruce pulp (previously extracted with acetone and water) into a flask, added 10 mL 0.1 M sodium deuteroxide, sealed flask and heated in oven at 88°C for 4 hours. Whole procedure was conducted under nitrogen.

5. Acetylation with acetic anhydride-d_6.

Of the methods described above, three were successful. Method 2 resulted in replacement of the 5 proton of vanillin with deuterium which simplified the spectrum (Figure 40 and Figure 41) by collapsing the aromatic multiplets between 7.0-7.5 ppm into singlets. Method 4 used less toxic reagents and a shorter reaction time to achieve exchange. The lignin sample was labelled and a deuterium spectrum obtained (Figure 42). The simplest method (5) was to incorporate deuterium into a known procedure. Lignin samples were acetylated using acetic anhydride-d_6. These samples were used to measure relaxation times. Deuteration method 1 did not work because water entered the sample and method 3 produced no appreciable change.

NMR Experiments:

Proton: Proton spectra were recorded on both the Bruker AC-E and AMX500 spectrometers at room temperature.

Carbon-13: Carbon-13 spectrum was recorded using an autoprogram called POWGATE.AU (power gated heteronuclear broadband decoupling).

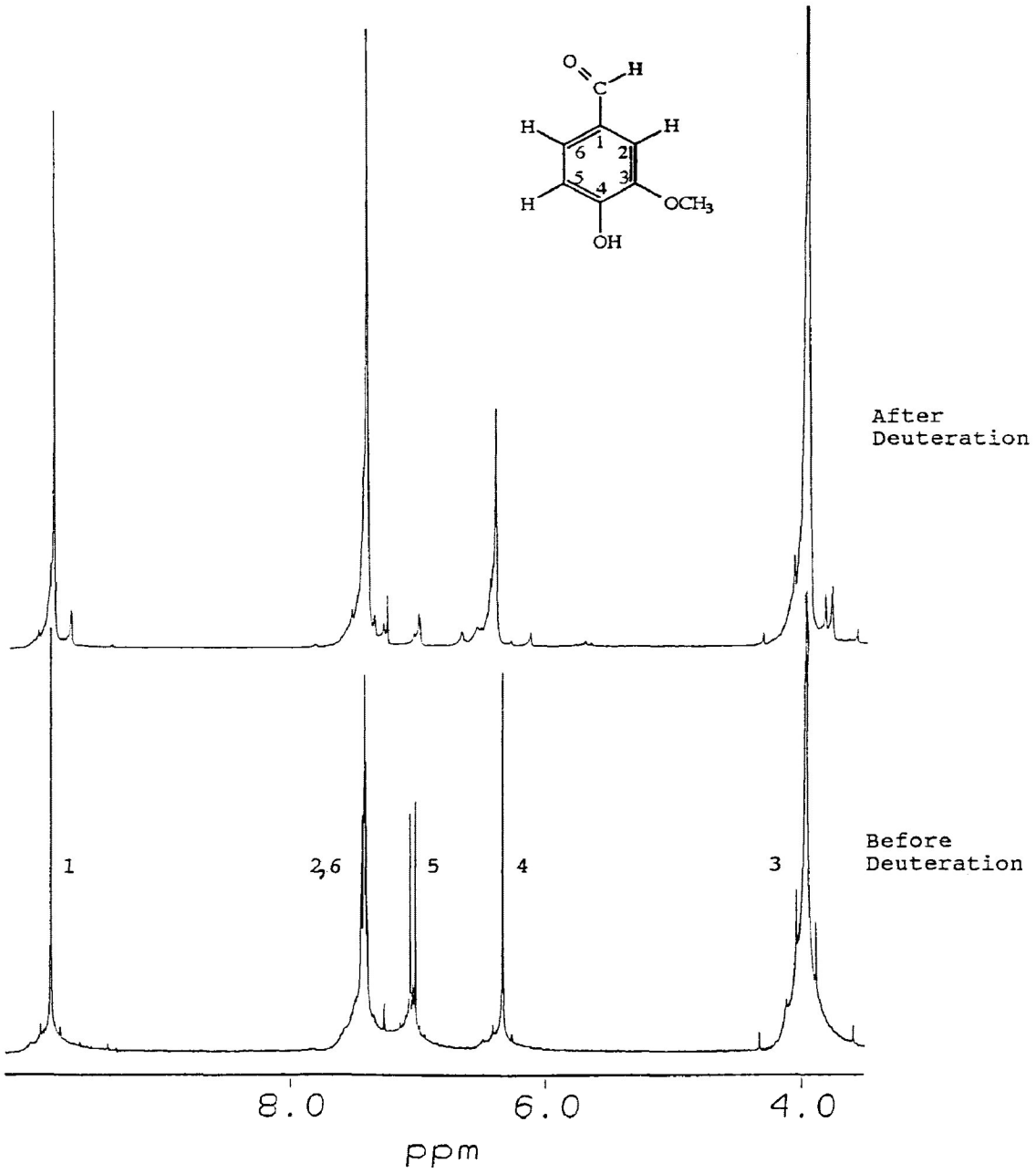

Figure 40 200 MHz proton spectra showing the collapse of vanillin multiplets between 7.0-7.5 ppm (deuteration method 2)

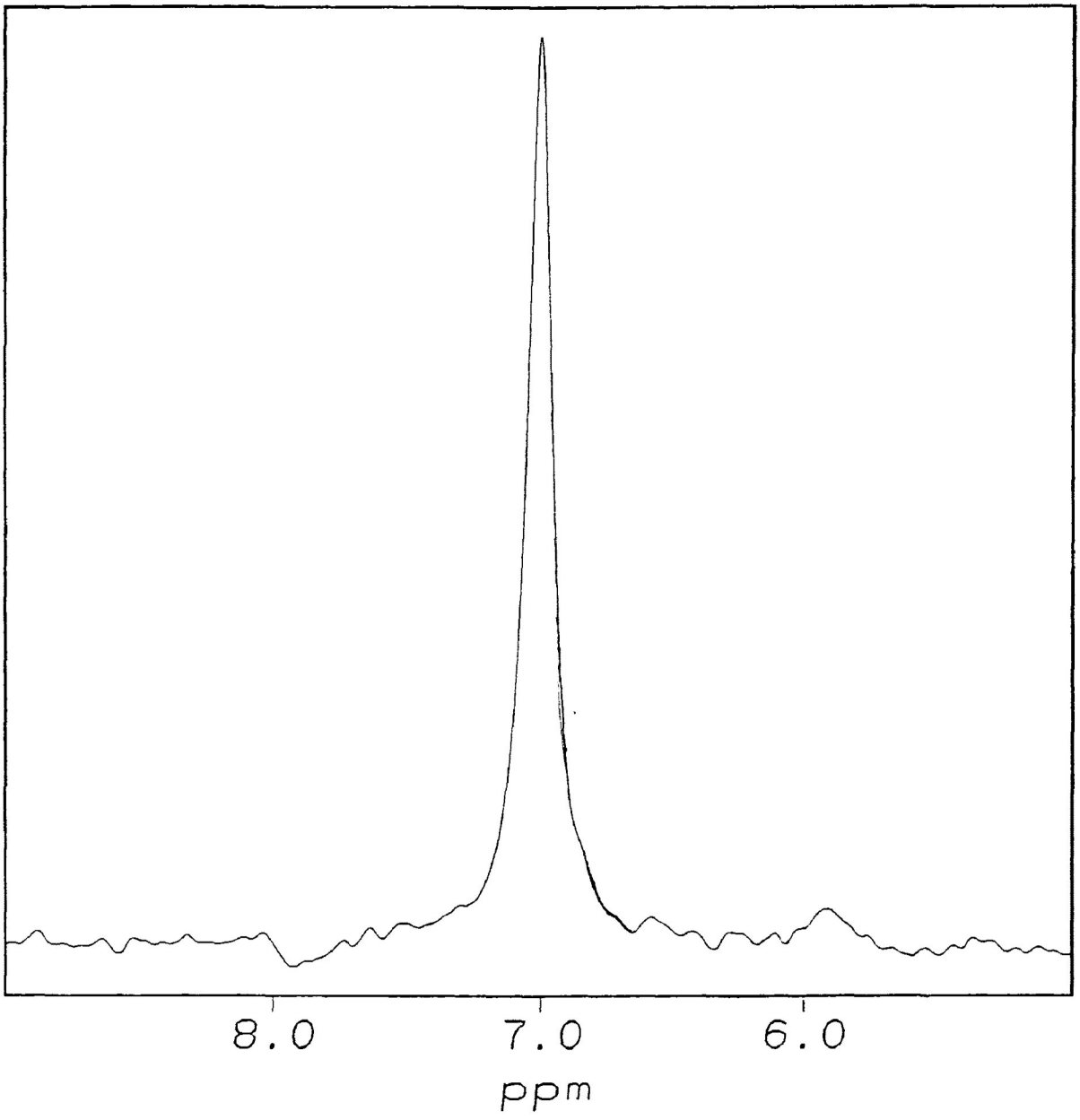

Figure 41 30.7 MHz deuterium spectrum of vanillin (deuteration method 2)

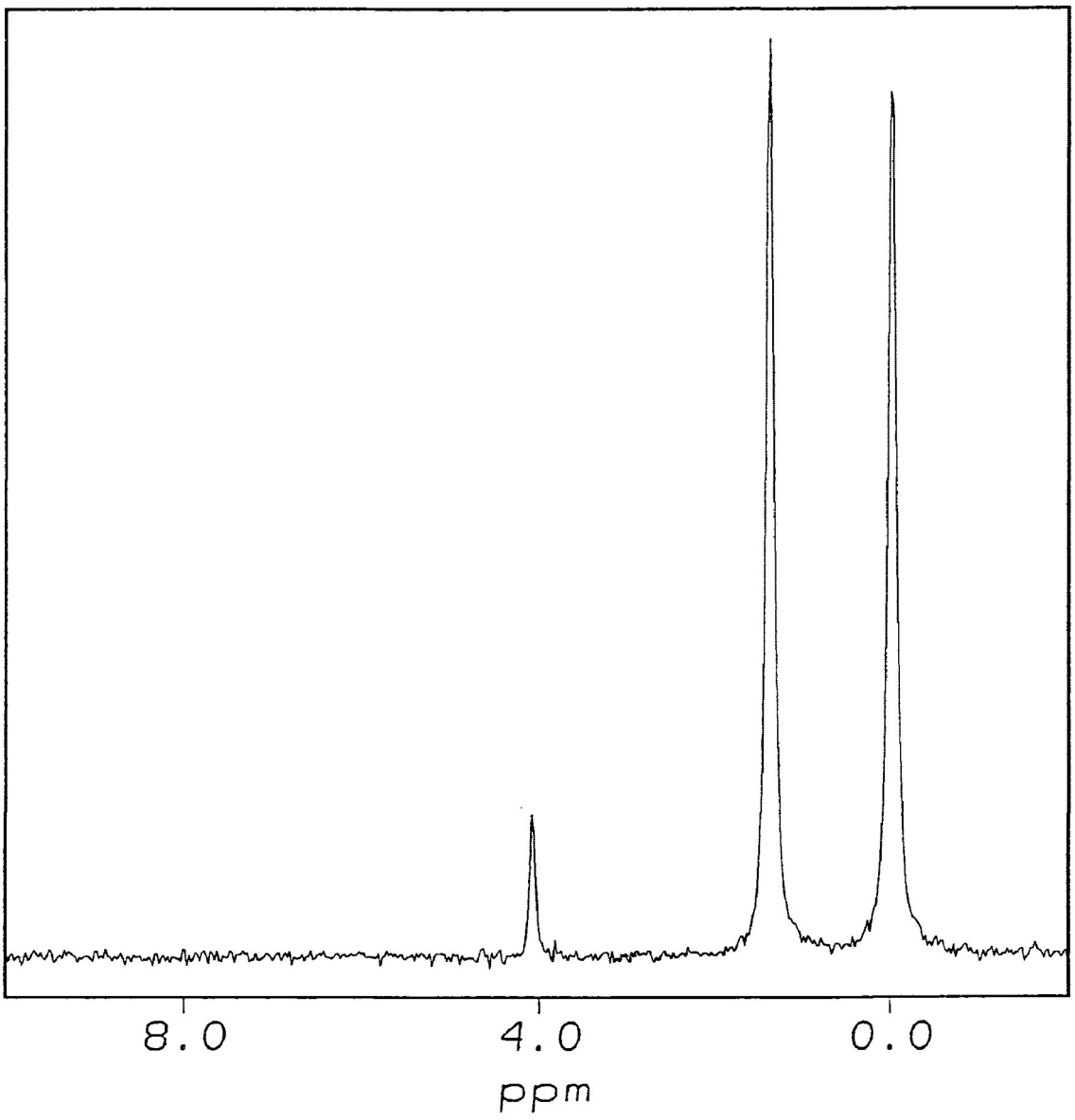

Figure 42 **30.7 MHz deuterium spectrum of ground milled spruce pulp (deuteration method 4)**

COSY: The pulse sequence was D1-90-D0-90 based on articles by Aue et al[14] and Nagayama et al[15]. There were 1K data points in F2 with a sweepwidth of 1602 Hz. There were 256 increments with 32 scans each.

NOESY: The pulse sequence was D1-90-D0-90-D9-90-FID[13] with a relaxation delay of 5 s and mixing time of 1.2 s. All other parameters were the same as for the COSY.

HOESY: The pulse sequence for a standard HOESY experiment based on articles by Yu and Levy and Rinaldi[19,20,21] is

^{1}H: D1-90-D0 D0-90-D9 BB

XNUC: D1 180 90-FID

There were 4K data points in F2 with a sweepwidth of 23809 Hz. The relaxation delay was 3.5 s and the mixing time was 2 s.

NOE Difference: The NOE difference program was based on an article by Kinns and Sanders[12]. There were 32 K data points with a sweepwidth of 3817 Hz. The cross-relaxation delay was set at 0.1 s.

HMBC[17,18]: The sweepwidth was 3623 Hz with 4K data points and F2 and a J_{CH} delay of 0.07 s or 7 Hz.

HMQC[16,17]: There were 4K data points with a sweepwidth of 3623 Hz in F2. Delay time for optimizing one bond proton-carbon couplings was 0.00178 s or 140 Hz.

Analysis of Deuterium Relaxation:

Deuterium relaxation spectra were obtained on a Bruker AC 200 spectrometer operating at 30.7 MHz for deuterium. The T_1 inversion recovery program (INVREC)

used a 180° - τ - 90° sequence with delays of 0.05 to 3000 ms. (Delay times were 0.05, 0.5, 1, 2, 4, 7, 10, 15, 20, 30, 45, 60, 80, 100, 150, 200, 300, 400, 500, 750, 1000, 1500, 2000, 3000 ms). Spectra were integrated on a Sun IPX Workstation using a Lorentzian peak fitting option after a baseline correction (polynomial = 5) in a Felix 2.10 program. Integrals and peak heights were plotted versus delay times. A non-linear fit[71] (see equation below) of the points up to 500 ms provided an initial rate approximation of T_1 values (Figure 43). T_1 values were also calculated using a double exponential equation applied to all the points (Figure 44).

$$I_t = I_\infty[1 - 2\exp(-t/T_1)] \qquad (15)$$

T_2 relaxation times at various sample concentrations were obtained by substituting the line width into the following equation[58].

$$\Delta\nu_{1/2} = 1/\pi T_2 \qquad (16)$$

T_1 and T_2 data obtained by the methods described above were plotted versus concentration and fit with quadratic and cubic equations.

T_1 and T_2 values were regressed versus concentration using polynomial least squares methods. The T_1/T_2 ratio, as a function of concentration, was calculated from these polynomial fits to the experimental data. This T_1/T_2 ratio was then compared to a T_1/T_2 ratio calculated using theoretical equations (equation 11) for deuterium relaxation. The correlation times leading to the theoretical T_1/T_2 ratios which matched the T_1/T_2 polynomial ratio were found. These are the correlation times reported in Figures 35 and 36.

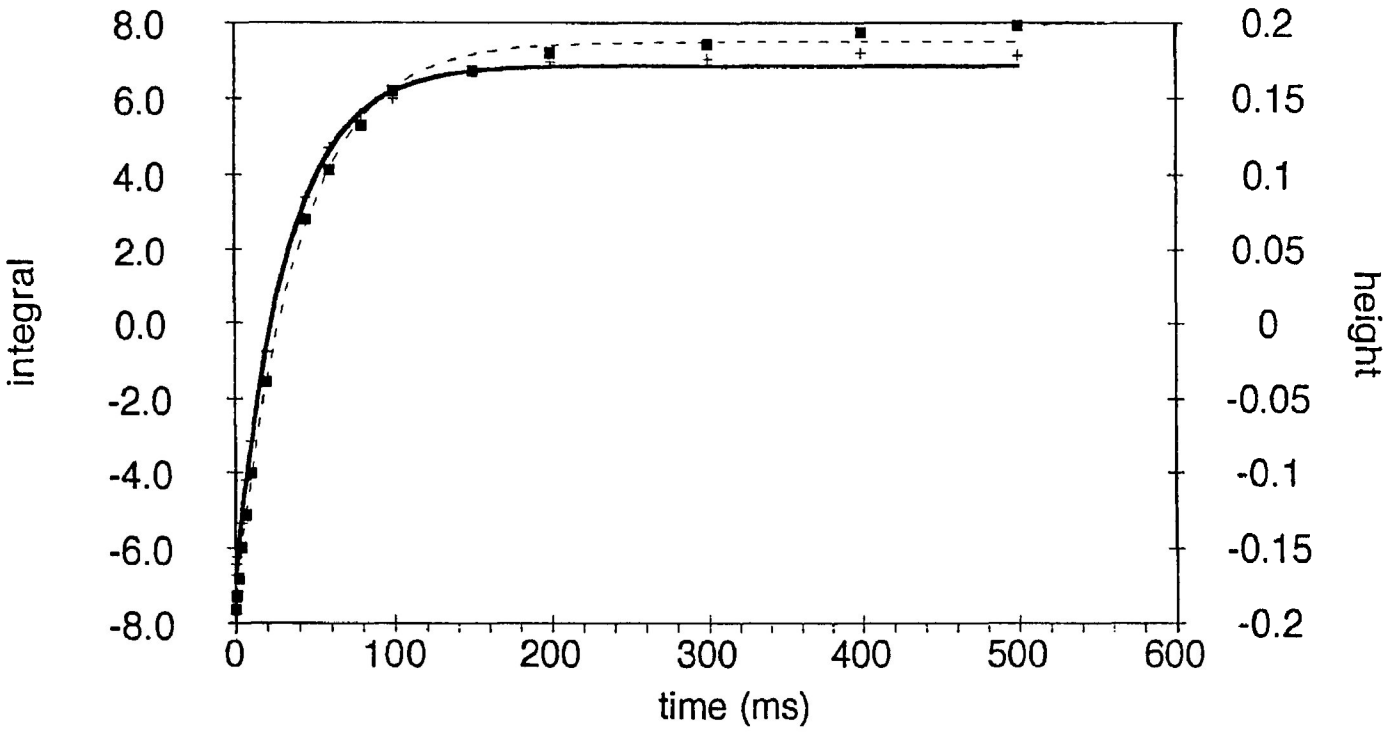

Figure 43 **Single exponential fit to inversion recovery integral (——) and height (····) data for molecular weight 2300**

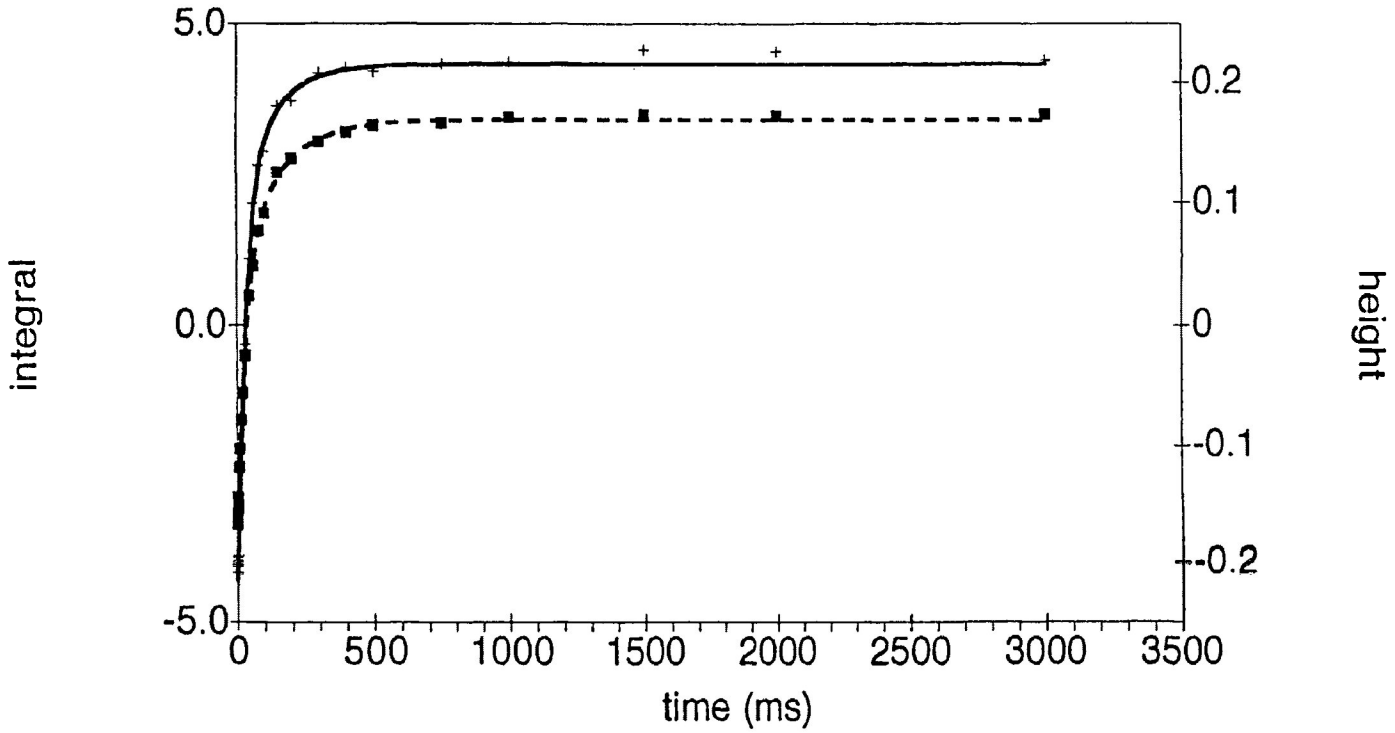

Figure 44 **Double exponential fit to inversion recovery integral (——) and height (····) data for molecular weight 480**

Polynomials (T_1/T_2) were plotted versus concentration and correlation time for each sample (Figure 45). Correlation time and concentration values were measured at various (T_1/T_2) values. Correlation time versus concentration was plotted.

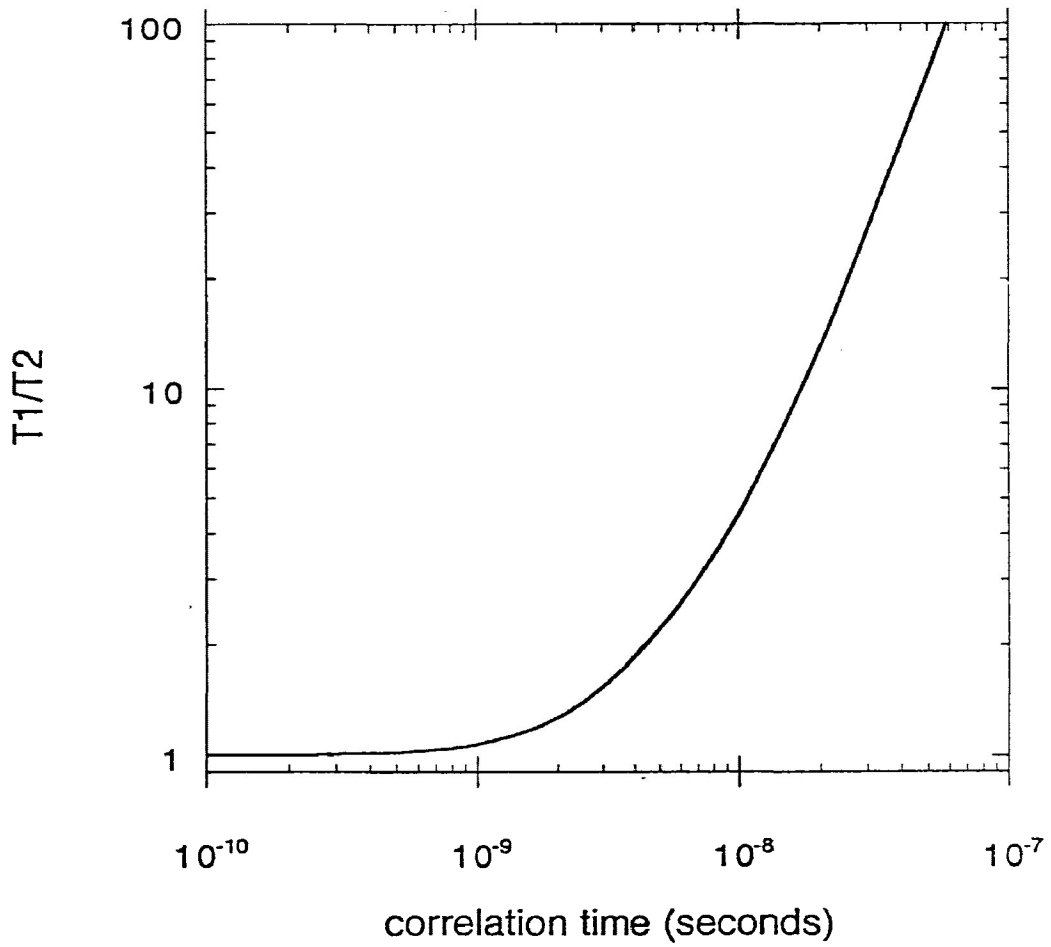

Figure 45 **Theoretical plot of T_1/T_2 versus correlation time for deuterium at 30.7 MHz**

REFERENCES

1. Sarkanen, K.V.; Ludwig, C.H. eds Lignins; John Wiley & Sons: New York, 1971, pp. 797, pp. 1, 2, 299-326.

2. Lin, S.Y.; Dence, C.W. eds Methods in Lignin Chemistry; Springer-Verlag: Berlin, 1992, pp. 4, 6.

3. Sjöström, E. Wood Chemistry; Academic Press: New York, 1981, p. 72, 76-77, 79.

4. Fengel, D.; Wegener, G. Wood; Walter de Gruyter: Berlin, 1984, pp. 230-232, 465.

5. Sjöström, E. Wood Chemistry; Academic Press: San Diego, 1993, pp. 63, 65, 81-86, 188-189.

6. Adler, E. *Wood Sci. Technol.*, 1977, 11, 169-218.

7. Derome, A.E. Modern NMR Techniques for Chemistry Research; Pergamon Press: Oxford, 1987, pp. 85, 188, 215-216.

8. Friebolin, H. Basic One- and Two-Dimensional NMR Spectroscopy; VCH Publishers: New York, 1991, pp. 20, 27, 82-84, 97, 228-229.

9. Kringstad, K.; Mörck, R. *Holzforschung*, 1985, 37, 237.

10. Mörck. R.; Kringstad, K. *Holzforschung*, 1985, 39, 109.

11. Nimz, H.H.; Lüdemann, H.-D. *Holzforschung*, 1976, 30, 33.

12. Kinns, M; Sanders, J.K.M. *J. Magn. Reson.*, 1984, 56, 518.

13. Neuhaus, D.; Williamson, M.P. The Nuclear Overhauser Effect in Structural and Conformational Analysis; VCH Publishers: New York, 1989, pp. 63-74, 79, 82, 83, 103-140.

14. Aue, W.P.; Bertholdi, E.; Ernst, R.R. *J. Chem. Phys.*, 1976, 64, 2229.

15. Nagayama, K.; Kumar, A.; Wüthrich, K.; Ernst, R.R. *J. Magn. Reson.*, 1980, 40, 321.

16. Bax, A.; Subramanian, J. *J. Magn. Reson.*, 1986, 67, 565.

17. Nakanishi, K. ed. One-Dimensional and Two-Dimensional NMR Spectra by Modern Pulse Techniques; University Science Books: Mill Valley, 1990, pp. 226-227.

18. Bax, A.; Summers, M.F. *J. Am. Chem. Soc.*, 1986, 108, 2093.

19. Yu, C.; Levy, G. *J. Am. Chem. Soc.*, 1984, 106, 6533.

20. Yu, C.; Levy, G.C. *J. Am. Chem. Soc.*, 1983, 105, 6994.

21. Rinaldi, P.L. *J. Am. Chem. Soc.*, 1983, 105, 5167.

22. Croasmun, W.R.; Carlson, R.M.K. Two-Dimensional NMR Spectroscopy; VCH Publishers: New York, 1994, pp. 295, 327, 406-407.

23. ur-Rahman, A. One And Two Dimensional NMR Spectroscopy; Elsevier: Amsterdam, 1989, pp. 273, 274, 361, 376-378, 395, 422.

24. Martin, G.E.; Zektzer, A.S. Two-Dimensional NMR Methods for Establishing Molecular Connectivity; VCH Publishers: New York, 1988, pp. 59, 240-242.

25. Ernst, R.R.; Bodenhausen, G.; Wokaun, A. Principles of Nuclear Magnetic Resonance in One and Two Dimensions; Clarendon Press: Oxford, 1987, pp. 504, 519, 520, 523.

26. Ede, R.M.; Brunow, G.; Simola, L.K.; Lemmetyinen, J *Holzforschung*, 1990, 44, 95.

27. Lundquist, K. *Acta Chem. Scand.*, 1979, B33, 418.

28. Ralph, J. *Magn. Reson. Chem.*, 1993, 31, 357.

29. Lundquist, K. *Nordic Pulp and Paper Research Journal*, 1992, 1, 4.

30. Karplus, M. *J. Chem. Phys.*, 1959, 30, 11.

31. Karplus, M. *J. Am. Chem. Soc.*, 1963, 85, 2870.

32. Shen, X.; Van Heiningen, A. *Can. J. Chem.*, 1992, 70, 1754.

33. Schraml, J.; Bellama, J.M. Two-Dimensional NMR Spectroscopy; John Wiley & Sons: New York, 1988, pp. 3, 141-142.

34. Sanders, J.K.M.; Hunter, B.K. Modern NMR Spectroscopy 2nd ed.; Oxford University Press: Oxford, 1993, pp. 2, 50, 161-164.

35. Bovey, F.A.; Jelinski, L.; Mirau, P.A. Nuclear Magnetic Resonance Spectroscopy 2nd ed.; Academic Press: San Diego, 1988, p. 82.

36. Ede, R.M.; Brunow, G. *J. Org. Chem.*, 1992, 57, 1477.

37. Singh, R.P. ed. The Bleaching of Pulp 3rd ed.; Tappi Press, 1979, pp.211-212.

38. Pan, X.; Lachenal, D.; LaPierre, C.; Monties, B.; Neirinck, V. *Holzforschung*, 1994, 48, 429.

39. Holmbom, R.; Ekman, R; Sjöholm, R.; Eckerman, C.; Thornton, J. *Jahrgang*, 1991, Heft 10A, V16.

40. Agnemo, R.; Gellerstedt, G. *Acta Chem. Scand.*, 1979, B33, 337.

41. Agnemo, R.; Gellerstedt, G; Lindfors, E.-L. *Acta Chem. Scand.*, 1979, B33, 154.

42. Reeves, R.H.; Pearl, I.A. *Tappi*, 1965, 48, 121.

43. Gellerstedt, G.; Agnemo, R. *Acta Chem. Scand.*, 1980, B34, 275.

44. Gellerstedt, G.; Hardell, H.-L.; Lindfors, E.-L. *Acta Chem. Scand.*, 1980, B34, 669.

45. Bailey, C.W.; Dence, C.W. *Tappi*, 1969, 52, 491.

46. Omori, S.; Dence, C.W. *Wood Sci. Technol.*, 1981, 15, 113.

47. Nonni, A.J.; Dence, C.W. *Holzforschung*, 1988, 42, 37.

48. Gellerstedt, G.; Agnemo, R. *Acta Chem. Scand.*, 1980, B34, 461.

49. Gellerstedt, G.; Zhang, L. in Photochemistry of Lignocellulosic Materials; American Chemical Society: Washington, 1993, pp. 129-146.

50. Lundquist, K. *Acta Chem. Scand.*, 1980, B34, 21.

51. Pan, X.; Lachenal, D.; LaPierre, C.; Monties, B. *J. Wood Chem. Technol.*, 1993, 13(2), 145.

52. Lundquist, K.; Stern, K. *Nordic Pulp and Paper Research J.*, 1989, 3, 210.

53. Lundquist, K.; Olsson, T. *Acta Chem. Scand.*, 1977, B31, 788.

54. Argyropoulos, D.S.; Bolkner, H.I.; Heitner, C.; Archipov, Y. *J. Wood Chem. Technol.*, 1993, 13(2), 187.

55. Spittler, T.D.; Dence, C.W. *Svensk Papperstid.*, 1977, 9, 275.

56. Lundquist, K.; Simonson, R.; Tingsvik, K. *Svensk Papperstid.*, 1979, 9, 272.

57. Tsang, P.; Wright, P.E.; Rance, M. *J. Am. Chem. Soc.*, 1990, 112, 8183.

58. Abragam, A. The Principles of Nuclear Magnetism; Clarendon Press: Oxford, 1961, pp. 271-272, 313-315, 441.

59. Mantsch, H.H.; Saitô, H.; Smith, I.C.P Progress in NMR Spectroscopy; Pergamon Press: Oxford, 1977, pp. 211-271.

60. Seelig, J.; MacDonald, P.M. *Acc. Chem. Res.*, 1987, 20, 221.

61. Smith, I.C.P. NMR of Newly Accessible Nuclei Vol.2; Academic Press: New York, 1983, pp. 1-26.

62. Shimuzu, H. *J. Chem. Phys.*, 1962, 37, 765.

63. Marshall, A.G.; Schmidt, P.G.; Sykes, B.D. *Biochem.*, 1972, 11, 3875.

64. Keniry, M.A.; Rothgeb, M.; Smith, R.L.; Gutowsky, H.S.; Oldfield, E. *Biochem.*, 1983, 22, 1917.

65. Leopold, M. *Acta Chem. Scand.*, 1950, 4, 1523.

66. Garver, T.M. Jr.; Maa, K.J.; Xu, E.C.; Holah, D.G. *Res. Chem. Intermed.*, 1995, 21, 503.

67. Archipov, Y.; Argyropoulos, D.S.; Bolker, H.I.; Heitner, C. *J. Wood Chem. Technol.*, 1991, 11(2), 137.

68. Lucas, H.J.; Mithel, F.W.; Scully, C.N. *J. Am. Chem. Soc.*, 1950, 72, 5491.

69. Kirby, G.W.; Ogunkoya, L. *J. Chem. Soc.*, 1966, 64, 6914.

70. Saito, I.; Sugiyama, H.; Yamamoto, A.; Muramatsu, S.; Matsuura, T. *J. Am. Chem. Soc.*, 1984, 106, 4286.

71. Leipert, T.K.; Marquardt, D.W. *J. Magn. Res.*, 1976, 24, 181.

72. Ede, R.M.; Kilpeläinen, I. *Res. Chem. Intermed.*, 1995, 21, 313.